Gondwana Research 141 (2025) 74–101

Contents lists available at ScienceDirect

Gondwana Research

journal homepage: www.elsevier.com/locate/gr

A review of Mesozoic geodynamic evolution of the North Makran (SE Iran): A tale of a Neo-Tethyan ocean vanished due to two coexisting subduction zones

Edoardo Barbero [a,*], Luca Pandolfi [b], Morteza Delavari [c], Asghar Dolati [c], Emilio Saccani [d], Maria Di Rosa [b], Michele Marroni [b,e]

[a] Istituto di Geoscienze e Georisorse, CNR, Torino, Via Valperga Caluso 35, 10125 Torino, Italy
[b] Dipartimento di Scienze della Terra, Università di Pisa, Via S. Maria 53, 56126 Pisa, Italy
[c] Faculty of Earth Sciences, Kharazmi University, Shahid Mofatteh St. 43, Tehran, Iran
[d] Dipartimento di Fisica e Scienze della Terra, Università di Ferrara, Via Saragat 1, 44123 Ferrara, Italy
[e] Istituto di Geoscienze e Georisorse, CNR, Pisa, Via G. Moruzzi 1, 56124 Pisa, Italy

ARTICLE INFO

Handling Editor: Jan Marten Huizenga

Keywords:
North Makran domain
Ophiolites
Subduction zones
Neo-Tethys geodynamics
Mesozoic-Cenozoic

ABSTRACT

This paper presents a synthesis of the geological features of each tectonic unit of the North Makran (SE Iran), integrating results of multidisciplinary analyses, including structural and stratigraphic studies, petrographic and geochemical analyses, thermobarometric studies, as well as biostratigraphic and geochronological dating. This wealth of data forms the basis for a novel geodynamic model of the Jurassic – Eocene evolution of the Neo-Tethys realm, which evolved between the Arabian Plate and the Lut Block. The features of the North Makran tectonic units support the existence of a mid-ocean ridge setting during the Jurassic – Early Cretaceous. Contrary to previous interpretations, the data from these tectonic units suggests a single oceanic basin separating the Arabian and Lut continental margins, without the interposition of a microcontinental block. In the Early Cretaceous, subduction initiation is recorded by volcanic arc assemblages accommodating the convergence between the Arabian Plate and Lut Block. The nucleation of an intra-oceanic subduction marked the separation of the North Makran Ocean from the Neo-Tethys. The Late Cretaceous was characterized by plume-related magmatism and the onset of the convergence in the North Makran Ocean, inducing its subduction beneath the Lut Block. This subduction is recorded by volcanic arc assemblage and high pressure and low-temperature metamorphism within a subduction complex. Meanwhile, intra-oceanic subduction persisted within the Neo-Tethys, accompanied by a subduction complex and arc magmatism. The final closure of the North Makran Ocean occurred during the Late Cretaceous –Late Paleocene with the progressive amalgamation of the two subduction complexes and the deformation of the interposing oceanic lithosphere. This study suggests that the subduction of a seamount chain in the North Makran Ocean played a key role in the shortening and closure of this basin. This research emphasizes the importance of considering multiple factors in understanding the tectonic evolution of the Neo-Tethys realm.

1. Introduction

The Alpine–Himalayan orogenic belt consists of a mosaic of continental microplates surrounded by ophiolite-bearing suture zones that extend from the eastern Mediterranean area to the Himalayan belt (Fig. 1a). This tectonic setting is the result of a long-lived geological history spanning from Paleozoic to the present day, characterized by processes such as rifting, oceanic spreading, subduction/obduction, volcanic arc activity and continental margin collision. These processes are all interconnected with the drifting of continental microplates from the northern margin of the Gondwana Plate and their progressive northward motion until their accretion at the southern margin of the Eurasian Plate (Fig. 1b, c; Stöcklin, 1968; Takin, 1972; Şengör and Yilmaz 1981; Dercourt et al. 1986; Ricou 1994; Barrier et al., 2018; Fergusson et al., 2016; Dilek and Furnes, 2019; Metcalfe, 2021).

One of the best examples of the tectonic setting resulting from this

* Corresponding author.
E-mail address: edoardobarbero91@gmail.com (E. Barbero).

https://doi.org/10.1016/j.gr.2025.01.016
Received 16 April 2024; Received in revised form 23 December 2024; Accepted 14 January 2025
Available online 12 February 2025

long-lived geological history is the Iranian area, where several ophiolite-bearing suture zones are distributed around continental microplates (Fig. 1a), forming a complex network of oceanic-derived terranes. This network mainly resulted from the interplay between two large oceanic basins: the Paleo-Tethys, which opened in the Silurian and closed in the Triassic, and the Neo-Tethys, whose opening occurred in the Late Permian – Triassic (Fig. 1b; Stöcklin, 1968; Şengör, 1984; Şengör et al., 1988; Stampfli, 2000; Agard et al., 2005; Stampfli and Hochard, 2009; Metcalfe, 2013). Reconstructing the tectonic evolution of the various Neo-Tethyan ophiolite-bearing suture zones is therefore a crucial step in understanding the geodynamic history of the Alpine–Himalayan orogenic belt in the Iranian area.

This paper focuses on the reconstruction of the Mesozoic to Cenozoic geodynamics of one of the most relevant suture zones of the Iranian region: the North Makran, where a stack of oceanic units of different ages and geodynamic significance is well exposed (Fig. 2a, b). This area plays an important role as the backstop of the present-day Makran Accretionary Prism, a regional structure resulting from the ongoing northward subduction of the Neo-Tethys oceanic lithosphere beneath the Lut Block, one of the continental microplates amalgamated with the Eurasian margin (Fig. 1a). Geodynamic reconstructions for the North Makran have so far been proposed by several authors (e.g., McCall and Kidd, 1982; Moghadam and Stern, 2015; Burg, 2018; Saccani et al., 2018; Ghasemi et al., 2022a). While these reconstructions are scientifically valuable, they have some limitations due to an overly regional-scale focus (e.g., Moghadam and Stern, 2015), or a lack of detailed studies because of the pioneering nature of the research (e.g., McCall and Kidd, 1982), or a focus on specific and restricted parts of the North Makran (e.g., Burg, 2018; Saccani et al., 2018), or again a reliance solely on petrological data without integration with multidisciplinary studies (e.g., Ghasemi et al., 2022a). A great amount of data was provided in the past few years by several authors, including the authors of this paper, who have conducted extensive multidisciplinary investigations in the western sector of the North Makran (e.g., Esmaeili et al., 2019, 2020; Ghasemi Siani et al., 2021, 2022a, 2022b; Sepidbar et al., 2020; Barbero et al., 2020a, b, 2021a, b, 2023a, b, c; Pandolfi et al., 2021; Moghadam et al., 2022; Saccani et al., 2022a, b). These studies have significantly enhanced our understanding of the western North Makran and demonstrated that extant geodynamic models are not fully satisfactory for explaining the recent geological evidence. For this reason, we present a

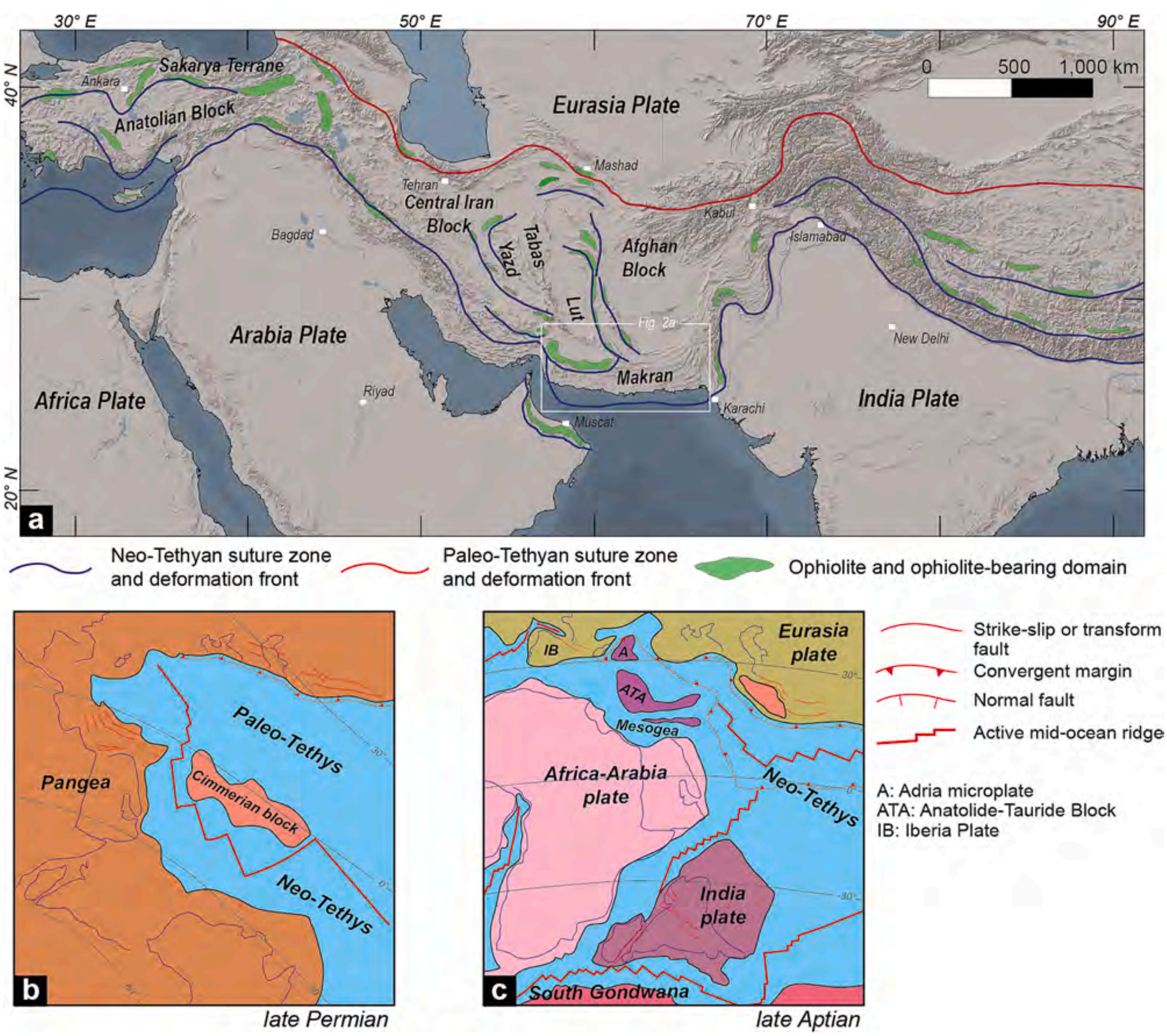

Fig. 1. a) general tectonic setting of the eastern mediterranean, middle east, and himalayan regions showing the main paleo- and neo-tethyan suture zones, as well as the main ophiolites and ophiolite-bearing domains (modified fromDilek and Furnes, 2009; Furnes et al., 2020; Marroni et al., 2020; Wan et al., 2021). The main continental plates and blocks are also shown. The box indicates the approximate position of Fig. 2a. Paleogeographic maps showing the Tethyan realms in the Late Permian (b) and the Early Cretaceous (c) (modified from Barrier et al 2018).

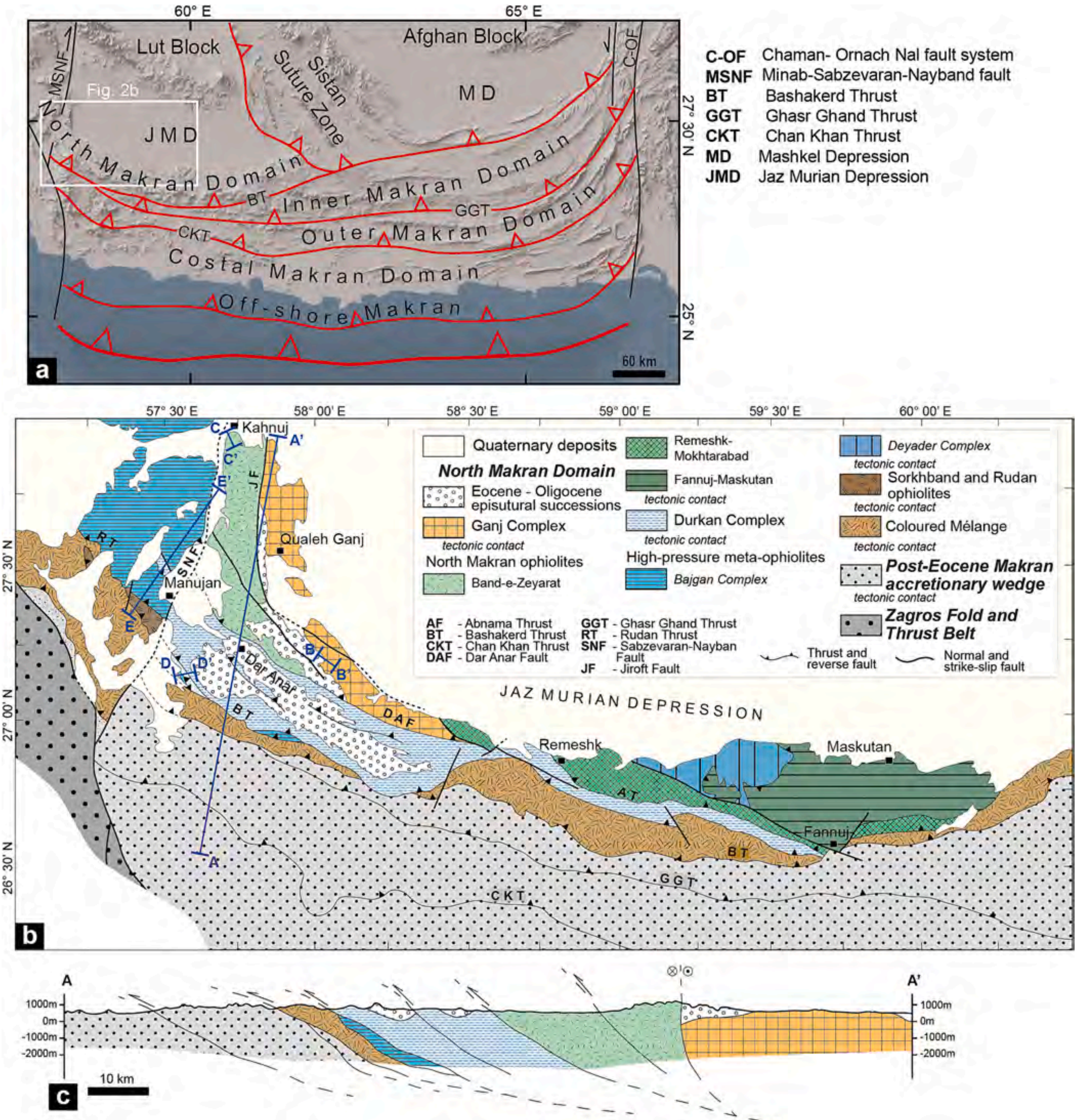

Fig. 2. a) shaded relief topography of the makran area showing the trace of the regional-scale thrusts, the main fault systems, and the main tectono-stratigraphic domains (fromDolati, 2010; Burg, 2018). The box indicates the location of Fig. 2b. b) Simplified structural map and geological cross-section (c) showing the main tectonic units within the North Makran domain. Traces of the cross sections shown in Figs. 3-6 are also shown in Panel b).

comprehensive review of the geological features of the western sector of the North Makran using a wide spectrum of published data derived from structural and stratigraphic studies, petrographic and geochemical analyses, as well as biostratigraphic and geochronological dating. We propose a new reconstruction of the geodynamic history of this area from the Permian to the Eocene, which will be discussed within the broader context of the Alpine–Himalayan orogenic belt. For the first time, this reconstruction integrates multidisciplinary data from the whole North Makran area, representing a step forward to understanding and interpreting the complex geodynamics of the whole Alpine–Himalayan system.

2. Geological and geodynamic setting of the Makran

The Makran Accretionary Prism (SE Iran-SW Pakistan, Fig. 2a) is one of the largest active accretionary prisms in the world. It is related to the Cretaceous to present convergence between the Arabian Plate and southern margin of the Lut Block (e.g., Farhoudi and Karig, 1977; McCall and Kidd, 1982; Glennie et al., 1990; Ricou, 1994; Koop et al., 2000; Barrier et al., 2018). Similar to other segments of the Alpine-Himalayan orogenic system in the Middle East, this convergent kinematics was associated with the closure of the Neo-Tethyan oceanic seaways through the formation of multiple, long-lived subduction zones (Fig. 1c; Dercourt et al., 1986; Stampfli and Borel, 2002; Agard et al., 2011; Barrier et al., 2018; Saccani et al., 2018; Burg, 2018;Stern et al., 2021; Wan et al., 2021). In the Makran, subduction processes are still active as indicated by geophysical and seismological data imaging the north-dipping subducting oceanic lithosphere of the Oman Sea (e.g., White and Klitgord, 1976; Kopp et al., 2000; Engdahl et al., 2006; Grando and McClay, 2007; Penney et al., 2017; Motaghi et al., 2020).

The Makran extends from west to east for ∼ 1000 km between the dextral Minab-Sabzevaran-Nayband and the sinistral Chamal-Ornach-Nal fault systems (Fig. 2a). Along the cross-strike direction (i.e., from south to north), this prism extends for 400–600 km, from the offshore deformation front in the Gulf of Oman to the depressions of Jaz Murian and Mashkel (Fig. 2a), corresponding to the present-day forearc basins of the active volcanic arcs. The Makran consists of an offshore and an onshore prism separated by a wide shelf composed of undeformed Miocene-Pliocene sediments (Burg, 2018). The offshore prism extends from the deformation front to the coastline and consists of an imbricate thrust-fold system associated with shale diapirism and normal faults (Kopp et al., 2000; Grando and McClay, 2007). In the onshore prism, four tectono-stratigraphic and thrust-bounded domains have been identified by Dolati (2010) and Burg et al. (2013). From north to south – that is from the uppermost to the lowermost structural position – these domains are the North, Inner, Outer, and Coastal Makran (Fig. 2a). The North Makran domain is a structurally complex stack of both metamorphic and non-metamorphic tectonic units, bounded by either high- or low-angle shear zones and records the pre-Eocene accretionary stage of the subduction complex (e.g., McCall and Kidd, 1982; McCall, 1985; Glennie et al., 1990; McCall, 1997; Saccani et al., 2018; Burg, 2018; Esmaeili et al., 2020; Pandolfi et al., 2021; Bröcker et al., 2021; Barbero et al., 2023a, b). The North Makran domain corresponds to the backstop of the post-Eocene onshore accretionary prism, which includes the Inner, Outer, and Coastal Makran (e.g., Dolati, 2010; Burg, 2018). These domains are separated by regional-scale thrusts (Fig. 2a) and consist of Eocene to Pleistocene mainly siliciclastic sedimentary successions reflecting deposition within southward-migrating and progressively younger trench and wedge-top basins (Platt et al., 1985; Dolati, 2010; Burg et al., 2008, 2013; Dolati and Burg, 2013; Mohammadi et al., 2016, 2017). These domains formed as a result of the progressive deformation and incorporation of the trench and wedge-top successions into the frontal part of the accretionary prism at different times during its Eocene – Pleistocene history. The tectonic units of the North Makran domain are well exposed in its western sector (Fig. 2b, c), whereas in the east, most of these units are covered by the deposits of the Jaz Murian basin or completely cut out along regional-scale thrusts.

3. The tectonic units of the western rim of the North Makran domain

The western North Makran domain consists of a south- to southwest-verging imbricate stack of tectonic units. Southward, this stack overlaps the Inner Makran along the Bashakerd thrust, an E-W trending, top-to-the-south shear zone considered to be Early Miocene in age (Burg et al., 2013). Northward, the stack is covered by the Quaternary deposits of the Jaz Murian depression. However, the boundary between the tectonic units of the North Makran domain and the deposits of the Jaz Murian depression is locally dissected by high-angle normal and strike-slip faults (Burg et al., 2013). The western boundary of the North Makran domain is instead represented by the Minab-Sabzevaran-Nayband dextral strike-slip fault system (Fig. 2a; Regard et al., 2010). Eastward, the North Makran domain disappears against the Nehbandan dextral strike-slip fault system along the western rim of the Sistan Suture Zone (Rashidi et al., 2022).

According to McCall (2002), Omrani et al. (2017), Saccani et al. (2018, 2022a, 2022b); Barbero et al. (2020b), Barbero et al. (2021a), Pandolfi et al. (2021) and Esmaeili et al. (2021), the imbricate stack of the North Makran domain, from top to bottom, includes the following tectonic units: 1) the Ganj Complex, as defined by Barbero et al. (2020a); 2) the North Makran Ophiolites, also known as the northern ophiolites, which include three tectonic units: the Band-e-Zeyarat ophiolite (Arvin et al., 2005; Ghasemi Siani et al., 2021; 2022a; Kananian et al., 2001; Ghazi et al., 2004; Burg, 2018; Barbero et al., 2020b, 2023b), the Remeshk-Mokhtarabad ophiolite (McCall, 2002; Hunziker et al., 2015; Burg, 2018; Monsef et al., 2019) and the Fannuj-Maskutan ophiolite (Hunziker et al., 2015; Moslempour et al., 2015; Burg, 2018; Sepidbar et al., 2020); 3) the Durkan Complex as defined by Barbero et al. (2021a, b); 4) the high pressure *meta*-ophiolites that include the Bajgan and Deyader Complexes as defined by Pandolfi et al. (2021) and Hunziker et al. (2017), respectively; 5) the Sorkhband ophiolites (also known as southern ophiolites) as defined by Delavari et al., (2016); 6) the Coloured Mélange (McCall and Kidd, 1982; Burg et al., 2013; Saccani et al., 2018).

The units from the North Makran domain, their internal tectonic structures, and their mutual tectonic relationships are sealed by the Late Paleocene – Early Eocene sedimentary deposits (McCall, 1985; Barbero et al., 2023a). However, the North Makran domain is affected by Early-Middle Miocene – Pliocene regional-scale brittle deformation (Burg, 2018; Barbero et al., 2023a), which is represented by normal and strike-slip faults as well as thrusts and associated folding, as testified by the occurrence of Late Paleocene – Early Eocene deposits within the main thrust zones (Barbero et al., 2023a). Nonetheless, this deformation did not change the architecture of the pre-Late Paleocene stack of tectonic units. Consequently, the present-day structure is regarded as representative of the pre-Late Paleocene tectonic setting (McCall, 1985; Burg, 2018).

3.1. *The Ganj Complex*

According to Barbero et al. (2020a), the Ganj Complex (Fig. 2b and 3a) represents a tectonic unit consisting of the remnants of a Turonian-Coniacian volcanic arc that was most likely formed in a relatively shallow marine environment within an extensional intra-arc setting. This complex is non-metamorphic and weakly deformed. The Ganj Complex crops out along a discontinuous 38 km-long and 15 km-wide belt located along the southwestern border of the Jaz Murian depression. Toward the west and southwest, the Ganj Complex is thrust over the North Makran ophiolites; however, these relationships are largely reworked by the N-S to NW-SE trending sub-vertical Jiroft fault. The Ganj Complex is unconformably overlain by the Eocene sedimentary deposits (Fig. 3b).

3.1.1. *Stratigraphic features*

According to Barbero et al. (2020a), the Ganj Complex can be divided into three stratigraphic units. The base is represented by a basal dyke swarm showing a transition to the volcano-sedimentary sequence that passes upward into a turbidite sequence (Fig. 3a). The thickness of the entire sequence is > 2000 m (Barbero et al., 2020a).

The dyke-swarm consists of groups of sub-parallel or crosscutting dykes (Fig. 3a), represented by a wide variety of rock-types, including andesites, dacites, rhyolites and subordinate basaltic rocks. These different rock types are evenly distributed in the study area with no observed crosscutting relationships. In the uppermost part of the dyke-swarm, the occurrence of sills marks the transition to the volcano-sedimentary sequence.

The volcano-sedimentary sequence consists of an assemblage of massive lava flows, pillow lavas, lava breccias and minor sedimentary deposits (Fig. 3a). The lower part of the volcano-sedimentary sequence is dominated by massive lava flows rarely intercalated with minor pillow lavas, lava breccias and rare turbidite beds. Towards the top, the volume of the lava flows, pillow lavas and minor turbidite beds progressively increase (Shaker Ardakani et al., 2009). Remnants of unconsolidated silty marls and marly limestones have been identified as soft clasts squeezed among the pillow lavas. The general features of the volcano-

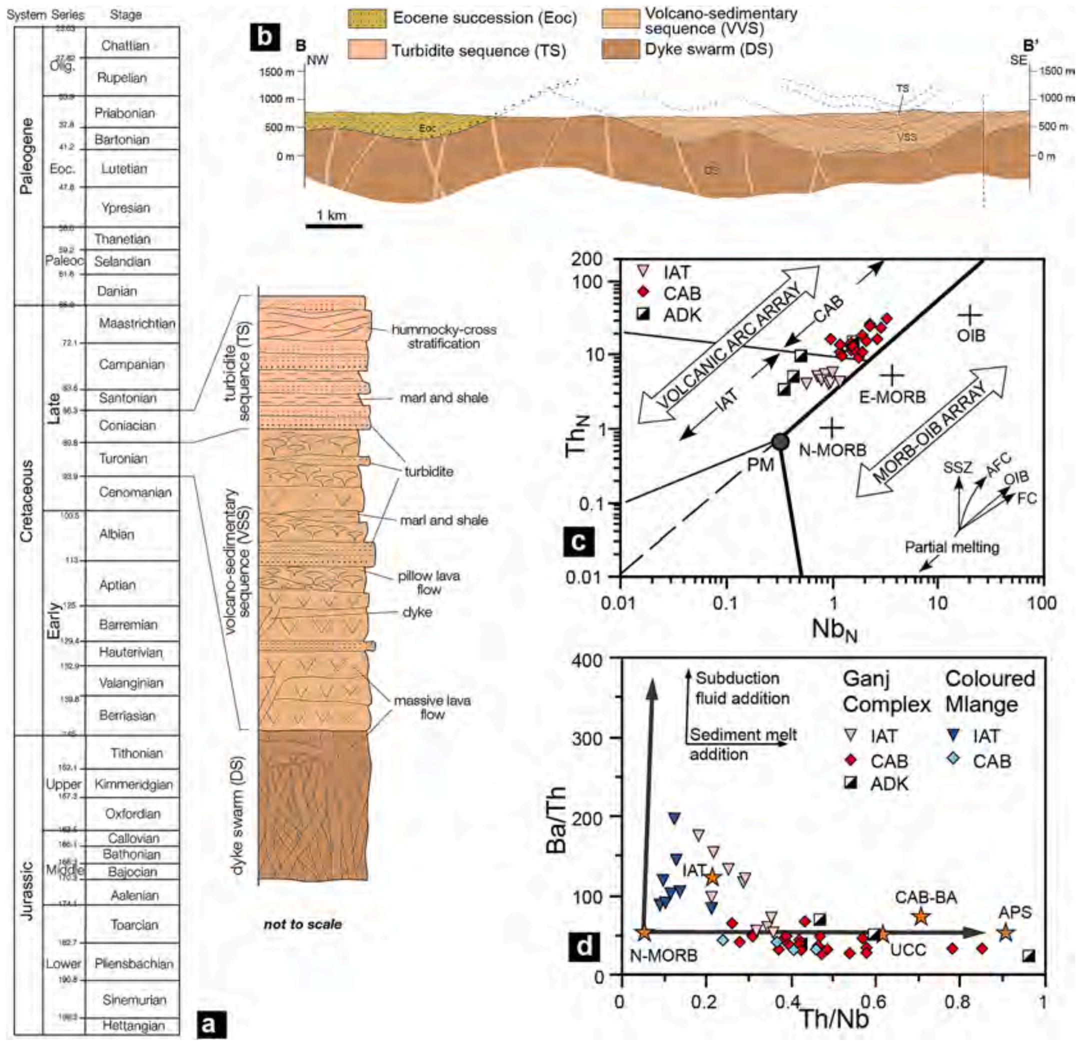

Fig. 3. Synthesis of the stratigraphic, structural, chronological, and geochemical features of the Ganj Complex. a) Schematic stratigraphic column for the Ganj Complex. The ages of these units are based on nannoplancton biostratigraphy (Barbero et al., 2020a); b) cross-section in the Mahallati area (see Fig. 2b for trace of the section) showing the structural setting; c) N-MORB-normalized Th vs. Nb discrimination diagram of Saccani (2015) for volcanic and subvolcanic rocks of the Ganj Complex (data from Barbero et al., 2020a). Abbreviations, N-MORB: normal-type mid-ocean ridge basalt; E-MORB: enriched-type mid-ocean ridge basalt; P-MORB: plume-type mid-ocean ridge basalt; OIB: alkaline oceanic within-plate basalt; alk: alkaline basalts; IAT: island arc tholeiite; CAB: calc-alkaline basalt; ADK: IAT and CAB with marked adakitic signature Vectors indicate the trends of chemical variation due to supra-subduction zone components (SSZ), assimilation-fractional crystallization (AFC), ocean island (plume type) components (OIB), and fractional crystallization (FC). Normalizing values, composition of typical N-MORB, E-MORB, and OIB (crosses), and the Primitive Mantle (PM) composition are from Sun and McDonough (1989); d) Ba/Th vs. Th/Nb diagram for volcanic and sub-volcanic rocks from the Ganj Complex. Data from the Coloured Mélange are also shown. The composition of average pelitic sediments (APS); upper continental crust (UCC); average calc-alkaline basalts and basaltic andesites (CAB-BA); average island arc tholeiitic basalts (IAT); normal-type mid-ocean ridge basalt (N-MORB) are indicated with orange stars. Data ; APS and UCC are from ; IAT, and CA-B-BA are calculated from 249, and 244 samples, respectively of basaltic rocks from various ophiolitic complexes (see for references).
Source: N-MORB are from Sun and McDonough (1989)Taylor and McLennan (1985)Saccani, 2015

sedimentary sequence and the occurrence of columnar basalts suggest that the volcanic rocks were erupted in sub-aerial or, eventually, very shallow-water (e.g., lacustrine or lagoonal) marine environments (Barbero et al., 2020a).

The turbidite sequence consists of a sequence of medium to thin-bedded turbidites composed of a medium- to coarse-grained arenites showing a transition into fine-grained laminated silty marls and marly limestones (Fig. 3a). In the coarse-grained arenites the occurrence of fragments of both carbonate and volcanic rocks, as well as remnants of shells and gastropods can be observed. Compositionally, the arenites are characterized by ubiquitous volcanic-derived minerals and rock fragments associated with variable, but generally moderate, amounts of calcareous rock fragments and bioclasts. This composition indicates sediments provenance from coeval, intrabasinal volcanic arc and carbonate platform source areas (Barbero et al., 2020a). This turbidite sequence was deposited in an outer platform environment influenced by a river-delta (Barbero et al., 2020a).

3.1.2. Geochemistry and petrogenesis of the magmatic rocks

The sub-volcanic and volcanic rocks of the Ganj Complex exhibit a wide variety of rock types, including basalts, basaltic andesites, andesites, dacites, and rhyolites. These different rock types share many geochemical features, such as a clear sub-alkaline nature with Nb/Y ratios ranging from 0.06 to 0.33, low contents of compatible elements (e.g., Cr, Ni, Co), enrichment in Th with respect to Nb (Fig. 3c), and enrichment in LREE (light rare earth elements) compared to HREE (heavy rare earth elements) (Barbero et al., 2020a). Based on immobile element geochemistry these authors recognized three different rock types with distinct geochemical affinities: calc-alkaline (CA), island arc tholeiites (IAT), and volcanic arc rocks with a marked adakitic signature (ADK). The CA rocks are characterized by significant enrichment in Th, La, and Ce coupled with Ta, Nb, P, and Ti depletion. They show LREE/MREE (MREE: medium REE), and MREE/HREE enrichments, (e.g., $La_N/Yb_N = 1.67 – 5.50$; $Sm_N/Yb_N = 1.10$—2.80, values normalized to the chondrite composition of Sun and McDonough (1989). Moreover, these rocks show a marked enrichment in Th relative to Nb (Fig. 3c). Compared to CA rocks, IATs show significant Ta and Nb depletion coupled with a little enrichment in Th contents and lack of Ti and P depletion. Their IAT nature is evidenced in the discrimination diagram in Fig. 3c. Compared to CA and IAT rocks, the rocks with ADK signature show similar contents of many incompatible elements. Nonetheless, their distinctive feature is an exceptionally high Sr content (380—982 ppm) coupled with very low HREE and Y contents. Barbero et al. (2020a) observed that some geochemical features of these basalts (particularly, the Sr-Y-Yb systematics) show similarities with adakitic rocks. However, their overall geochemistry does not fully align with the definition of "typical" adakites. Consequently, these authors concluded that the ADK group is represented by both CA and IAT rocks showing significant adakitic signature.

Petrogenetic modelling based on Cr-Y and Ba/Th − Th/Nb co-variation, as well as REE compositions (Barbero et al., 2020a) indicates that CA rocks derived from ~ 10—12 % partial melting in the spinel-facies mantle of a depleted lherzolite residual after MORB-type melt extraction, which was metasomatized by subduction components significantly enriched in Th through the addition of 0.5 – 0.7 % sediment melt (Fig. 3d). The IATs were formed by 15 – 17 % partial melting in the spinel-facies mantle of a depleted lherzolite predominantly enriched by subduction-derived aqueous fluids, thought minor contribution by sediment melt addition cannot be excluded (Fig. 3d). Petrogenetic modelling shows that the REE composition of the ADK basalts can be explained by 15 % partial melting of a depleted lherzolite with the addition of variable amounts (1—3 %) of an adakitic melt component. In summary, Barbero et al. (2020a) suggested that volcanic rocks and dykes from the Ganj Complex were formed in a volcanic arc tectonic setting on the southern margin of the Lut Block during the Late Cretaceous.

3.1.3. Structural setting and deformation history

According to Barbero et al., (2020a), the Ganj Complex is weakly deformed. No evidence of orogenic metamorphism has been found in the Ganj Complex, which, together with the Eocene deposits, was affected by a gentle folding phase followed by a faulting phase represented by high-angle strike-slip and normal faults (Fig. 3e). The folding phase consists of upright folds with N-S to NW-SE trending fold axes and a disjunctive axial planar cleavage. The faulting phase dismembered the Ganj Complex into several tectonic slices.

3.1.4. Chronological constraints

The chronological constraints include the biostratigraphic dating of marls collected at the top of the volcano-sedimentary sequence and within the turbidite sequence (Barbero et al., 2020a). Dating was performed using calcareous nannofossils assemblages. The main nannofossil species identified in the marls at the top of the volcano-sedimentary sequence suggest a Turonian age, whereas the turbidite sequence provided nannofossils assemblages indicating a Turonian-Coniacian age (Fig. 3a).

3.2. The North Makran ophiolites

The North Makran ophiolites include the Band-e-Zeyarat, Remeshk-Mokhtarabad and Fannuj-Maskutan ophiolites, each representing a fragment of the same Early to Late Cretaceous oceanic basin, known as the North Makran Ocean (Desmons and Beccaluva, 1983; Arvin et al., 2005; McCall, 2002; Kananian et al., 2001; Ghazi et al., 2004; Hunziker et al., 2015; Moslempour et al., 2015; Burg, 2018; Monsef et al., 2019; Barbero et al., 2020b; Sepidbar et al., 2020; Ghasemi Siani et al., 2021; 2022a, 2022b; Saccani et al., 2022a). These non-metamorphic ophiolites experienced two deformation phases during their incorporation within the accretionary prism and subsequent exhumation (Barbero et al., 2023b). The North Makran ophiolites extend along a narrow belt approximately 400 km-long, spanning from the Minab-Sabzevaran-Nayband and Chaman-Ornach Nal strike-slip fault systems (Fig. 2b). This belt, generally less than 15 km wide, is WNW-ESE striking in most of its extent but is N-S striking in the westernmost area. Here, the boundary between the Band-e-Zeyarat ophiolite and the Bajgan Complex is defined by the Sabzevaran-Nayband Fault. Northward, the North Makran ophiolites are tectonically juxtaposed to the Ganj Complex or covered by the Quaternary deposits of the Jaz-Murian Depression. Southward, they are thrust over the Durkan Complex in the easternmost area, whereas in the westernmost region, the boundary is marked by the Dar Anar Fault. The North Makran ophiolites are unconformably overlain by Late Paleocene − Early Eocene sedimentary deposits (Fig. 4b).

3.2.1. Stratigraphic features

The Remeshk-Mokhtarabad and Fannuj-Maskutan ophiolites display the same stratigraphic log, consisting of a complete ophiolite sequence ranging from mantle peridotites to the volcanic section and the related sedimentary cover (Hunziker et al., 2015; Moslempour et al., 2015; Burg, 2018; Monsef et al., 2019; Sepidbar et al., 2020). However, Saccani et al. (2022a) demonstrated that the peridotitic rocks in these ophiolites are represented by ultramafic cumulates forming the lower oceanic crust. This feature is also observed in the Band-e-Zeyarat ophiolite, which includes only the crustal section (Arvin et al., 2005; Ghasemi Siani et al., 2021; 2022a; Kananian et al., 2001; Ghazi et al., 2004; Burg, 2018; Barbero et al., 2020b, 2023b).

A stratigraphic log for the North Makran ophiolites has been reconstructed by integrating all available data in the different sequences of the study area (Fig. 4a). This log includes, from bottom to top: ultramafic rocks at the base, representing the lower crustal sequence; an intrusive sequence starting with a layered lower crust sequence passing upward to upper-level gabbros intruded by minor plagiogranites bodies; a sheeted dykes complex, and an extrusive sequence topped by deep-marine sedimentary rocks (Fig. 4a).

The ultramafic rocks consist of plagioclase-bearing lherzolites, clinopyroxene-bearing harzburgites, dunites, plagioclase-dunites, and podiform chromitites (Moslempour et al., 2015; Burg, 2018; Saccani et al., 2022a). The lower crustal mafic sequence is characterized by a magmatic layering ranging from centimetres to metres in thickness, with alternating levels of olivine gabbros, troctolites, pegmatitic olivine gabbros, anorthosites, and wehrlites (Barbero et al., 2020b). The gabbros show a well-developed magmatic foliation defined by the preferred orientation of the mineral assemblages, especially plagioclase and pyroxene.

The upper intrusive sequence mainly consists of isotropic rocks, including fine-grained and coarse-grained gabbros, ferrogabbros, and diorites, all intruded by small bodies and dykes of plagiogranites (Fig. 4a). In the Band-e-Zeyarat ophiolite, plagiogranites are particularly abundant at the top of the intrusive complex, near the transition between isotropic gabbros and the sheeted dyke complex. In addition, the isotropic gabbros are frequently crosscut by basaltic dykes, which are particularly abundant at the uppermost part of the intrusive sequence.

The sheeted dyke sequence consists of mutually intrusive, parallel, and sub-parallel dykes of varying colours and grain sizes. These dykes typically display doleritic textures and range in thickness from 10 cm to 3 m.

The volcanic sequence stratigraphically overlays the sheeted dyke complex (Fig. 4a) through a transitional zone of pillow and massive lava flows cut by abundant sills and dykes ranging from a few decimetres to a few metres in thickness. Pillow breccias are also interlayered at several stratigraphic levels. They consist of centimetric- to pluridecimetric-sized

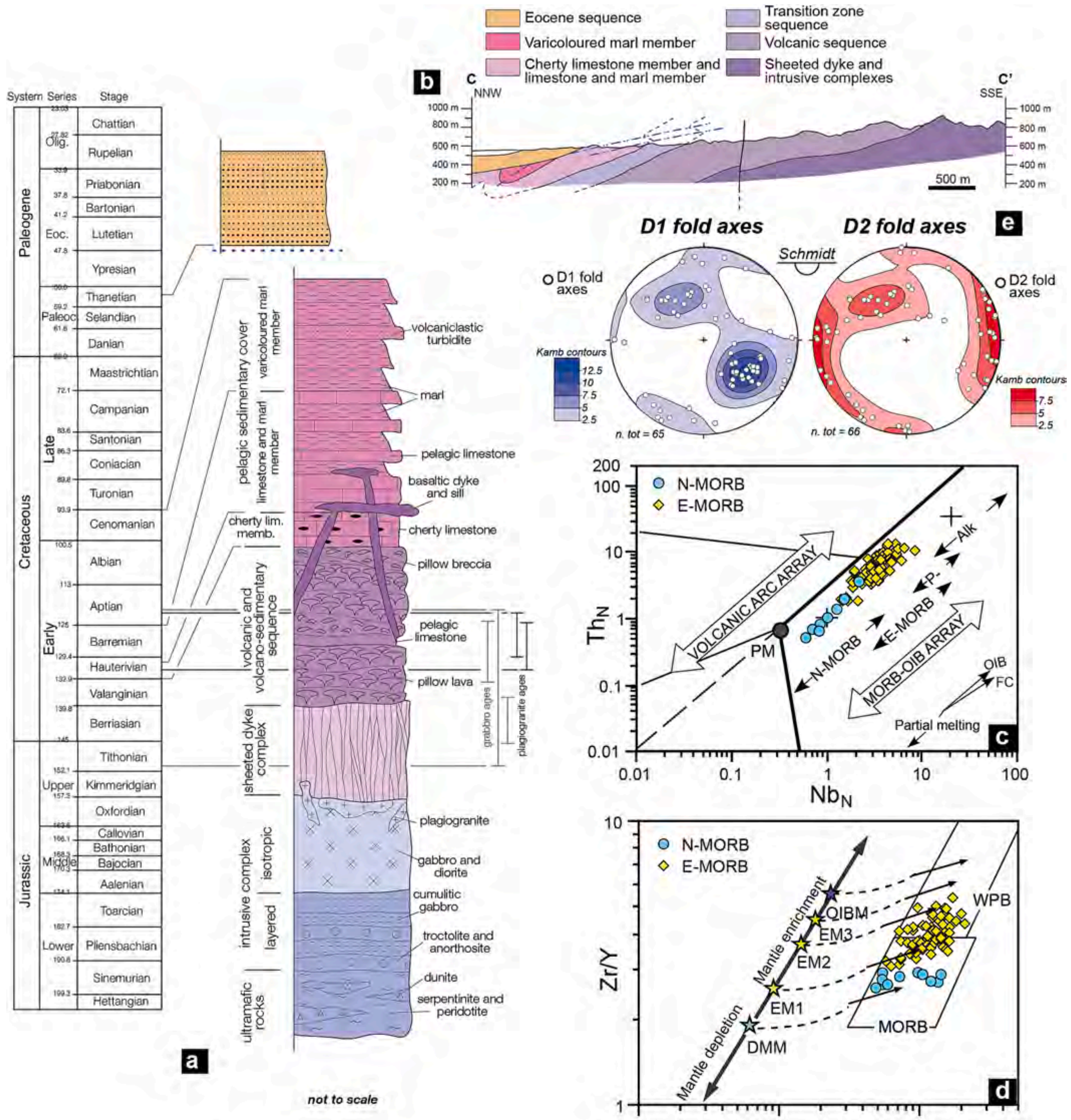

Fig. 4. Synthesis of the stratigraphic, structural, chronological, and geochemical features of the North Makran ophiolites. a) Schematic stratigraphic column showing the crustal architecture of the ophiolite sequence and the different members of the sedimentary cover. Radiometric ages for the intrusive sequence are indicated with grey and black segments (data). Biostratigraphic age based on nannoplancton biostratigraphy are also indicated (data from); b) geological cross-section of the Band-e-Zeyarat ophiolite and its sedimentary cover showing the structural setting near the Kahnuj city (see b for trace of the section); c) N-MORB-normalized Th vs. Nb discrimination diagram of for volcanic and subvolcanic rocks of the North Makran ophiolites (data from). Abbreviations and compositions as in c; d) Zr/Y vs. Zr diagram (modified from) for volcanic and subvolcanic rocks of the North Makran ophiolites (data from). Stars indicate different mantle source compositions ranging from the depleted MORB mantle (DMM;) to DMM sources progressively enriched by plume-type component (EM1, EM2, EM3) and enriched oceanic island mantle source (OIBM). Dashed lines indicate partial melting trends, whereas arrows indicate open system fractional crystallization trends (calculated based on , and . Abbreviations, MORB: mid-ocean ridge basalt; N-MORB: normal-type MORB; E-MORB: enriched-type MORB; WPB: within-plate basalt; e) Stereographic plots showing mesoscale data for the axis of D1 and D2 deformation stages.

Source: Kananian et al., 2001; Ghazi et al 2004; Hunziker, 2014; Khalatbari-Jafari et al., 2016; Sepidbar et al., 2020; Ghasemi Siani et al., 2021; Barbero et al., 2020bBarbero et al., 2023bFig. 2Saccani (2015)Barbero et al., 2020b; Saccani et al., 2022bFig. 3Pearce and Norry, 1979Barbero et al., 2020b, Saccani et al., 2022bWorkman and Hart, 2005Pearce and Norry (1979), Saccani et al. (2003)Bortolotti et al. (2018)

fragments of pillow basalts, pelagic limestones, and cherts, set in a fine-grained glassy matrix. A transition to the overlying pelagic sedimentary cover is represented by pillow and massive lava flows interlayered with thin, discontinuous layers of pelagic marls and limestones (Fig. 4a). These layers show soft-sediment deformations, suggesting that lava flows were emplaced onto weakly consolidated sediments.

The pelagic sedimentary cover has been reconstructed in detail in the Band-e-Zeyarat ophiolite by Barbero et al. (2023b). This cover can be subdivided into three members, which, from bottom to top, include: the cherty limestone member, which transitions gradually to the limestone and marl member, consisting of well-stratified sequence of marls and limestones beds (Fig. 4a). The last member is represented by the post-Barremian-Cenomanian(?) varicoloured marl member, characterized by marls with widespread intercalation of volcaniclastic arenites (Fig. 4a). Petrographic analysis of arenites indicates that the siliciclastic fragments derived from quartz-rich volcanic arc rocks. The sedimentary cover is intruded by basaltic dykes and sills.

The Fannuj-Maskutan ophiolite is unconformably overlain by Maastrichtian shallow-water limestones and, locally, by turbiditic sandstones interbedded with andesitic lava flows (Dolati, 2010). These deposits are lacking in the Band-e-Zeyarat and Remeshk-Mokhtarabad ophiolites.

3.2.2. *Geochemistry and petrogenesis of magmatic rocks*

Geochemical data on intrusive rocks from the Band-e-Zeyarat ophiolites have been presented in Barbero et al. (2020b), whereas data for the Remeshk-Mokhtarabad and Fannuj-Maskutan ophiolites were presented in Hunziker (2014) and Saccani et al. (2022a). Ultramafic and mafic cumulates display a wide range in major and trace elements compositions reflecting variation in mineral abundances. These rocks show low TiO_2, P_2O_5, and incompatible element contents, whereas MgO, Cr, Co, and Ni contents are generally high (see Barbero et al., 2020b for details). Their overall geochemical features indicate crystallization from parental liquids with a general MORB affinity. The intrusive rocks show olivine + plagioclase + clinopyroxene + magnetite crystallization order (Hunziker, 2014; Saccani et al., 2022a), which is the typical crystallization order of tholeiitic magma series formed in mid-oceanic ridge settings (Beccaluva et al., 1983). Plagiogranites, likewise, appear to be differentiated products of MORB-type melts. Isotropic gabbros and quartz-diorites show either N-MORB or E-MORB chemical affinity (Hunziker, 2014; Barbero et al., 2020b).

Sheeted dykes, individual dykes, massive lavas, and pillow lavas mainly consist of basalts, basaltic andesites, and Fe-basalts with minor andesites and dacites, and very rare rhyolite dykes (Barbero et al., 2020b; Saccani et al., 2022a). Volcanic and sub-volcanic rocks from the North Makran ophiolites share the same chemical features and petrogenetic processes. In fact, these units include sub-alkaline tholeiitic rocks showing both N-MORB and E-MORB affinities (Ghazi et al., 2004; Moslempour et al., 2015; Khalatbari-Jafari et al., 2016; Esmaeili et al., 2019; Barbero et al., 2020b, Sepidbar et al., 2020; Saccani et al., 2022a) (Fig. 4c). N-MORBs and E-MORBs can be distinguished based on incompatible elements and REE compositions. N-MORBs have very low Nb/Y ratios (0.08 – 0.11) and low Y, Zr, Nb, Th, Ta, and LREE. They show flat N-MORB-normalized incompatible elements patterns (e.g., $Th_N/Nb_N = 0.8 – 1.9$; $Th_N/Yb_N = 0.8 – 1.6$; $Nb_N/Yb_N = 0.9 – 1.4$) with LREE/HREE depletion ($La_N/Yb_N = 0.5 – 0.9$) and flat MREE-HREE patterns ($Sm_N/Yb_N = 0.9$——1.2) (Ghazi et al., 2004; Hunziker, 2014; Barbero et al., 2020b, Saccani et al., 2022a).

In contrast, E-MORBs exhibit Nb/Y ratios (0.14——0.42) and moderate enrichment of Th, Ta, and Nb relative to Tb, Y, and Yb, with $(Th/Yb)_N = 2.6 – 13$, $(Ta/Yb)_N = 2.0 – 8.1$, and $(Nb/Yb)_N = 2.0 – 5.6$. These E-MORBs show LREE enrichment with respect to MREE and HREE with $(La/Yb)_N = 1.2$——4.0, $(La/Sm)_N = 1.2 – 2.2$, and $(Sm/Yb)_N = 1.1 – 2.0$ (Ghazi et al., 2004; Hunziker, 2014; Barbero et al., 2020b, Saccani et al., 2022a). The E-MORB affinity of these rocks is evident in the Th-Nb discrimination diagram, where they plot in the field for subduction-unrelated settings, within the compositional field for rocks with E-MORB affinity (Fig. 4c).

Petrogenetic modelling based on several incompatible elements, such as REE, Th, Nb, and Zr indicate that N-MORBs derived from partial melting of a depleted MORB mantle (DMM) with negligible enrichment by ocean island basalts (OIB)-type (plume-type) components. E-MORBs, on the other hand, derived from varying degrees of partial melting of a DMM source variably enriched by OIB-type components (Barbero et al., 2020b; Saccani et al., 2022a) (Fig. 4d). Differences in the chemistry of E-MORBs within and between ophiolitic units can be attributed to variations in the extent of: mantle enrichment (Fig. 4d), partial melting degrees, melting depths, or a combination of these factors. Ghazi et al. (2004), Barbero et al. (2020b), and Saccani et al. (2022a) suggested that the North Makran ophiolites represent a chemically composite oceanic crust, which record an Early Cretaceous incipient mantle plume activity and varying degrees of plume-ridge interaction in the Neo-Tethys.

3.2.3. *Structural setting and deformation history*

The structural setting of the North Makran ophiolites has been recently studied in detail for the Band-e-Zeyarat ophiolite (e.g., Barbero et al., 2023b), whereas only regional-scale studies have been done for the Remeshk-Mokhtarabad and Fannuj-Maskutan ophiolites (McCall, 1985; Dolati, 2010; Hunziker, 2014). All these ophiolites show similar regional-scale structural positions, stratigraphic architectures, and lithological and geochemical features of the magmatic rocks. Therefore, we assume that the Remeshk-Mokhtarabad and Fannuj-Maskutan ophiolites underwent a deformation history comparable to that of the Band-e-Zeyarat ophiolite.

The Band-e-Zeyarat ophiolite consists of a N-S striking tectonic units bordered by high-angle fault zones and unconformably covered by an Eocene siliciclastic succession (Fig. 2b, 4a). This ophiolite shows a polyphase deformation history recently described by Barbero et al (2023b). Three deformation phases, referred to as D1, D2, and D3, have been recognized. Mesoscale structures associated with the D1 and D2 phases are observed within the sedimentary cover, where bedding provides excellent markers for deformation. The D1 phase is characterized by overturned sub-isoclinal to close folds, with an axial planar foliation (S1) developed only in marly and less competent beds (Fig. 4b). The S1 foliation represents a pressure solution cleavage, indicating deformation at shallow structural levels within the Makran Accretionary Prism (Barbero et al., 2023b). The orientation of the fold axes is variable, ranging from N- to NW- and ESE-trend (Fig. 4e), likely due to later deformation events. The D1 phase occurred during the incorporation of fragments of oceanic lithosphere into the Makran Accretionary Prism (Barbero et al., 2023b). The D1 folds are deformed by a second generation of open to tight folds (D2) with sub-horizontal axial planes (Fig. 4b, e), associated with a local weak axial planar cleavage (Barbero et al., 2023b). The fold axes are sub-horizontal and exhibit variable orientation, ranging from N-S to NE-SW and NW-SE trend (Fig. 4e). Similar to the D1 folds, the variation in fold axes orientation suggests later deformation events during a strike-slip faulting stage (i.e., the D3 phase). The D2 phase occurred during the progressive exhumation of the Band-e-Zeyarat ophiolites (see discussion in Barbero et al., 2023b). The D1 and D2 structures are unconformably sealed by the Eocene siliciclastic succession (Fig. 4b). Both the Band-e-Zeyarat ophiolite and the Eocene succession are deformed into a domal antiform structure that is cut by high-angle faults (D3 phase). The D3 antiform is characterized by the magmatic intrusive sequence at its core and volcanic-sedimentary sequences along its borders, where high-angle faults rework the antiform limbs (Barbero et al., 2023b). These faults show strike-slip kinematics and define fault-bounded structural blocks, with different orientations of the D1 and D2 structural elements due to rotation induced by strike-slip deformation. On a larger-scale, this rotation affected the whole North Makran ophiolites. In fact, the orientation of regional folds, thrusts, and dykes within the sheeted dyke complex changes from E-W to NW-SE and NNW-SSE from the eastern to the western North Makran. This trend variation is also observed in other tectonic units of the North Makran (e.g., Durkan Complex, Coloured Mélange, see Fig. 2a, b). This evidence likely indicates a clockwise rotation of the western margin of the North Makran domain relative to the eastern North Makran during the post-accretion tectonic evolution. The D3 structures accommodate this rotation, which has been associated with right-lateral faulting along the Minab-Sabzevaran-Nayband fault system (e.g., McCall, 1985; Stoneley, 2005; Barbero et al., 2023b).

3.2.4. Chronological constraints

Chronological constraints for the magmatic rocks are primarily available for the Band-e-Zeyarat ophiolite, based on K/Ar amphibole, Ar/Ar amphibole and U/Pb zircon methods. Early studies by McCall (1985) and Hassanipak et al. (1996) used K/Ar dating on amphibole in gabbros obtaining ages between 126 ± 2.5 and 131 ± 2.5 Ma and 124 ± 4 to146 ± 5 Ma, respectively (Fig. 4a). Later, Ghazi et al. (2004) used Ar/Ar dating on amphiboles from gabbros to yield ages of 140.7 ± 2.2, 142.9 ± 3.5 and 141.7 ± 1.0 Ma (Fig. 4a). More recent LA-ICP-MS zircon U/Pb dating by Barbero et al. (2020b) and Ghasemi Siani et al.

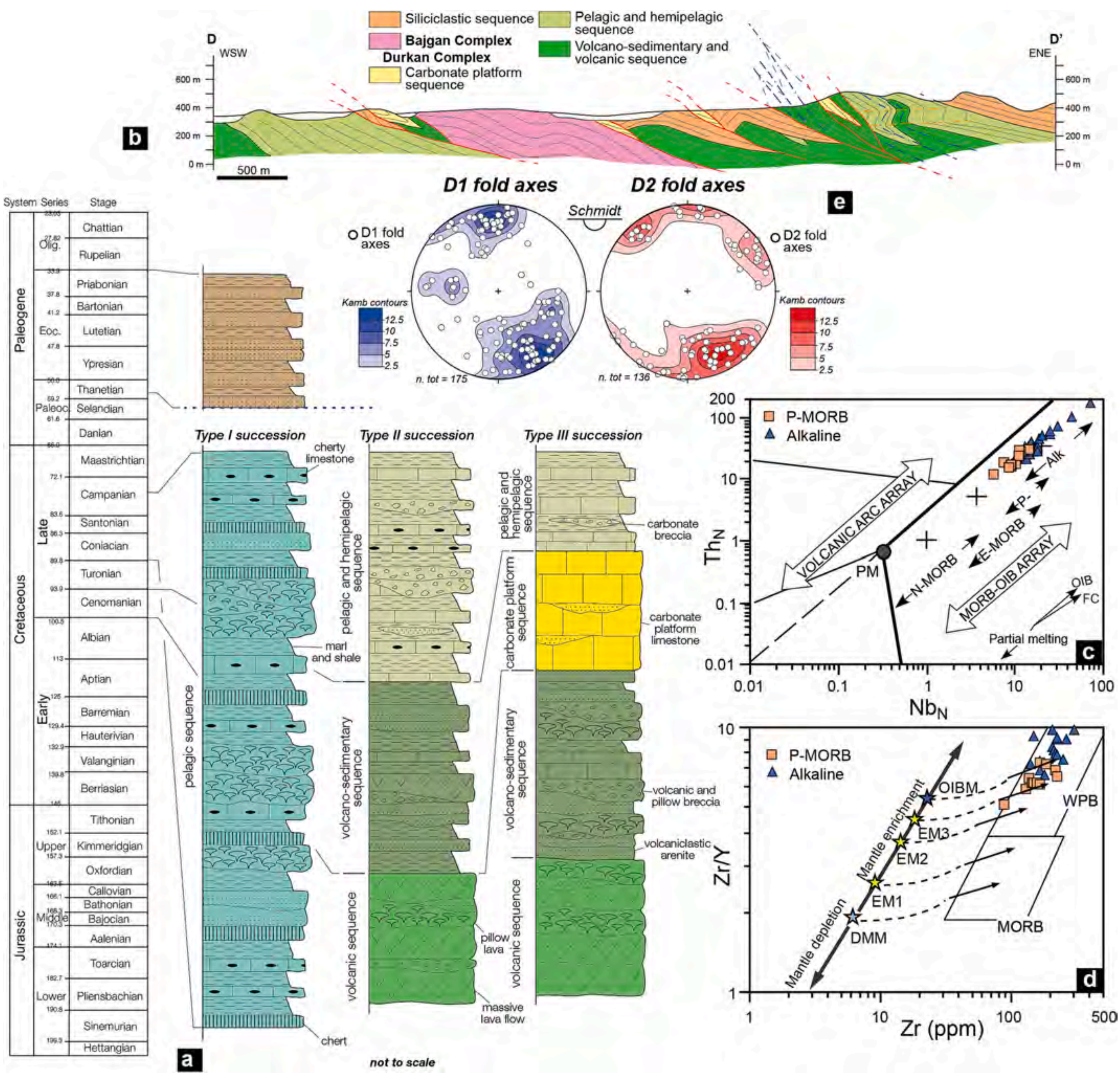

Fig. 5. Synthesis of the stratigraphic, structural, chronological, and geochemical features of the Durkan Complex. a) Schematic stratigraphic columns reconstructed for the Durkan Complex in the western North Makran; chronological constraints for the distinguished stratigraphic units are based on nannoplancton biostratigraphy (data from Barbero et al., 2021a); b) geological cross-section showing the structural setting of the Durkan Complex in the western North Makran (see Fig. 2b for trace of the section); c) N-MORB-normalized Th vs. Nb discrimination diagram of Saccani (2015) for *meta*-volcanic and volcanic rocks from the Durkan Complex (data from Barbero et al., 2021a, b). Abbreviations and compositions as in Fig. 3c; d) Zr/Y vs. Zr diagram (modified from Pearce and Norry, 1979) for *meta*-volcanic and volcanic rocks from the Durkan Complex (data from Barbero et al., 2021a, b). Abbreviations, compositions, and trends as in Fig. 4d, P-MORB: plume-type mid-ocean ridge basalt; e) Stereographic plots showing mesoscale data for the axis of the D1 and D2 deformation phases.

(2021) provided ages of 122–129 Ma and 126.0 ± 1.3, 126.4 ± 1.7 Ma, 128.5 ± 1.3, to 130.8 ± 1.8 Ma for plagiogranite and plagiogranic dykes, respectively (Fig. 4a). These data collectively indicate a lowermost Early Cretaceous age for the Band-e-Zeyarat ophiolite sequence, spanning from Berriasian to Barremian (Fig. 4a). While no radiometric dating is available for the Fannuj-Maskutan and Remeshk-Mokhtarabad ophiolites, geological evidence and biostratigraphic dating of the overlying sedimentary cover (Dolati, 2010) support the hypothesis that the ages of the Band-e-Zeyarat ophiolite can be extended to all the North Makran ophiolites.

Nannofossil-based biostratigraphic dating of the sedimentary cover of the Band-e-Zeyarat ophiolite, performed by Barbero et al. (2023b), indicates a lower Hauterivian and upper Hauterivian – Barremian age for the cherty limestone and limestone and marl members, respectively (Fig. 4a). In addition, McCall (1985) reported Cenomanian foraminifera at the top of the varicoloured marl lithofacies (Fig. 4a), suggesting that the younger part of the sedimentary cover of the Band-e-Zeyarat ophiolite extends into the Late Cretaceous. In both the Remeshk-Mokhtarabad and Fannuj-Maskutan ophiolites, the overlying sedimentary rocks consists of pelagic limestones and hemipelagic red marls containing nannofossils no younger than Barremian (Dolati, 2010).

3.3. The Durkan Complex

The Durkan Complex extends along an ESE-WNW trending belt with a length of about 300 km and a maximum width of 30 km (Fig. 2b). Southward, the boundary between the Coloured Mélange and Durkan Complex is represented by the Bashakerd thrust (Fig. 2b, c), whereas to the north the boundary with the North Makran ophiolites is marked by the Abnama thrust. In the westernmost areas, this boundary is reworked by the Dar Anar fault. Eastward, the Durkan Complex progressively disappears along the Bashakerd thrust, whereas to the west, it is crosscut by the NNE-striking dextral Sabzevaran Fault. In the westernmost area, the Durkan Complex is unconformably covered by the Late Paleocene – Early Eocene sedimentary deposits (Fig. 5a).

The Durkan Complex has long been regarded as part of a single tectonic unit together with the Bajgan Complex; this assemblage was known as Bajgan-Durkan Complexes (McCall and Kidd, 1982; McCall, 2002; Hunziker et al., 2015; Burg, 2018). These authors interpreted the Bajgan-Durkan Complexes as a continental ribbon detached from the Lut Block. Recently, the Durkan Complex has been re-interpreted as an independent tectonic unit consisting of a stack of tectonic slices, mostly representing the remnants of a Late Cretaceous oceanic seamounts chain that was tectonically disrupted during its involvement in a subduction zone (Barbero et al., 2021a; b; 2023a). The structural evolution of the Durkan Complex indicates underplating under blueschist facies metamorphic conditions, followed by exhumation to shallower structural levels within an accretionary prism (Barbero et al., 2023a).

3.3.1. Stratigraphic features

The Durkan Complex consists of a stack of tectonic slices, each characterized by a coherent stratigraphic succession showing distinct deformation and metamorphic imprints (Barbero et al., 2021a; 2023a). In the western area of the Durkan Complex, Barbero et al. (2021a) identified three different types of successions referred to as Type-I, –II and –III, each including both magmatic and sedimentary rocks derived from different seamount environments (Fig. 5a, b). The type-I succession is characterized by a pelagic sequence consisting of thin-bedded red cherts and cherty limestones alternating with shales and shaly marls along with minor volcaniclastic arenites and pillow breccias (Fig. 5a). Pillow basalts are frequently interbedded within this sequence. The low vesicularity of the basalts suggests their eruption in a relatively deep-water setting (Barbero et al., 2021a). This type of succession represents the remnants of a seamount during its deep-water stages of formation, characterized by sedimentation and volcanic activity in a pelagic depositional environment (Barbero et al., 2021a).

The Type-II succession begins with a basal volcanic sequence showing a transition to a volcano-sedimentary sequence that, in turn, gradually passes upward to a pelagic and hemipelagic sedimentary sequence (Fig. 5a, b). The volcanic sequence is made up of alternating massive lava flows, pillow lavas, and volcaniclastic arenites and breccias. The volcano-sedimentary sequence consists of alternating volcaniclastic arenites and breccias, shales and siltstones. Within this sequence, limestone layers, as well as minor massive lava flows have been identified. The occurrence of pelagic foraminifera in the limestones suggests that this succession originated in a relatively deep-water environment. The pelagic and hemipelagic sedimentary sequence consists of cherty limestones, shales, shaly marls, cherts, and minor carbonate breccias and volcaniclastic arenites (Fig. 5a). The stratigraphic features of the Type-II succession indicate a depositional setting along and at the base of a seamount flank during the relatively shallow-water shield stage of seamount growth (Barbero et al., 2021a).

The Type-III succession is characterized by a volcanic sequence passing upward to a volcano-sedimentary sequence (Fig. 5a). This sequence is capped by a carbonate platform sequence that, in turn, passes upward to a pelagic and hemipelagic sequence at the top (Fig. 5a). The volcanic sequence is characterized by pillow and massive lava flows alternating with volcaniclastic arenites. The volcano-sedimentary sequence is composed of alternating volcanic rocks, volcaniclastic arenites and breccias, shales, as well as turbidites with a mixed carbonate-volcanic composition (Fig. 5a). In addition, minor platform-derived massive limestones are interbedded within the sequences (Fig. 5a), suggesting a shallow-water depositional setting, further supported by the significantly high vesicularity of the pillow lavas. The shallow-water carbonate platform sequence consists of massive limestones alternating with subordinate volcaniclastic arenites with no evidence of lava flows. The uppermost hemipelagic and pelagic sequence marks the drowning of the carbonate platform. The stratigraphy of Type-III succession records shallow-water volcanic activity associated with carbonate platform sedimentation and is comparable with the stratigraphic successions formed in a seamount summit setting during the shallow-water shield growth stage (Barbero et al., 2021a).

In the eastern area of the Durkan Complex, Hunziker (2014) and Hunziker et al. (2015) identified a pre-Cretaceous rock assemblage along the thrust with the Fannuj-Maskutan ophiolite, including tectonic slices of trondhjemites, diorites, plagiogranites, and granites associated with basalts and recrystallized limestones. The granites are intruded into well-bedded recrystallized limestone, which is cut by basaltic dykes, and covered by basaltic pillow-lavas. McCall (1985) interpreted the limestones as Jurassic shelf deposits. Hunziker et al. (2015) also reported the occurrence of Valanginian sediments interlayered with the pillow-lavas.

3.3.2. Geochemistry and petrogenesis of magmatic rocks

The magmatic rocks of the Durkan Complex are mainly represented by basalts and ferrobasalts and minor trachytes and rhyolites showing different degrees of deformation and metamorphic overprinting. Basaltic and *meta*-basaltic rocks display geochemistry ranging from transitional P-MORB to alkaline OIBs (Fig. 5c; Barbero et al., 2021b). Both P-MORB and alkaline series show variable contents of major elements and compatible trace elements, suggesting formation from melts at different fractionation stages (Barbero et al., 2021b). P-MORBs and OIBs can be distinguished based on incompatible elements and REE compositions. P-MORBs are mainly found in the Type-I succession, less abundant in the Type-II succession and absent in Type-III. They are characterized by transitional Nb/Y ratios (0.7 – 1.0) and relatively high TiO_2, P_2O_5, Nb, Th, and Ta contents with relatively low Y contents. Incompatible element contents, normalized to N-MORB (Sun and McDonough, 1989), display significant enrichment of Th, Ta, and Nb relative to Yb, as exemplified by high $(Th/Yb)_N$ (26.1 – 47.3), $(Ta/Yb)_N$ (14.7 – 20.6), and $(Nb/Yb)_N$ (12.2 – 18.2) ratios. These rocks show mild LREE enrichment with respect to HREE, as well as moderate depletion of HREE compared to MREE, as summarized by the $(La/Yb)_N$ (4.44 – 7.86) and $(Sm/Yb)_N$ (1.18 – 3.16) ratios. The Durkan P-MORBs have geochemical features highly similar to those of many P-MORBs erupted in modern mid-ocean ridge settings influenced by plume-type activity (e.g., Haase and Devey, 1996; Le Roex et al., 1983; Sun and McDonough, 1989). In fact, these rocks plot in the field for very enriched MORB compositions (P-MORB) erupted in subduction-unrelated oceanic settings (Fig. 5c).

Alkaline basalts and ferrobasalts are mainly found in the Type-II and Type-III successions but are absent in the Type-I. They show a clear alkaline affinity, indicated by high Nb/Y ratios ranging from 1 to 4. These rocks have high contents of TiO_2, P_2O_5, Th, Nb, and Ta, while Y absolute abundance (18.5—–33.0 ppm) is relatively low. Incompatible element contents normalized to the N-MORB (Sun and McDonough, 1989) display marked enrichment in Th, Ta, and Nb relative to Yb, with very high $(Th/Yb)_N$ (37.9 – 161), $(Ta/Yb)_N$ (28.3 – 87.4), and $(Nb/Yb)_N$ (22.0 – 65.3) ratios coupled with a slight enrichment in Th relative to Ta and Nb (e.g., $Th_N/Nb_N = 1.6 – 2.7$). Chondrite-normalized REE patterns show marked LREE/HREE (e.g., $La_N/Yb_N = 9.26 – 28.07$) and MREE/HREE (e.g., $Sm_N/Yb_N = 3.5 – 8.4$) enrichments, which are higher than those of P-MORBs. The overall geochemical features of these basaltic rocks are very similar to those of the within-plate alkaline volcanic rocks typically forming oceanic islands (e.g., Safonova et al., 2016, and references therein). The alkaline basalts plot within the field for subduction unrelated alkaline basalts and cluster around the composition of OIB (Fig. 5c; Saccani, 2015).

Petrogenetic modelling based on several incompatible elements, such as REE, Th, Nb, Zr, Y, and TiO_2 carried out by Barbero et al. (2021b) indicates that the Durkan basaltic and *meta*-basaltic rocks were generated from partial melting of a depleted sub-oceanic mantle source that was metasomatized by OIB-type (plume-type) chemical components in a within-plate oceanic setting. These authors suggested that the chemical differences between P-MORBs and OIBs can be explained by variations in: 1) amount of OIB-type enrichment; 2) partial melting degree; 3) the depths of melting (i.e., spinel- or garnet-facies mantle). Fig. 5d shows that, compared to the North Makran ophiolites (Fig. 4d), both P-MORBs and alkaline basalts derived from partial melting of enriched to very enriched mantle sources. Petrogenetic evidence suggests that the oceanic lithosphere onto which the Durkan seamounts was forming was characterized by an important mantle plume activity during the Late Cretaceous (Barbero et al., 2021b).

3.3.3. *Structural setting and deformation history*

To the east of Remeshk, the Durkan Complex constitutes a rather thin tectonic elements bounded by mainly E-W striking thrust, which separates it from the North Makran ophiolites and the Coloured Mélange to the north and to the south, respectively (Fig. 2b; Hunziker 2014; Hunziker et al., 2015). Close to the contact with the North Makran ophiolites, this complex is characterized by top-to-SSW shear zones associated with the main thrust surfaces (Hunziker, 2014). Associated with thrusts, meso- and macro-scale folds have been observed, showing NW- to W-trending axes and southward vergence (Hunziker, 2014). As observed in the eastern sector of the North Makran ophiolites, a Campanian-Maastrichtian – Paleocene shallow-water marine succession unconformably seals the deformation of the Durkan Complex (Burg, 2018). In addition, later NW-SE and NE-SW conjugates fault systems crosscut the thrust and fold structures (Hunziker, 2014).

To the west of Remeshk (Fig. 2b), the Durkan Complex shows different stratigraphic features (see section 3.3.1) and a distinct structural setting. It consists of a series of tectonic slices unconformably sealed by a Late Paleocene – Eocene succession, which are bordered by NW- to NNW-striking and NE- to E- dipping thrusts, showing top-to W-SW sense of shearing (Fig. 5b; Barbero et al., 2023a). The stratigraphic succession within each tectonic slice is affected by polyphase deformation. The D1 phase include sub-isoclinal to tight similar folds, characterized by thinned and stretched limbs with a NW- to NNW-trending axes and W-vergence (Fig. 5e). The overturned limbs of the macro-scale anticline are usually characterized by pluridecametric-thick reverse shear zones, which include blocks of marbles and *meta*-basalts within a matrix of *meta*-volcaniclastic materials. These shear zones mainly represent the border of each tectonic slices (Barbero et al., 2023a). The D1 folds are associated with an axial planar foliation (S1), which exhibit varying dynamic recrystallization depending on the rock type. This ranges from chlorite, amphibole, epidote, and albite in the *meta*-basalts, chlorite, white mica, calcite, quartz, and albite in the *meta*-volcaniclastic rocks and varying proportions of calcite, white mica, chlorite, and quartz in *meta*-sedimentary rocks. Thermobarometric modelling indicates P-T conditions of 0.6–1.2 (±0.2) GPa and 160–310 (±20) °C during the formation of the S1 axial planar foliation, consistent with blueschist facies conditions (Barbero et al., 2023a). The D2 deformation phase is characterized by open to close asymmetric and parallel folds, which deform the D1 structural elements (Fig. 5e) producing Type 3 interference pattern (Ramsay, 1967). D2 folds mainly show NW-SE trending axes and NE- to N-vergence (Fig. 5e). The axial planar foliation (S2) corresponds to a disjunctive cleavage in the more competent beds, such as marble and *meta*-arenites, and a crenulation cleavage in shales, both of which are not associated with metamorphic recrystallization. These features of the S2 foliation (i.e., disjunctive and crenulation cleavage without metamorphic recrystallization) indicate that the D2 occurred at shallower structural levels compared to the D1 blueschist phase. The D1 and D2 structures are sealed by a Late Paleocene – Eocene succession (Fig. 5b). However, *meso*-scale structures and the involvement of the Late Paleocene – Eocene succession along the thrusts indicate a brittle reactivation of the D1 shear zones during the post-Eocene, corresponding to the D3 deformation phase (Fig. 5b; Barbero et al., 2023a).

3.3.4. *Chronological constraints*

The chronological constraints are based on biostratigraphic dating obtained through an integrated approach using radiolarians, foraminifera and calcareous nannofossils assemblages (Barbero et al., 2021a). The pelagic sequence of the Type-I is Coniacian-Campanian in age, whereas the limestones from the volcano-sedimentary sequence of the Type-II succession are Cenomanian (Fig. 5a). Similarly, the limestones from the Type-III succession sampled in the shallow-water carbonate platform sequence have yielded Cenomanian assemblages (Fig. 5a).

Hunziker et al. (2015) provided U/Pb zircon ages for the magmatic rocks cropping out along the tectonic boundary with the Fannuj-Maskutan ophiolite. The magmatic zircon from the granites yielded concordant ages of 176.0 ± 1.0 Ma and 170.0 ± 1.0 Ma. In the diorites, the dominant zircon population yielded concordant or intercept ages between 160.3 ± 0.8 Ma and 165.6 ± 1.7 Ma. In addition, the same authors have obtained U/Pb zircon ages spanning from 158.7 ± 1.3 Ma to 160.5 ± 1.4 Ma for trondhjemites and from 164.4 ± 1.9 Ma to 137.6 ± 2.5 Ma for plagiogranites.

3.4. *The high pressure meta-ophiolites*

The high pressure *meta*-ophiolites include the Bajgan and Deyader Complexes, which are characterized by the high pressure – low temperature (HP-LT) metamorphic imprint. These complexes crop out in two different areas, approximately 250 km apart from each other (Fig. 2b). The metamorphic imprint indicates that the high pressure *meta*-ophiolites represent fragments of oceanic lithosphere deformed and metamorphosed in a subduction setting. The deformation history of these *meta*-ophiolites includes the deep underplating at the base of an accretionary prism and the exhumation up to shallow structural levels (Pandolfi et al., 2021).

The Bajgan Complex is exposed over an area of about 2400 km^2, bounded by the Sabzevaran fault to the east and the Rudan thrust to the south (Fig. 2b). This complex was previously interpreted as an assemblage of metamorphic rocks derived from sedimentary and magmatic protoliths of Paleozoic (or older) age (McCall and Kidd, 1982; Dorani et al., 2017), representing the metamorphic basement of a continental microplate (e.g., McCall, 1985; Hunziker et al., 2015; Burg, 2018). Recently, Pandolfi et al. (2021), Barbero et al. (2023c), and Saccani et al. (2024) have shown unambiguously that the Bajan Complex consists of Late Jurassic to Early Cretaceous *meta*-ophiolites and related *meta*-sedimentary rocks, both affected by HP-LT metamorphism during the Late Cretaceous.

The Deyader Complex is exposed in a tectonic window of about 400 km^2 (Fig. 2b). This complex is overthrust by the Remeshk-Mokhtarabad ophiolite along a sub-horizontal thrust, whereas the boundary with the Fannuj-Maskutan ophiolite is marked by a WNW-ESE trending fault. To the north, the Deyader Complex is covered by the Quaternary deposits of the Jaz Murian depression.

3.4.1. *Stratigraphic features*

The Bajgan Complex has recently been studied in detail by Pandolfi et al. (2021), Barbero et al. (2023c), and Saccani et al. (2024). According to these authors, this complex includes several tectonic slices representative of crustal sections of oceanic lithosphere consisting of *meta*-ophiolites and *meta*-sedimentary. The *meta*-ophiolites include, from bottom to top, serpentinites, representing remnants of the lower crust ultramafic cumulates section, topped by *meta*-intrusive rocks derived from the metamorphism and deformation of a primary sequence of anorthosite, melagabbro, and gabbro, with minor plagiogranites (Fig. 6a, b). The *meta*-volcanic rocks are derived from the metamorphism of massive and pillow lava basalts (Barbero et al., 2023c). The transition between the *meta*-volcanic and *meta*-sedimentary rocks is represented by a thick level of *meta*-volcaniclastic rocks (Fig. 6a, b). The *meta*-sedimentary rocks include quartzites, marbles, micaschists, calcschists and paragneisses derived from a pristine deep-sea, pelagic succession including cherts, limestone and turbidites (Fig. 6a).

The Deyader Complex consists of three slices deformed under different P-T conditions ranging from greenschist to blueschist metamorphic conditions. These slices largely consist of foliated and massive *meta*-basic rocks (Saccani et al., 2022b) associated with micaschists, calcschists, and marbles whose protoliths were represented by shales, sandstones, and limestones (Hunziker et al., 2017). The *meta*-basic rocks occur in a large outcrop, up to ~ 30 km^2 in size, and include coarse-

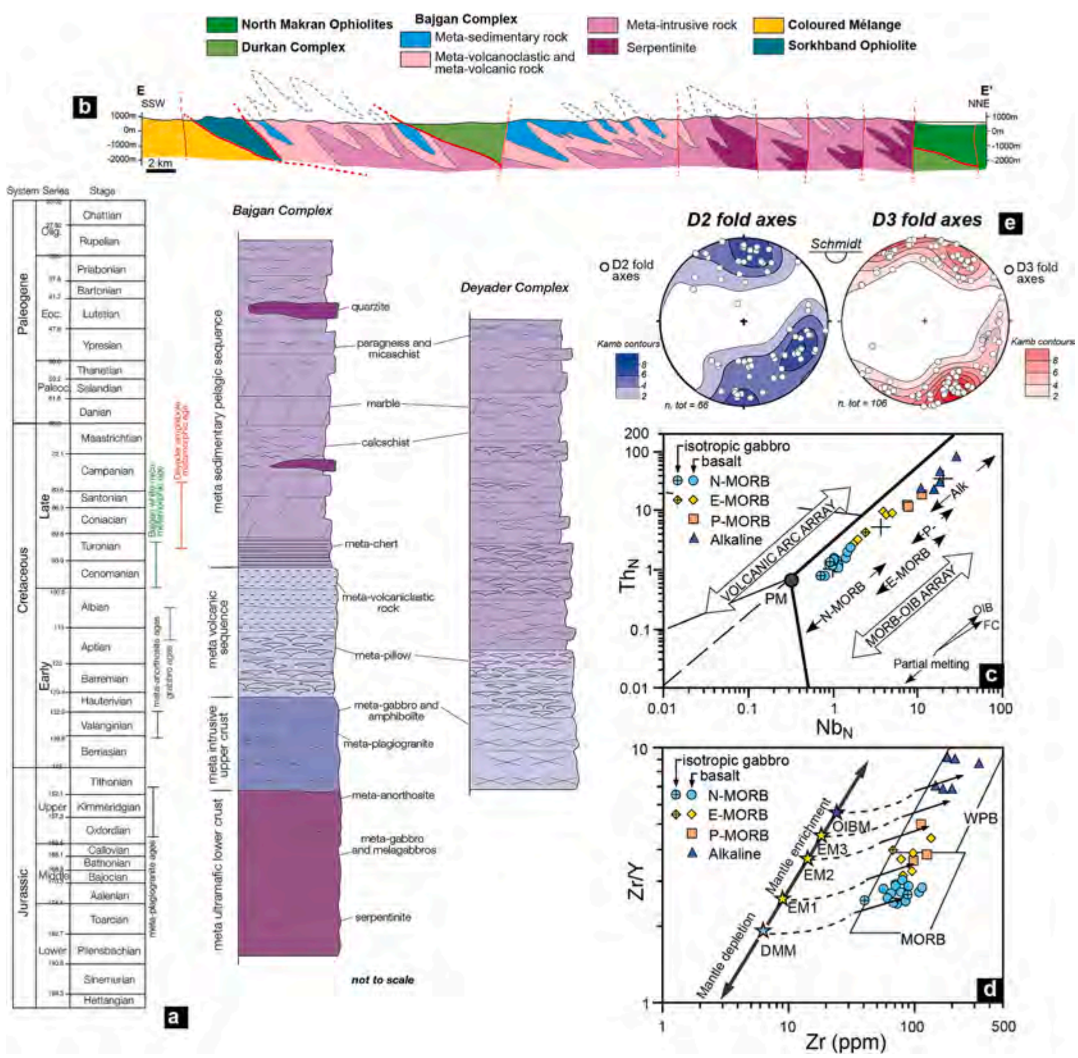

Fig. 6. Synthesis of the stratigraphic, structural, chronological, and geochemical features of the high pressure *meta*-ophiolites. a) schematic stratigraphic columns for the Bajgan and Deyader Complexes showing the reconstructed lithostratigraphy. Radiometric magmatic and metamorphic ages for different metamorphic rocks of the Bajgan Complex are shown as coloured segments; b) geological cross-section showing the structural setting of the Bajgan Complex and its tectonic relationship between the Sorkhband ophiolite and the Durkan Complex in the Manujan area (see Fig. 2b for trace of the section); c) N-MORB-normalized Th vs. Nb discrimination diagram of Saccani (2015) for *meta*-volcanic and *meta*-intrusive rocks from the high pressure *meta*-ophiolites (data from Barbero et al., 2023c). Abbreviations, compositions, and trends as in Fig. 3c; d) Zr/Y vs. Zr diagram (modified from Pearce and Norry, 1979) for *meta*-volcanic and *meta*-intrusive rocks from high pressure *meta*-ophiolites (data from Barbero et al., 2023c). Abbreviations, compositions, and trends as in Fig. 4d, 5d; e) Stereographic plots showing mesoscale data of the axis of the D2 and D3 deformation phases.

grained, layered blueschists, fine-grained blueschists, and foliated sequences of blueschists alternating with calcschists and marbles. The protoliths of these rocks were represented by gabbros, basalts, and volcaniclastic sequences (Fig. 6a, b; Hunziker et al., 2017; Saccani et al., 2022b).

3.4.2. Geochemistry and petrogenesis of magmatic protoliths

Based on $TiO_2 - Al_2O_3 - MgO - CaO$ co-variations, Barbero et al. (2023c) suggested that the magmatic protoliths of the Bajgan serpentinites were represented by ultramafic cumulitic rocks, which can be basically subdivided in two groups: 1) plagioclase lherzolites and harzburgites; 2) plagioclase-wehrlites and plagioclase-websterites. Incompatible trace element contents are very low in all rock types, whereas compatible elements, such as Cr (651–3488 ppm) and Ni (1070–2537 ppm), show high abundance. Chondrite-normalized REE patterns show negative Eu anomalies indicating early crystallization and removal of plagioclase (Barbero et al., 2023c). In summary, the geochemistry of the serpentinites are compatible with compositions of ultramafic cumulitic rocks largely dominated by olivine with subordinate pyroxene and plagioclase (Pandolfi et al., 2021). The magmatic affinity of ultramafic cumulitic rocks cannot reliably defined because the composition of these rocks is largely dependent on cumulus processes rather than melt composition. Therefore, from the chemical data it can only be postulated that these rocks were characterized by early crystallization of plagioclase, which is a feature typically observed in MORB-type magmatic series (Beccaluva et al., 1983).

The protoliths of the *meta*-intrusive rocks are represented by anorthosites, cumulitic gabbros, isotropic gabbros, and plagiogranites. Anorthosites show high Al_2O_3 and CaO, as well as low TiO_2, FeO_t, and MgO contents coupled with marked Eu positive anomaly (Pandolfi et al., 2021; Barbero et al., 2023c; Saccani et al., 2024). The *meta*-gabbros with cumulitic texture are characterized by low TiO_2, FeO_t, and P_2O_5 contents along with high MgO contents and very low incompatible trace element contents (Pandolfi et al., 2021). Barbero et al. (2023c) and Saccani et al. (2024) suggested that chemical compositions of these rocks resemble those of MORB-type gabbros. The *meta*-gabbros with isotropic texture show quite different chemical features compared to the *meta*-gabbros with cumulitic texture. They are characterized by comparatively higher TiO_2, FeO_t, and P_2O_5 contents. These rocks display a clear sub-alkaline affinity, with Nb/Y ratios ranging from 0.07 to 0.36 (Barbero et al., 2023c). Based on incompatible element and REE contents, Barbero et al. (2023c) suggested that isotropic gabbro protoliths of the Bajgan *meta*-ophiolites include both N-MORB and E-MORB type gabbros (Fig. 6c). Plagiogranites are characterized by low Nb/Y ratios (0.19 – 0.30), which suggest a sub-alkaline affinity (Pandolfi et al., 2021). Based on Th − Nb co-variation during fractional crystallization of MORB primary melts, Barbero et al. (2023c) suggested that plagiogranites from the Bajgan Complex originated by different degrees of fractional crystallization starting from an N-MORB type primary melt.

The *meta*-volcanic rocks of the Bajgan and Deyader Complexes derived from four distinct chemical groups of basaltic protoliths including N-MORB, E-MORB, P-MORB, and alkaline basalts (Fig. 6c; Pandolfi et al., 2021; Saccani et al., 2022b, 2024; Barbero et al., 2023c). N-MORBs show relatively high TiO_2 contents coupled with relatively low P_2O_5 and Nb values. They exhibit a sub-alkaline affinity with very low Nb/Yb ratios (0.06 – 0.13). N-MORB-normalized (Sun and McDonough, 1989) incompatible elements compositions display no relative enrichment of Th, Ta, and Nb relative to Yb, as exemplified by low $(Th/Yb)_N$, $(Ta/Yb)_N$, and $(Nb/Yb)_N$ ratios, which are all included between 0.8 and 2.0. These rocks show Th − Nb co-variation similar to that observed in typical N-MORB (Fig. 6c). Chondrite-normalized REE contents are characterized by depletion of LREE with respect to MREE and HREE with $(La/Yb)_N = 0.51 - 0.81$. E-MORB protoliths also display a sub-alkaline affinity with, however, Nb/Y ratios (Nb/Y = 0.35 to 0.45) higher than those of N-MORBs. Compared to N-MORBs, they show higher contents of P_2O_5, Nb, Ta, and Th, as well as LREE. These *meta*-basalts show Th, Ta, and Nb enrichment relative to Yb (e.g., $Th_N/Yb_N = 8.7 - 12.6$, $Ta_N/Yb_N = 5.4 - 7.4$, and $Nb_N/Yb_N = 4.5 - 6.1$). They also show slight LREE enrichment relative to MREE and HREE, as testified by the $(La/Sm)_N$ and $(La/Yb)_N$ ratios that are in the range 1.49–1.70 and 2.44–3.20, respectively (Barbero et al., 2023c; Saccani et al., 2024). P-MORBs are only found in the Deyader Complex (Fig. 6c). They can easily be distinguished from N- and E-MORBs based on transitional Nb/Y ratios (0.6 – 0.8) and comparatively higher TiO_2, P_2O_5, Nb, Th, and Ta contents, as well as by higher $Th_N/Yb_N = (15.6 - 21.1)$, $Ta_N/Yb_N = (10.5 - 14.2)$, and $Nb_N/Yb_N = (9.4 - 11.6)$ enrichments. They show mild LREE enrichment with respect to HREE, as well as moderate depletion of HREE compared to MREE, as summarized by the $(La/Yb)_N$ (3 – 6) and $(Sm/Yb)_N$ (1.8 – 2.2) ratios. Alkaline basalts are only found in the Bajgan Complex. These rocks show a clear alkaline affinity, as suggested by the high (i.e., 0.88 – 1.82) Nb/Y ratios. Compared to N-, E-, and P-MORBs, they show slightly higher contents of P_2O_5, Nb, Ta, and Th. Alkaline basalts show very high $Th_N/Yb_N = (40.9 - 108)$, $Ta_N/Yb_N = (24.9 - 54.6)$, and $Nb_N/Yb_N = (15.8 - 37.1)$ enrichments, as well as marked LREE/MREE and LREE/HREE enrichments with $(La/Sm)_N$, $(Sm/Yb)_N$, and $(La/Yb)_N$ ratios that are in the range 2.26——3.33, 3.05 – 6.63, and 7.01——20.08, respectively (Saccani et al., 2022b; Barbero et al., 2023c). In the tectonic discrimination diagram of Fig. 6c, they plot in the field for subduction-unrelated settings, namely within the compositional field for typical ocean island basalts (Saccani, 2015).

Based on petrological and lithostratigraphic evidence, Pandolfi et al. (2021) and Saccani et al. (2022b) suggested that the Bajgan and Deyader Complexes are represented by *meta*-ophiolites formed in oceanic tectonic settings characterized by different compositions of their mantle sources (Fig. 6d). N-MORB volcanic protoliths were generated in mid-ocean ridge settings from depleted mantle sources, whereas the very enriched OIB-type protoliths were generated in within-plate seamounts associated with plume–type activity. The slightly enriched E-MORBs and the enriched P-MORBs were generated in mid-ocean ridge settings variably influenced by plume-type activity.

3.4.3. Structural setting and deformation history

The Deyader Complex outcrops as a tectonic window below the North Makran ophiolites in the northern-eastern North Makran domain, whereas a north-dipping normal fault system separate it from the Jaz Murian depression. It represents an antiformal stack of several tectonic slices composed of *meta*-sedimentary and *meta*-volcanic rocks showing pumpellyite-actinolite to blueschist facies metamorphic recrystallization (Hunziker, 2014; Hunziker et al., 2017). The blueschist mainly consists of up to kilometric thick tectonic slices mainly composed of ophiolitic rocks, *meta*-basalts, and *meta*-sedimentary rocks (e.g., marble and shales). The Deyader Complex is severely deformed by meso- and macro-scale folds well exposed within the *meta*-sedimentary succession. These folds mainly show NW-SE trending axis, with bedding and foliation dipping to NE and SW (Hunziker, 2014). McCall (1985) recognize two subsequent tectono-metamorphic events associated with a dynamic recrystallization along axial planar foliations. These structures are crosscut by thrusts and reverse faults that record a post- metamorphic, Cenozoic imbrication within the North Makran domain.

The Bajgan Complex includes an assemblages of different tectonic slices composed of metamorphic rocks showing a NW-SE trending schistosity (Fig. 6e; Pandolfi et al., 2021). NW-SE trending mylonitic shear zones border the different tectonic slices. The result of a recent multiscale structural study suggests that this complex is deformed by four deformation phases, namely D1, D2, D3, and D4 (Pandolfi et al., 2021). The D1 structures are observed as relicts at both meso- and microscopic scale in low-strain domains along the D2 structures. These relicts consist of a S1 continuous foliation and rootles isoclinal folds. The S1 foliation is characterized by aggregates of chlorite and white mica in *meta*-volcaniclastic rocks and in micaschists. Thermobarometric estimation of the S1 mineral assemblages suggests a metamorphic event at blueschist facies conditions (T = 250–295 °C, P = 0.52–0.94 GPa) at depth of c. 17–31 km (Pandolfi et al., 2021). The main structures documented from map- to micro-scale are related to the D2 phase. They include tight to isoclinal folds with NW-SE to N-S trending axes (Fig. 6e) and shear zones showing S-SW sense of shearing. The D2 folds are associated with an axial planar foliation representing a continuous and pervasive schistosity from meso- to micro-scale. A thermobarometric study indicates that deformation and recrystallization during the D2 deformation event took place during two main steps along a retrograde path (i.e., early D2: T = c. 450 °C, P = 0.80–1.10 GPa; late D2: T = 315–350 °C, P = 0.28–0.57 GPa) (Pandolfi et al., 2021). The D3 deformation phase is characterized by close to open cylindrical folds showing sub-horizontal axes trending from NW-SE to NE-SW (Fig. 6e). The folds are associated with a S3 axial planar foliation corresponding to a crenulation cleavage or a disjunctive cleavage in the most competent rocks. The features of the S3 cleavage suggest semi-brittle to brittle deformation at shallower structural levels with respect to those of the D1 and D2 phases (Pandolfi et al., 2021). Middle Eocene (41.95 ± 0.07 Ma) felsic dykes intruded the Bajgan Complex and crosscut the D1, D2, and D3 structures providing limit deformation ages for these events. Both the Bajgan Complex and the felsic dykes are deformed by D4 open to gentle folds with axes trending from E-W to NW-SE and axial planar foliation characterized by a NE-SW striking disjunctive cleavage with no *syn*-kinematic recrystallization. The D1 and D2 deformation phases record underplating at blueschist facies conditions at the base of an accretionary prism and subsequent deformation within the subduction channel, respectively, whereas D3 phase indicate progressive exhumation of the deeply underplated units (Pandolfi et al., 2021).

3.4.4. Chronological constraints

U/Pb zircon dating of the felsic *meta*-intrusive rocks from the Bajgan Complex range from 156 ± 6 Ma to 112 ± 4 Ma, i.e., from Late Jurassic to Early Cretaceous. These ages have been interpreted as the ages of the protoliths (Fig. 6a, Pandolfi et al., 2021). In addition, the Ar/Ar dating of the metamorphic white mica from the micaschists have provided ages ranging from about 91 to 100 Ma (Pandolfi et al., 2021). No paleontological dating is available because the fossils have been totally recrystallized during the metamorphism. However, an Early Cretaceous age can be proposed for the *meta*-sedimentary rocks according to the Late Jurassic-Early Cretaceous age of *meta*-intrusive rocks and the Late Cretaceous age of the metamorphism (Pandolfi et al., 2021).

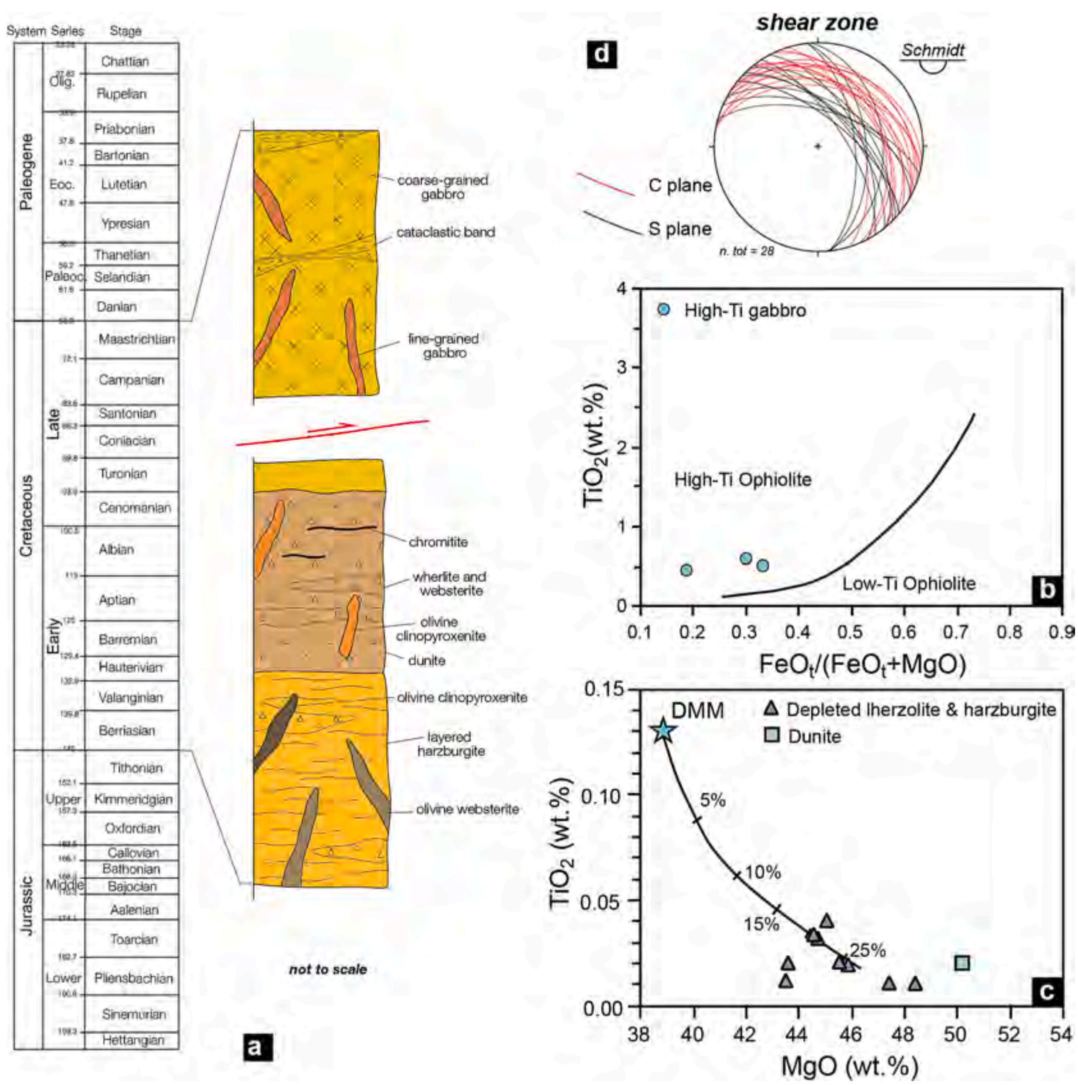

Fig. 7. Synthesis of the stratigraphic, structural, chronological, and geochemical features of the Sorkhband Ophiolite. a) stratigraphic columns for the upper and the lower tectonic slices of the Sorkhband ophiolite. The inferred ages are from McCall (1985) and Moghadam et al (2022); b) TiO_2 vs. FeO_t /(FeO_t + MgO) discrimination diagram (Serri, 1981) for gabbros from the upper ophiolite tectonic slice (data from Delavari et al., 2016); c) Variation of TiO_2 vs. MgO for peridotites from the lower tectonic slice (data from Delavari et al., 2016). Partial melting trend shows the Ti-Mg co-variation in residual spinel peridotites during anhydrous polybaric near-fractional melting of the depleted MORB mantle (DMM) source (Workmann and Hart, 2005) calculated using the model of Niu (1997). Numbers along the lines indicate percent melting; d) stereographic plots showing the mesoscale data from the shear zones bordering the Sorkhband ophiolite.

Chronological constraints about the Deyader Complex have been first provided by Delaloye and Desmons (1980). A K/Ar ages of 87.9 ± 5 Ma have been obtained on metamorphic amphibole by these authors. Recently, Bröcker et al. (2021) report an age of the blueschist metamorphism of about 84 Ma (± <1–3 Ma).

3.5. The Sorkhband ophiolite

The Sorkhband ophiolite (Rajabzadeh and Moosavinasab, 2013) is represented by a large body of about 20 km^2 cropping out between the Bajgan Complex at the top and the Coloured Mélange at the bottom (Fig. 2b; McCall, 2002; Najafazdeh et al., 2008; Behzadi and Shahabpour, 2011; Jannessary et al., 2012; Rajabzadeh and Moosavinasab, 2013; Delavari et al., 2016; Moghadam et al., 2022). The boundary with the Bajgan Complex is the NW-SE trending Dastgerd thrust whereas the boundary with the Coloured Mélange is the NNW-SSE trending Rudan thrust (Fig. 2b).

3.5.1. Stratigraphic features

The Sorkhband ophiolite consists of two different tectonic slices (Fig. 7a; Delavari et al., 2016). The upper slice includes only lower crust rocks, whereas the lower tectonic slice mainly consists of upper mantle peridotites and ultramafic rocks at the upper mantle-lower crust transition (Fig. 7a). The upper slice consists of an about 100 m-thick sequence of coarse-grained gabbros cut by dykes of fine-grained gabbros (Delavari et al., 2016). Most of the gabbros show a cataclastic fabric, though undeformed gabbros with well-preserved magmatic textures locally occur. The lower slice consists of a well-exposed thick sequence of mantle peridotites with remnants of the overlying lower oceanic crust (Fig. 7a; Najafzadeh et al., 2008; Jannessary et al., 2012; Rajabzadeh and Moosavinasab, 2013; Moghadam et al., 2022). At its base, the sequence includes layered diopside-bearing harzburgites associated with minor lenses of dunites (Fig. 7a). Abundant dykes of olivine clinopyroxenite to olivine websterite crosscut dunites and harzburgites. Harzburgites and dunites locally show traces of magmatic impregnation by basaltic melts represented by clinopyroxene cumulates at the contact and/or near the olivine clinopyroxenite and websterite dykes. The harzburgites show a gradual transition to a thick level of dunites with minor bands of wehrlites and websterites (Fig. 7a). The dunites are cut by dykes of ol-bearing clinopyroxenites (Fig. 7a). Ore bodies of chromitites have been found in the dunites showing textures changing from disseminated in thick dunitic layers to cumulate in chromite-rich dunites and to massive in chromitite layers (Moghadam et al., 2022). Bands of chromitites have also been observed inside the mantle peridotite (Fig. 7a).

3.5.2. Geochemistry and petrogenesis of magmatic rocks and mantle peridotites

Gabbros and fine-grained gabbroic dykes show an isotropic texture and relatively low TiO_2, P_2O_5, and Y contents with high Mg#. These rocks are depleted in incompatible elements with respect to the N-MORB composition. Nonetheless, they show N-MORB-normalized ratios similar to those of N-MORB-type gabbros (e.g., $Th_N/Yb_N = 0.5 – 1.0$), $Ta_N/Yb_N = 0.6 – 1.0$, and $Nb_N/Yb_N = 0.7 – 1.0$) coupled with no enrichment in Th relative to Ta and Nb (e.g., $Th_N/Nb_N = 0.8 – 1.2$). Chondrite-normalized REE compositions show the typical features of N-MORB rocks with a marked LREE depletion ($La_N/Yb_N = 0.44–0.62$). Delavari et al. (2016) suggested that Sorkhband gabbros were generated in a mid-ocean ridge setting from a DMM-type mantle with no influence from either enriched mantle components or subduction-related components. In fact, in the discrimination diagram in Fig. 7b they plot in the field for ophiolitic gabbros formed at mid-ocean ridge settings.

According to Delavari et al. (2016) and Moghadam et al. (2022), the Sorkhband peridotites represent the upper mantle-lower crust transition zone and consist of depleted lherzolites, harzburgites, stratiform chromitites, chromite-rich dunites, and dunites. Crosscutting dykes of olivine websterite and olivine clinopyroxenite are frequent. Incompatible element contents are low in lherzolites and very low in harzburgites. Depleted lherzolites show chondrite-normalized (Sun and McDonough, 1989) REE patterns featuring marked LREE/MREE and LREE/HREE depletion with $Sm_N/Yb_N = 0.12$ and $La_N/Yb_N = 0.04–0.07$. In contrast, harzburgites show chondrite-normalized REE patterns characterized by depletion of MREE with respect to both LREE and HREE ($La_N/Sm_N = 2.06 – 2.57$ and $Sm_N/Yb_N = 0.34 – 0.65$). According to Moghadam et al. (2022), major- and trace-element compositions of clinopyroxene and spinel in olivine-websterite and clinopyroxenite dykes and chromitites indicate crystallization from melts similar to boninites and low-Ti forearc basalts. Moghadam et al. (2022) proposed that the Sorkhband peridotites formed in a forearc setting during the initial subduction of the Neo-Tethys Ocean beneath the Lut block during the Late Cretaceous. In fact, the overall chemistry of these peridotites is compatible with that of sub-arc depleted lherzolites and harzburgites residual after high degrees of partial melting of a MORB-type mantle, as exemplified in Fig. 7c.

3.5.3. Structural setting and deformation history

The Sorkhband ophiolite constitutes a NW-SE trending lenticular tectonic element sandwiched between the Coloured Mélange, to the south, and the Bajgan Complex, to the north. In this ophiolite, a strong strain partitioning is observed, with the deformation localized along the basal and roof tectonic contacts and an internal poorly deformed domain. The basal and southern tectonic contact is hundreds of meters-thick shear zone, consisting of elongated and boudinaged slices of marbles, *meta*-basalts and serpentinized peridotites separated by NW-SE trending shear planes, gently dipping to the north-east (Fig. 7d). The *meso*-scale S-C structures indicate a top-to-the SW sense of shearing (Fig. 7d). The roof tectonic contact shows similar features, with up to hundreds of meters-long and tens of metres-thick slices of amphibolite of the Bajgan Complex included between the shear zones. Meso-scale data indicate top-to the southwest or south sense of shearing along this contact.

3.5.4. Chronological constraints

The age of these ophiolites is still unknown as radiometric datings are lacking. However, their structural position between Jurassic and Cretaceous ophiolites and *meta*-ophiolites suggest that they are reasonably Cretaceous in age, as suggested by Ghazi et al. (2004) and Delavari et al. (2016).

3.6. The Coloured Mélange

The Coloured Mélange is also known as Coloured Mélange Complex (McCall and Kidd, 1982; McCall, 2002; Saccani et al., 2018), or as Imbricate Zone (Burg et al., 2013; Burg, 2018), or as Southern Makran ophiolitic mélange (Esmaeili et al., 2020). It crops out along the entire length of the North Makran domain, i.e., an area about 500 km long with a width ranging from 15 to 2–3 km (Fig. 2b). However, in some places, the Coloured Mélange is completely cut off along its lower boundary. This mélange is an assemblage of tectonic slices and can be regarded as a tectonic mélange formed by offscraping of oceanic lithosphere, including the deep-sea sedimentary deposits. Its lower boundary is the WNW-ESE trending Bashakerd thrust, along which the Coloured Mélange overlaps the Inner Makran (Fig. 2b, c). The upper boundary, separating the Coloured Mélange from the Sorkhband ophiolite and from the Durkan Complex, corresponds to the WNW-ESE trending Rudan and Bandkosh thrusts, respectively. The Coloured Mélange is unconformably covered by the Late Paleocene – Early Eocene sedimentary deposits. However, slices of these deposits are involved in the thrust zones at the boundary with the Sorkhband ophiolite and the Durkan Complex.

3.6.1. Stratigraphic features

The slices of the Coloured Mélange are represented by sedimentary, magmatic, and metamorphic rocks, locally forming distinct incomplete sequences that include different lithologies (Fig. 8a). Overall, the slices mainly consist of (in order of decreasing volumetric abundance) volcanic rocks, cherts, limestones, mantle serpentinites, gabbros, shales, serpentinized cumulate peridotites, and plagiogranites. According to McCall (1983) and Esmaeili et al. (2021), slices of turbidites also occur. The magmatic rocks are representative of different oceanic tectonic settings, not only for their geochemical feature but also for their age.

The serpentinites are mantle peridotites, consisting of harzburgites associated with bodies of dunites, wehrlites and websterites (McCall, 1983). These ophiolites bear chromitite ore bodies, analogous to those of the Sorkhband ophiolite. Saccani et al. (2018) have recognized several slices of basalts, all covered by cherts (Fig. 8a). Their geochemical features indicate that the Coloured Mélange incorporates a wide range of volcanic rocks formed in distinct tectonic settings. McCall (1983) reported the occurrence of carbonate rocks consisting of Globotruncana-bearing biomicrites and Orbitolina-bearing reefal limestones (Fig. 8a). In addition, the occurrence of blocks of Globigerina-bearing limestones is also reported (McCall, 1983, 1985). Blocks of metamorphic rocks are also widespread. Most of these consist of massive marbles, *meta*-basalts and *meta*-volcaniclastic rocks (Fig. 8a). The *meta*-basalts are represented by HP-LT fine-grained schists with abundant glaucophane amphibole (Saccani et al. 2018). In addition, Esmaeili et al. (2021) described lenticular slices of amphibolites showing tectonic relationships with bodies of foliated serpentinites (Fig. 8a). The amphibolites show intercalations with discontinuous levels of bedded to massive marbles.

3.6.2. Geochemistry and petrogenesis of magmatic rocks

The mafic volcanic and *meta*-volcanic rocks in the Coloured Mélange consist of both subduction-related and subduction-unrelated rock types (Fig. 8b). Subduction-unrelated rocks-types include N-MORBs, E-MORBs, Late Cretaceous P-MORBs, alkaline basalts, and basalts with geochemical features strongly resembling those of oceanic plateau basalts (OPB) (Fig. 8b; Saccani et al., 2018; Esmaeili et al., 2019). All these rock types but OPB-like rocks, have chemical features similar to those of their counterparts forming the ophiolitic and *meta*-ophiolitic units described above. In contrast, OPB-like rocks, are exclusively found within the Coloured Mélange and show overall geochemical features very similar to those of E-MORBs (Fig. 8b) bearing, however, the very flat chondrite-normalized REE patters, which typically characterize the OPBs from many oceanic settings (Saccani et al., 2018, and references therein). In fact, these rocks show $(La/Yb)_N$, $(Sm/Yb)_N$, and $(La/Sm)_N$ ratios between 0.9 and 1.1. All these rocks have been interpreted as remnants of the Mesozoic Neo-Tethys sector located between the

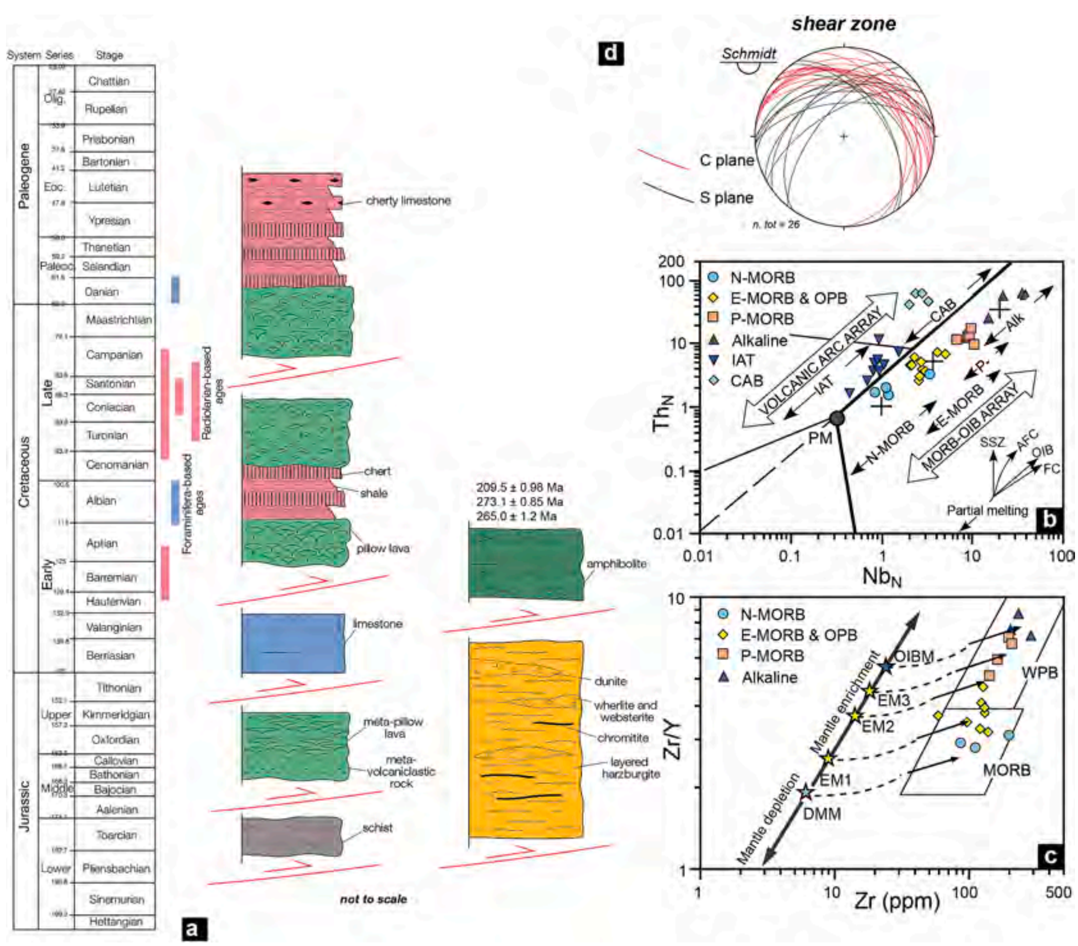

Fig. 8. Synthesis of the stratigraphic, structural, chronological, and geochemical features of the Coloured Mélange. a) schematic and reconstructed stratigraphic columns of different blocks within the Coloured Mélange. The coloured boxes indicate the radiolarian-based biostratigraphic ages for cherts associated with basalts (data from Saccani et al., 2018, Esmaeili et al., 2019) and the foraminifera-based ages for limestones (data from McCall, 1985). Radiometric ages for amphibolites are also reported (data from Esmaeili et al., 2021); c) N-MORB-normalized Th vs. Nb discrimination diagram of Saccani (2015) for *meta*-volcanic and volcanic rocks from the Coloured Mélange (data from Saccani et al., 2018). Abbreviations and compositions as in Fig. 3c, OPB: oceanic plateau basalt; d) Zr/Y vs. Zr diagram (modified from Pearce and Norry, 1979) for *meta*-volcanic and volcanic rocks from the Coloured Mélange (data from Saccani et al., 2018). Abbreviations, compositions, and trends as in Fig. 4d, 5d, OPB: oceanic plateau basalt; d) stereographic plot showing the orientation of bedding and shear zones within the Coloured Mélange in the Manujan area.

Arabian Plate and the Lut Block (Saccani et al., 2018; Esmaeili et al., 2019). The occurrence of enriched basalts, such as E-MORBs, OPBs, and alkaline basalts within the Coloured Mélange strongly point out for a Late Cretaceous mantle plume activity in this Neo-Tethys sector (Saccani et al., 2018). Likewise, Esmaeili et al. (2019) proposed that E-MORBs, P-MORBs, and alkaline basalts were formed through the partial melting of heterogeneous mantle sources, which were metasomatized by deep-mantle OIB-type components and were erupted in a mid-ocean ridge featuring plume-ridge interaction. Fig. 8c shows that the composition of subduction-unrelated basalts in the mélange are compatible with progressively enriched mantle sources. Subduction-related rocks within the Coloured Mélange include Early Cretaceous IATs and Late Cretaceous CABs varieties (Fig. 8b). Saccani et al. (2018) suggested that these rock types originated from depleted mantle sources that underwent different subduction-related metasomatisms prior to melting. In particular, CAB rocks show a marked influence from sediment melt addition, whereas IATs show chemical compositions compatible with subduction fluid addition (Fig. 3d). These petrological features suggest that Early Cretaceous IATs and Late Cretaceous CABs were generated in different volcanic arc settings or different portions of a single volcanic arc (Saccani et al., 2018).

3.6.3. Structural setting and deformation history

The Coloured Mélange corresponds to an assemblage of metric- to decametric-thick blocks showing lozenge-type shape. Generally, the blocks have been juxtaposed with each other by cm- to dm-thick shear zones without the presence of a sedimentary matrix enclosing them. The shear zones are ESE-WNW to NW-SE trending (Fig. 8d) and are characterized at the *meso*-scale by foliated cataclasites with S-C structures indicating reverse kinematic and top-to-the south-west sense of shearing (Fig. 8d). Only in some areas, the Coloured Mélange consists of blocks within a matrix composed of deformed and sheared serpentinites (McCall, 1983). Inside the thicker blocks, stratigraphic relationships between volcanic rocks, pelagic sedimentary rocks, and turbidites can be recognized (Saccani et al., 2018; Esmaeili et al., 2019, 2020). In this specific tectono-stratigraphic situation, the bedding is at low-angle, with the shear zones bordering the blocks and the bedding strike sub-parallel to the shear planes (Fig. 8d). These structural features, along with nature of the blocks forming the Coloured Mélange, suggest that it represents a tectonic chaotic complex (e.g., Festa et al., 2022) formed through the imbrication, deformation, and mixing of fragments of oceanic lithosphere and its sedimentary cover including pelagic and trench turbiditic successions (Saccani et al., 2018; Esmaeili et al., 2019, 2020).

3.6.4. Chronological constraints

Saccani et al. (2018) provided biostratigraphic dating of the cherts overlying the basalts using radiolarian assemblages. The results indicate that the volcanic arc tholeiites range from Early (late Hauterivian – early Aptian) to Late (latest Cenomanian – lower late Campanian) Cretaceous (Fig. 8a). In contrast, the calc-alkaline rocks and OPBs are Late Cretaceous in age (early Coniacian – Santonian and early Turonian – early Campanian, respectively). McCall (1983) reported an Albian age for limestones consisting of Globotruncana-bearing biomicrites and Orbitolina-bearing reefal limestones. However, the most important occurrence is represented by blocks of Globigerina-bearing limestones of Early Paleocene age, indicating that the processes leading to the origin of the Coloured Mélange began in the Early Paleocene (Fig. 8a).

Radiometric dating is scarce. The only available data were provided by Esmaeili et al. (2021), who reported U/Pb zircon ages of 209.5 ± 1.0 Ma (Late Triassic), 273.1 ± 0.9 Ma (Late- Early Permian), and 265.0 ± 1.2 Ma (Middle Permian) for the magmatic protoliths of amphibolites (Fig. 8a).

4. Discussion

A thorough examination of the existing data on the Makran tectonic units allows us to revise the geodynamic reconstructions of the North Makran domain published so far and to propose an update of its Mesozoic- Early Cenozoic geodynamic evolution. In section 4.1, we will briefly describe the extant geodynamic models of the area, whereas in section 4.2, we will critically evaluate these models by outlining points that contrast with new data from the authors of this paper. Finally, in section 4.3, we will propose a new geodynamic reconstruction, accompanied by 2-D sketches of the Makran, showing the Jurassic to Early Cenozoic plate tectonics in the Neo-Tethys realm and the associated Arabian Plate and the Lut Block.

4.1. Previous geodynamic reconstructions of the Makran area

The first geodynamic reconstruction of the Makran was proposed by McCall and co-workers (e.g., McCall and Kidd, 1982; McCall, 1997; McCall, 2002). These works summarized the results of the 1970 s-1980 s geological mapping at scales of 1:100,000 and 1:250,000. McCall and Kidd (1982) distinguished eight geotectonic zones and discussed their significance within a new geodynamic model of this area. From north to south, these provinces were defined as follows: the Jaz Murian depression, the Inner Makran Spreading Zone, the Bajgan – Durkan zone, the Coloured Mélange zone, the Eocene-Oligocene flysch, the Oligocene-Miocene flysch, the Miocene neritic zone, and the Mio-Pliocene neritic zone (McCall and Kidd, 1982). These zones are mainly bounded by tectonic contacts and each of them was considered as a distinct paleogeographic element during the Mesozoic-Cenozoic evolution of the Makran. The present-day structural position in the prism was considered as reflecting the original paleogeographic location within the former Neo-Tethys Ocean (McCall and Kidd, 1982). According to McCall and Kidd (1982) and McCall (1997), the Bajgan-Durkan zone was a key zone for reconstructing the Middle Jurassic to the Late Cretaceous paleogeography of the Neo-Tethys. This zone was described by McCall and Kidd (1982) and McCall (1997) as an assemblage of undated metamorphic rocks of the Bajgan Complex that are stratigraphically covered by the Cretaceous shelf carbonate sequence of the Durkan Complex (Fig. 9). Rare tectonic slices of Permian and Jurassic shallow-water limestone are also associated with the Cretaceous sequence. Based on the Permian – Cretaceous age of the carbonate succession of the Durkan Complex and its supposed stratigraphic relationship with the metamorphic rocks of the Bajgan Complex, the Bajgan-Durkan zone was interpreted as a microcontinent and its sedimentary cover. This microcontinent is thought to have completely separated the main oceanic branch, i.e., the Neo-Tethys Ocean, remnants of which are now preserved in the Coloured Mélange, from the Fannuj Ocean. The latter is currently represented by several ophiolites in the geotectonic province called Inner Makran Spreading Zone (referred to as the Northern ophiolites in this paper). In this geodynamic model, the Bajgan-Durkan complexes in the Makran were correlated with the Sanandaj-Sirjan zone in the Zagros belt (e.g., Ghasemi and Talbot, 2006), whereas the Inner and the Outer Zagros ophiolitic belts could be correlated with the Inner Makran Spreading Zone and the Coloured Mélange, respectively (McCall, 1997; see also Moghadam and Stern, 2015 and reference therein). McCall and Kidd, (1982) postulated that the northern oceanic basin (i.e., the Fannuj Ocean) represented a Jurassic – Cretaceous back-arc basin (Fig. 9) that opened in response to the northward subduction of the Neo-Tethys below the Bajgan-Durkan continental ribbon. This assumption was based on the scattered occurrence of calc-alkaline rocks within some sectors of the Inner Makran Spreading Zone and on a comparison with the Zagros belt. In fact, the Sanandaj-Sirjan zone is characterized by Middle Jurassic-Early Cretaceous volcanic arc complexes (e.g., Berberian et al., 1982; Hassanzadeh and Wernicke, 2016; Zhang et al., 2018) and Early to Late Cretaceous back-arc basin (e.g., Moghadam and Stern, 2015; Hassanzadeh and Wernicke, 2016), which were interpreted as the evidence for the start of the subduction in the Neo-Tethys realm. During the Late Cretaceous – Paleocene, convergent kinematics affected both the Neo-Tethys and the Fannuj Ocean. The Bajgan-Durkan

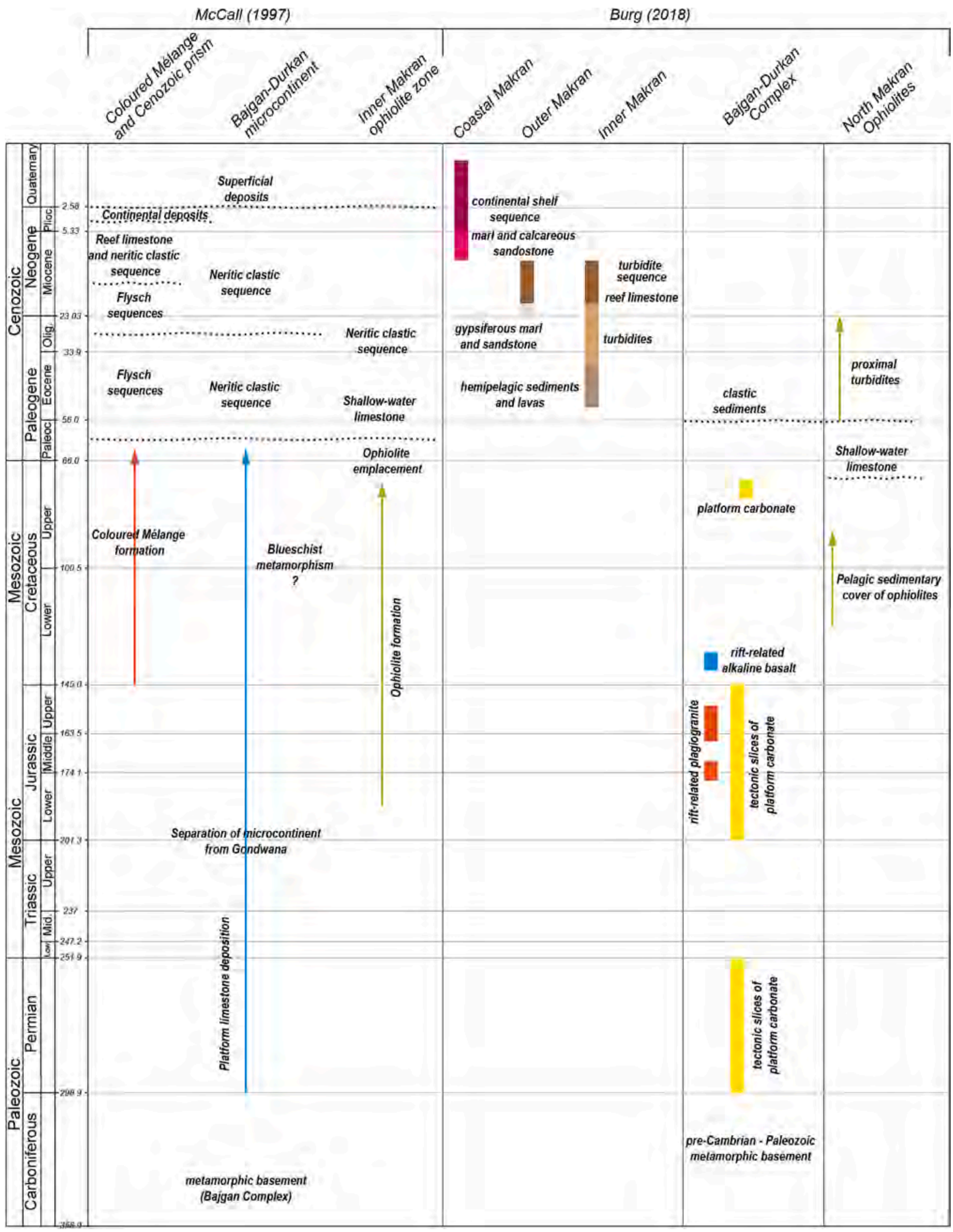

Fig. 9. Summary of the stratigraphic, magmatic, and tectonic events in the Makran Accretionary Prism according to the geodynamic models of McCall (1997) and Burg (2018). Blue dotted lines represent regional stratigraphic unconformities.

microcontinent was believed to have separated an actively forming accretionary complex to the south (e.g., the Coloured Mélange), and a closing ocean to the north (i.e., the Fannuj Ocean) (McCall and Kidd, 1982; McCall, 1997). These authors proposed that the closure of the northern basin was related to a subduction zone accounting for the occurrence of blueschists along the southern margin of the Jaz Murian depression (e.g., the Deyader Complex). By the Eocene, the former microcontinent collided with the Lut Block (i.e., the Eurasian Plate), and the ophiolites in the Inner Makran Spreading Zone were obducted onto the Bajgan-Durkan microcontinent. These ophiolites now mark this suture zone. The unconformable deposition of Eocene siliciclastic deposits onto this tectonic assemblage provides a chronological constrain for the formation of the suture zone (e.g., McCall and Kidd, 1982; Fig. 9).

Following the works of McCall and co-authors, over the past 20 years several papers have been published on specific aspects of the North Makran domain tectonic units, including their tectono-stratigraphic architecture and biostratigraphy (e.g., Dolati, 2010; Haghipour et al., 2012; Hunziker et al., 2015; Mohammadi et al., 2016, 2017; Burg et al., 2008, 2013; Saccani et al., 2018; Esmaeili et al., 2020; Barbero et al., 2020a, 2021a, 2023b), the tectono-magmatic characterization and dating of the ophiolites and *meta*-ophiolites (e.g., Ghazi et al., 2004; Hunziker, 2014; Delavari et al., 2016; Esmaeili et al., 2019; Monsef et al., 2019; Barbero et al., 2020b, 2021b; Ghasemi Siani et al., 2021, 2022a, 2022b; Sepidbar et al., 2020; Pandolfi et al., 2021; Moghadam et al., 2022; Saccani et al., 2022a, b), and their tectono-metamorphic evolution (e.g., Dorani et al., 2017; Hunziker et al., 2017; Omrani et al., 2017; Pandolfi et al., 2021; Bröcker et al., 2021; Barbero et al., 2023a). The geodynamic implications of part of these new data have been discussed by Burg (2018), who reviewed several years of work in the onshore Makran Accretionary Prism. He proposed to subdivide the prism into four tectono-stratigraphic domains (i.e., the North, Inner, Outer, and Coastal Makran) and presented a geodynamic reconstruction of the Mesozoic-Cenozoic evolution of the Makran. These domains are separated by major thrust zones and are distinguished according to the age of the stratigraphic successions, structural architecture, and timing of tectonic deformation phases (Burg, 2018). For example, the North Makran domain reflects a pre-Eocene convergent evolution, whereas the Inner, Outer, and Coastal Makran record post-Eocene –Mio-Pliocene accretionary stages. Using data from the eastern North Makran domain, Hunziker et al. (2015) and Burg (2018) adopted the McCall's hypothesis of existence of a microcontinent separating two oceanic branches. They interpreted the northern ocean (i.e., the Fannuj Ocean of McCall and Kidd, 1982) as having opened in response to rifting along the southern margin of the Lut Block. According to Burg (2018), remnants of the Fannuj Ocean are preserved in the North Makran ophiolites, whereas the remnants of the microcontinental block are now found in the Bajgan and Durkan Complexes. The Bajgan-Durkan microcontinent experienced a Late Jurassic – Early Cretaceous rifting stage, followed by the emplacement of a volcanic arc associated with the northward subduction of the Neo-Tethys beneath the Bajgan-Durkan continental ribbon since the Early Cretaceous (Fig. 9; Burg, 2018). Different types of granites and plagiogranites, first attributed to the Durkan Complex by Hunziker et al. (2015), were interpreted as the sole remnants of this rifting stage, as no typical continental crust rocks have been found. In contrast, indirect evidence for the Early to Late Cretaceous arc include volcanic sequences onto the North Makran ophiolites (Hunziker, 2014) and an increase in detrital zircon grains sourced from a volcanic arc during the Cretaceous – Miocene turbidites of the Inner and Outer Makran (Mohammadi et al., 2016, 2017; Burg, 2018). However, Cretaceous volcanic arc rocks have not yet been identified in the Bajgan and Durkan Complexes. Convergent kinematics persisted during the Late Cretaceous – Paleocene as evidenced by the formation of blueschists, an accretionary wedge south of the Bajgan-Durkan microcontinent, and the obduction of the North Makran ophiolites (Burg, 2018).

The Late Cretaceous – Paleocene tectonic stage is followed by a phase of tectonic quiescence, during which Eocene – Early Oligocene turbidites (i.e., the present-day successions of the Inner and Outer Makran) were deposited (Fig. 9; Burg, 2018). These turbidites were deposited on top of the Late Cretaceous – Paleocene accretionary prism (i.e., the tectonic units of the North Makran domain) and were fed by the prism itself, with paleocurrent orthogonal to the trench. Oligocene and Miocene turbidites were also deposited in more distal locations, directly atop the subducting oceanic lithosphere. During the Miocene – Present-day, this trench – wedge- top tectonostratigraphic assemblage was imbricated and folded as indicated by the folding and thrusting deformation in the Inner, Outer, and Coastal Makran. This deformation is related to the continuous convergence of the Arabian Plate and Lut Block, which is accommodated by the ongoing subduction in the Makran and by continent–continent collision in the Zagros (e.g., Agard et al., 2011; Burg, 2018).

Another significant geodynamic reconstruction of the North Makran domain has been proposed by Saccani et al. (2018), who suggested an update on the Late Cretaceous – Paleocene evolution based on new geochemical data on basaltic rocks and biostratigraphic data on the associated cherts. These authors identified Late Cretaceous basalts within the Coloured Mélange, suggesting the existence of oceanic island and oceanic plateaux in the Neo-Tethys during this age. Saccani et al. (2018) also proposed that these oceanic reliefs played a significant role during the convergent stages, causing regional shortening of the convergent margin, which controlled the imbrication of the tectonic units and the obduction of the North Makran ophiolites onto the Bajgan-Durkan microcontinent. Although this model was based just on data from the Coloured Mélange and does not provide a comprehensive update of the geodynamic evolution of the area, it was the first to propose that oceanic islands and plateaux existed in the Neo-Tethys Ocean and that their role during the convergent stage should be considered in future geodynamic reconstructions.

4.2. *Critical evaluation of the existing models and key points for the North Makran geodynamic evolution*

The data reviewed in this paper indicates that some constraints in the previous geodynamic models require critical discussion. One of the major controversial points is the interpretation of the Bajgan-Durkan Complexes as a Paleozoic microcontinent (McCall and Kidd, 1982; Burg, 2018). The Late Jurassic – Early Cretaceous ages of the magmatic protoliths from the Bajgan Complex (Fig. 10) allow us to exclude that it represents a Paleozoic or pre-Paleozoic continental basement as previously believed. On the contrary, the Jurassic – Cretaceous age, the N-MORB, E-MORB, and OIB chemical affinities of the *meta*-gabbros and *meta*-basalts, and the stratigraphic architecture of the Bajgan Complex demonstrate that it is an assemblage of *meta*-ophiolites and their *meta*-sedimentary cover derived from the subduction of different portions of the Neo-Tethys oceanic basin. This conclusion aligns with the regional-scale reconstruction for the Neo-Tethys realm during the Jurassic – Early Cretaceous, which shows a wide oceanic domain existing between the Arabian and Eurasian Plates (e.g., Şengör et al., 1988; Barrier et al., 2018). Further support comes by the comparison between the ages and geochemical compositions of the Bajgan Complex *meta*-ophiolites with those of the North Makran ophiolites and the Deyader Complex (Fig. 10). In fact, the similar age range and shared N- and E-MORB geochemical affinities of these ophiolites and *meta*-ophiolites (Fig. 10) strongly suggest that they originated from the deformation of different sectors of the same Late Jurassic – Cretaceous oceanic basin. Consequently, the hypothesis of a small continental microplate separating two distinct oceanic basins should be discarded in the future geodynamic reconstructions of the North Makran domain.

Another point of contrast with previous models is the occurrence of rocks with supra-subduction zone geochemical affinity within two units with distinct structural positions. Contrary to what proposed by McCall and Kidd (1982), Late Cretaceous calc-alkaline and island arc tholeiites

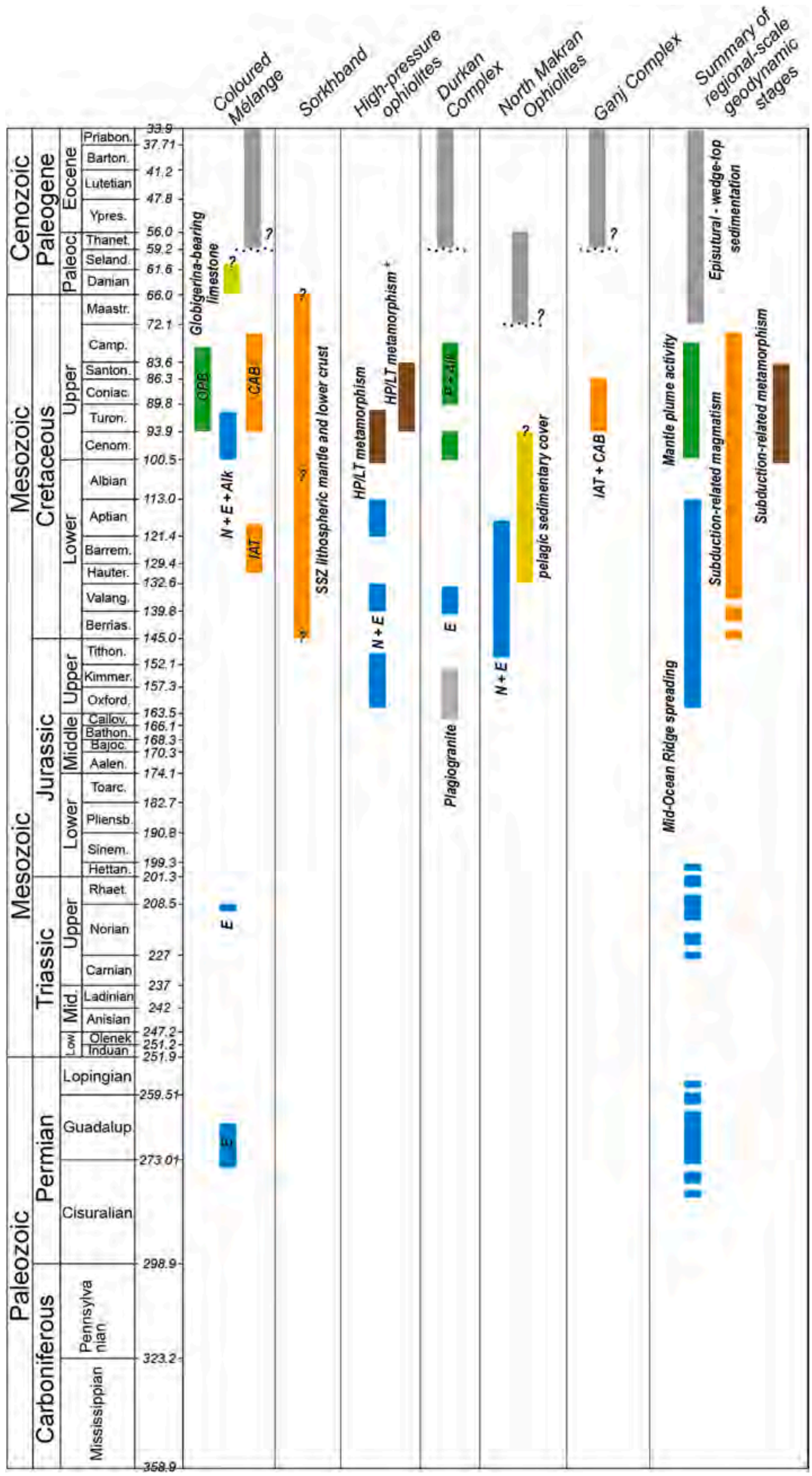

Fig. 10. Summary of the stratigraphic, magmatic, and tectonic events recognized in the tectonic units of the North Makran and a synthesis of the ages of the different geodynamic stages. The colours indicate the different type of events. Data , 2020b, 2021a, 2023b), , Brocker et al (2021), . Abbreviations: N: normal-type MORB; E: enriched-type MORB; P: Plume-type MORB; Alk: Alkaline basalt; OPB: oceanic plateau basalt; SSZ: supra-subduction zone; IAT: island arc tholeiite; CAB: calc-alkaline basalt; HP-LT: high pressure – low temperature.

Source: Delaloye and Desmons (1980), McCall (1983, 1985), Ghazi et al. (2004), Dolati (2010), Hunziker et al. (2015), Delavari et al. (2016), Saccani et al. (2018), Barbero et al. (2020aGhasemi Siani et al., (2021), Pandolfi et al. (2021)Esmaeili et al. (2021)

rocks are found exclusively in the Ganj Complex and are not peculiar of all the North Makran ophiolites. These volcanic arc rocks are significantly younger than the N- and E-MORB magmatic rocks of the North Makran ophiolites, suggesting the existence of a volcanic arc in specific sectors of the basin and distinct magmatic stages with different age and chemical affinity (Fig. 10). Early to Late Cretaceous volcanic and ultramafic rocks with supra-subduction zone chemical affinity are also found within the Coloured Mélange (Fig. 10), which occupies a structural position distinct from that of the Ganj Complex. In addition, two belts with HP-LT metamorphism are found in two separate structural positions within the tectonic stack, providing evidence for two distinct subduction complexes. The southern belt occurs as dismembered blocks within the Coloured Mélange, whereas the northern belt is represented by high pressure *meta*-ophiolites and part of the Durkan Complex. Restoring the original positions of these supra-subduction zone rocks and the HP-LT metamorphic units is critical for discussing the location of ancient subduction zones in the new geodynamic model, which will be reviewed in the next section.

The stratigraphic, biostratigraphic, and petrological data from the Durkan Complex provide additional fundamental constraints for the geodynamic evolution of the Makran. Specifically, the western part of this complex includes successions formed in a Late Cretaceous seamount where P-MORB and OIB magmatisms, as well as shallow-water and pelagic sedimentation took place (Fig. 10). Remnants of Permian and Jurassic continental margin shelf sequences and rift-related magmatic rocks, as described by McCall (1985) and Hunziker et al. (2015) were not found stratigraphically associated with the Late Cretaceous succession, suggesting that this complex cannot be interpreted as a continuous passive margin succession. Moreover, there is no evidence of a pristine stratigraphic relationship between the Durkan and the Bajgan Complexes, contrary to what previously believed (McCall, 1985; Burg, 2018). Instead, the different ages, P-T metamorphic conditions, and the structural data indicate a tectonic relationship between these complexes. Thus, interpreting the Durkan Complex as a tectonically disrupted seamount chain (Barbero et al., 2021a, 2021b, 2023a) is a central clue for proposing a new geodynamic model.

The wealth of structural data reviewed in this paper represent fundamental constraints for better describing the convergent stages that affected the Makran. In fact, the Late Cretaceous age of the main metamorphism of the Bajgan Complex (Fig. 10) provides a crucial age constraint for these convergent stages. Similar to the hypothesis postulated by McCall and Kidd (1982), these data confirm the existence of a Late Cretaceous subduction zone associated with an accretionary prism. The deformation history and style described in the Deyader Complex, the Durkan Complex, and the North Makran ophiolites, indicate their deformation within an accretionary prism, further supporting the existence of a subduction complex where the accretion of fragments of oceanic lithosphere occurred at different depths of the prism (Fig. 10). As previously suggested by McCall (1985), the ages of the successions unconformably resting on top of these units allow for constraining the accretionary deformation phases to the Late Cretaceous – Paleocene times (Fig. 10). In addition, the structural setting of the Coloured Mélange, with tectonic slices composed of succession of different ages, natures, and metamorphic degrees, is compatible with the deformation in both the frontal and deeper parts of an accretionary prism. Collectively, these data represent a significant advancement in understanding the convergent deformation that affected the Makran. Their geodynamic significance will be discussed in the next section.

Finally, similar to what was proposed by McCall and Burg (e.g., McCall and Kidd, 1982; McCall, 1997; Burg, 2018), the consistency of the structural data and the direction of transport along the main thrust zones within the different units suggest that the position of each unit in the tectonic stack likely reflects its original paleogeographic location within the former Neo-Tethys realm. This assumption forms the basis of the geodynamic reconstruction described in the following sections.

4.3. New model for the North Makran geodynamic evolution

The different steps of the Jurassic – Eocene geodynamic evolution of North Makran domain are described here to propose a new geodynamic scenario for the opening and closure of the Neo-Tethys Ocean between the Arabian and Lut continental margins. Unlike previously published geodynamic models, we emphasize that the new model considers the results of multidisciplinary studies performed on all the North Makran tectonic units.

4.3.1. Jurassic – Early Cretaceous stage: Oceanic spreading

The opening of the Neo-Tethys Ocean dates back to the Permian and started with continental rifting along the northern Gondwana margin (Dercourt et al., 1986; Şengör et al., 1988; Robertson and Searle, 1990; Stampfli and Borel, 2002; Barrier et al., 2018). In the Middle East sector, this ocean evolved between the Arabian Plate and the Lut Block from the Triassic up to the Cenozoic (Barrier et al., 2018). Remnants of the Late Permian – Early Triassic rifting and early oceanic spreading stages of the Neo-Tethys are rare within the collisional and accretionary belts of the Middle East region. These remnants correspond to both pelagic succession (i.e., limestone and radiolarites) and volcano-sedimentary assemblages in the Oman Mountains (e.g., Robertson and Searle, 1990; Chauvet et al., 2011) and in the Zagros collisional belt (Ghasemi and Talbot, 2006). In the North Makran domain, amphibolites within the Coloured Mélange, whose protoliths date to the Permian and Late Triassic, likely record the rifting and early oceanic spreading of the Neo-Tethys (Fig. 10). In fact, the transitional to E-MORB geochemical affinity of the amphibolites suggest their interpretation as metamorphosed mafic rocks formed during the plume-associated rifting of the northern Gondwana margin. This finding testifies to the progressively opening of the Neo-Tethys during the Late Permian – Late Triassic in the Makran (Esmaeili et al., 2021). The spreading stage of the Neo-Tethys Ocean is recorded by the *meta*-ophiolites now preserved in the Bajgan Complex. The stratigraphic architecture, the geochemical composition of *meta*-basalts and *meta*-gabbros, and U/Pb ages of the *meta*-intrusive rocks indicate that this complex is composed of remnants of Late Jurassic – Early Cretaceous oceanic lithosphere, providing evidence for the existence of a mid-ocean ridge since at least the Late Jurassic (Fig. 11a). This interpretation aligns well with recently published Early to Middle Jurassic age data on gabbros and plagiogranites from the Haji-Abad *meta*-ophiolites in the Zagros belt (Moghadam et al., 2017). Unlike the geodynamic reconstruction proposed by McCall and Kidd (1982) and Burg (2018), the re-interpretation of the Bajgan Complex as Mesozoic *meta*-ophiolites implies the existence of a single oceanic basin actively spreading during the Jurassic – Early Cretaceous and separating the Arabian and Lut passive margins without the interposition of a micro-continental block (Fig. 11a). At this time, there is no evidence for an active subduction zone or subduction-related magmatism in the entire Makran domain (Fig. 11a).

4.3.2. Early Cretaceous stage: First subduction inception

During the Early Cretaceous, the kinematic evolution in the Neo-Tethys realm changed with the onset of convergence between the Arabian Plate and the Lut Block (e.g., Agard et al., 2011; Barrier et al., 2018). This convergence was accommodated by the nucleation of subduction zones, as recorded by both arc magmatism and HP/LT metamorphism within the neighbouring Neo-Tethyan orogenic belts (e.g., Agard et al., 2006; Burg, 2011; Angiboust et al., 2016; Moghadam et al.,

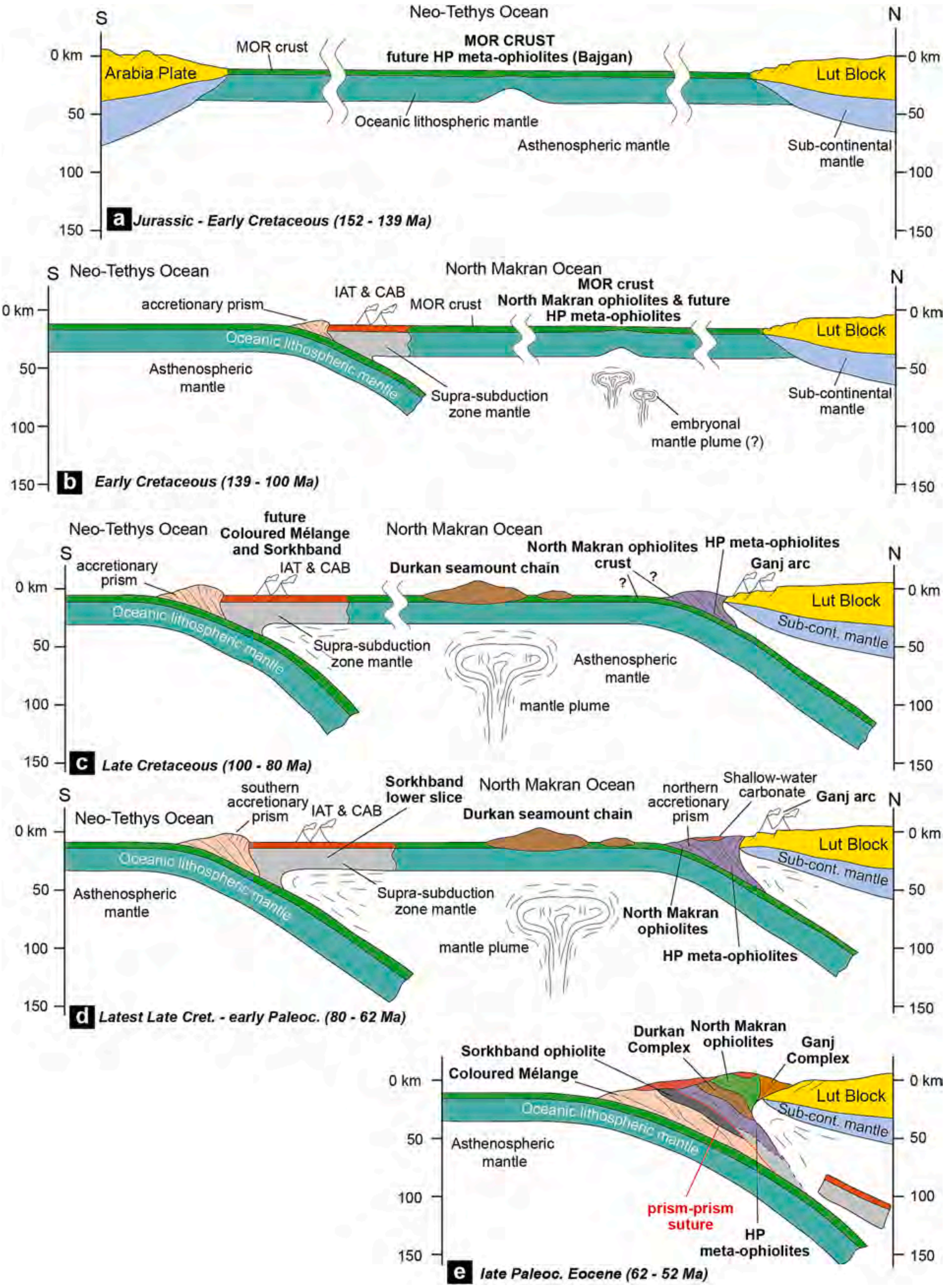

Fig. 11. 2D lithospheric-scale cartoons showing the Jurassic – Eocene geodynamic history for the North Makran domain.

2017; Rolland et al., 2020; Muñoz-Montecinos et al., 2021). In the North Makran domain, this convergent kinematics is testified by the formation of an intra-oceanic subduction zone, evidenced by volcanic arc assemblages within the Coloured Mélange and the supra-subduction zone peridotites of the Sorkhband ophiolite (Fig. 11b). In detail, the Early Cretaceous IAT rocks formed within a volcanic arc setting associated with the intra-oceanic subduction of the Neo-Tethys oceanic lithosphere (Fig. 11b). The pelagic sedimentary cover of the volcanic arc rocks within the Coloured Mélange indicate a subduction-related magmatism in a deep-water setting (i.e., forearc; Fig. 11b). Accordingly, the Sorkhband ophiolites represent the upper mantle-lower crust transition of a forearc domain (Fig. 11b). During the Early Cretaceous, the development of the intra-oceanic subduction delineated two distinct oceanic branches in the Makran based on their position relative to the subduction zone, namely the Neo-Tethys Ocean and the North Makran Ocean (Fig. 11b). Thus, the Sorkhband ophiolites, the North Makran ophiolites, and the high pressure *meta*-ophiolites derived from the North Makran Ocean, whereas the Coloured Mélange (Fig. 2b, c) includes the remnants of the Neo-Tethys Ocean. From the Early Cretaceous onwards, the oceanic lithospheres of the two oceanic branches followed different evolutionary paths. The lithosphere of the Neo-Tethys was consumed in the intra-oceanic subduction, whereas the lithosphere of the North Makran Ocean was characterized by continued oceanic spreading and the formation of N- to E-MORB oceanic crust (i.e., North Makran Ophiolites and high pressure *meta*-ophiolites in Fig. 11b). Petrogenetic modelling for E-MORB rocks suggests partial melting of lherzolite enriched by OIB-type chemical components in both garnet- and spinel-facies. This indicates that the asthenospheric mantle beneath the mid-ocean ridge was influenced by plume-type chemical component connected to an embryonal rise of a mantle plume (e.g., Barbero et al., 2020b, 2023c; Saccani et al., 2022a, b). Therefore, the petrogenetic data indicate that the North Makran Ocean during the Early Cretaceous was a mature oceanic basin perched at the rear of the intra-oceanic subduction. It was characterized by an active mid-ocean ridge spreading showing plume-ridge interaction with no evidence of subduction-related magmatism (Fig. 11b).

4.3.3. *Late Cretaceous stage: Second subduction inception and mantle plume activity*

During the Late Cretaceous, the North Makran Ocean experienced significant tectono-magmatic and geodynamic events that modified the physiography of the basin and its northern margin. The tectono-magmatic and tectono-sedimentary evolutions reconstructed for the Durkan and Ganj Complexes record the beginning of plume- and volcanic arc-related magmatism, respectively (Fig. 10,11c). The stratigraphic architecture and geochemistry of the basalts and *meta*-basalts in the Durkan Complex indicate sedimentation and magmatism within a Late Cretaceous seamount chain formed as consequence of an active mantle plume (Fig. 11c). Evidence for this plume includes the clear P-MORB and alkaline nature of the volcanic rocks along with the petrogenetic modelling, which demonstrate partial melting of OIB-type asthenospheric mantle within garnet stability field during the ascent of a mantle plume (Barbero et al., 2021b). In contrast, the Late Cretaceous volcanic arc succession preserved in the Ganj Complex provides evidence of active subduction of oceanic lithosphere. The structural position of the Ganj Complex as the uppermost unit of the North Makran domain, its less intense folding deformation with respect to other tectonic units, and the moderate- to shallow-water marine setting of its eruptions indicate that this arc cannot correspond to the Early Cretaceous arc associated with the intra-oceanic subduction of the Neo-Tethys Ocean (Fig. 11c). In addition, a simple *retro*-deformation analysis based on the top-to-the-south sense of shear of the deformations observed in the different units (see previous sections and Burg et al., 2013) suggest that the original location of the Ganj volcanic arc was to the north of the North Makran Ocean (Fig. 11c). These considerations imply that the Late Cretaceous Ganj arc was associated with the northward subduction of the lithosphere of the North Makran Ocean beneath the Lut Block (Fig. 11c). This conclusion is further supported by the occurrence of *meta*-ophiolites with Late Cretaceous HP-LT metamorphism along the southern margin of the Eurasian Plate (Bröcker et al., 2021; Angiboust et al., 2016; Bonnet et al., 2020a; Agard et al., 2005), which indicates the regional presence of subduction complexes along the northern margin of the Neo-Tethyan oceanic realm. The Late Cretaceous IAT and calc-alkaline volcanic rocks nowadays preserved in the Coloured Mélange indicate that magmatism associated with the intra-oceanic subduction of the Neo-Tethys oceanic lithosphere remained active during this period (Fig. 11c; Saccani et al., 2018; Burg, 2018). Therefore, the Late Cretaceous was characterized by two distinct subduction zones in the Makran Neo-Tethys. Some considerations can be proposed to explain the nucleation of a new subduction zone beneath the continental margin of the Lut Block during the Late Cretaceous. This new subduction could have been induced by the high convergence rate (i.e., slightly more than 6 cm/a) of Arabia and Eurasia between 105–80 Ma (Agard et al., 2007). In this period, such high convergence rate could not have been fully accommodated by the intra-oceanic subduction, thus requiring the formation of a new subduction zone below the Lut Block. In addition, numerical modelling suggested that mantle plume can induce the nucleation of subduction zones both in intra-oceanic settings and beneath continental margins (Whattam and Stern, 2015; Rodriguez et al., 2021; Cloetingh et al., 2021). The ocean-continent transition zone can act as a zone of weakness where a new subduction zone might originate (e.g., Pandey et al., 2019; Zhou et al., 2020). At present, there are insufficient data to fully understand the effective mechanism that led to the subduction of the North Makran Ocean. However, the slightly older age of the plume-related basalts compared to the volcanic arc rocks of the Ganj Complex suggests that a combination of plume activity, fast convergence rate, and possible pre-existing weakness along the Lut margin contributed to its formation.

4.3.4. *Latest Cretaceous – Early Paleocene stage: Progressive oceanic closure by coexistence of two subduction zones*

During this period convergence in the Neo-Tethys realm led to the progressive closure of the North Makran Ocean, the incorporation of fragments of its oceanic lithosphere in the northern subduction complex, and in the formation of the tectonic stack nowadays observed in the North Makran (Fig. 11d). The early stages of oceanic lithosphere accretion are recorded by the deformation history of the *meta*-ophiolites and the North Makran ophiolites. In fact, the features of the D1 and D2 deformation phases, as along with the thermobarometric and geochronological data from the *meta*-ophiolites (Delaloye and Desmons, 1980; Hunziker et al., 2017; Pandolfi et al., 2021) indicate underplating at the base of the subduction complex involving slices of the North Makran oceanic lithosphere (Fig. 11d). These data agree with dating and P-T paths obtained for other blueschist units found in the area of Iranshar, at the eastern termination of the North Makran domain (Omrani et al., 2017; Bröcker et al., 2021), as well as in the southeast Zagros (Agard et al., 2011; Angiboust et al., 2016; Moghadam et al., 2017; Bonnet et al., 2020a). Together, this evidence strongly supports the existence of an active subduction complex during Late Cretaceous at the southern margin of the Eurasian Plate. Likewise, the structural evolution of the non-metamorphic North Makran ophiolites and the features of the D1 deformation phase suggest that these units were incorporated at shallow structural level within the same subduction complex (Fig. 11d). Due to the absence of a metamorphic recrystallization, the age of their incorporation into the prism can be inferred from the age of the stratigraphic succession of the units and the oldest sedimentary succession resting unconformably on top of them. According to Dolati (2010), Burg et al. (2013), and Burg (2018), the unconformable deposition of a Maastrichtian-Paleocene succession above the already deformed Remeshk-Mokhtarabad and Fannuj-Maskutan ophiolites indicate that the accretion of the North Makran ophiolites occurred during the latest Cretaceous (Figs. 10, 11d).

During the Early Paleocene, a significant amount of shortening induced multiple compressional tectonic events in the Makran, as recorded by the structural evolution of the Durkan Complex, the Sorkhband ophiolites, and the Coloured Mélange (Fig. 11d). Starting with the Durkan Complex, the occurrence of the D1 phase sub-isoclinal folds and shear zones along the fold limbs indicate the imbrication of several tectonic slices detached from a subducting seamount during compressional tectonic events (Barbero et al., 2023a). P-T data indicate the underplating of seamount material at blueschist facies (Barbero et al., 2023a). The structural setting of the Sorkhband ophiolites also records significant shortening; specifically, the reverse shear zones along the basal and roof tectonic contact of this unit indicates its emplacement during compressional tectonic events. It is worth noting that the basal shear zone is responsible for the overthrusting of the former SSZ forearc crust-mantle sequence onto the southern subduction complex, now represented by the Coloured Mélange (Fig. 11d). Finally, the structural setting of the Coloured Mélange, with reverse shear zones separating imbricated tectonic slices, records a significant amount of shortening and compressive tectonics. The lithological composition of the rocks in the tectonic slices and their Jurassic to Early Paleocene ages likely indicate that they correspond to fragments of oceanic lithosphere of the Neo-Tethys Ocean and, its sedimentary cover, as well as trench successions deformed in the frontal part of a subduction complex (Burg, 2018; Saccani et al., 2018). In addition, the occurrence of Early – Late Cretaceous IAT and CAB basalts indicate that also the forearc crust were involved in the compressional events that formed the Coloured Mélange. Unfortunately, age constraints for this shortening are still limited, although they can be indirectly inferred from the youngest ages of the deformed succession and the oldest ages of the unconformable succession resting on top of the Coloured Mélange, the Sorkhband, and the Durkan Complex. The evidence that the youngest age of the blocks in the Coloured Mélange is Early Paleocene (McCall, 1983), and that Late Paleocene – Eocene deposits unconformably rest onto the Durkan Complex (McCall, 1983; Barbero et al., 2023a) temporally constrain the deformation to the Paleocene. However, older tectonic accretion during the Cretaceous cannot be ruled out. Another consequence of this significant amount of shortening is the folding and faulting of the Ganj arc along southern margin of the Lut Block, as indicated by its structural setting (Fig. 11d).

4.3.5. *Late Paleocene – Eocene stage: Amalgamation of two subduction complexes*

At a larger scale, the compressive deformation that occurred during the latest Cretaceous – Early Paleocene resulted in the final closure of the North Makran Ocean. This event was marked by the slicing of the SSZ crust-mantle section onto the southern subduction complex, the complete subduction of the remaining oceanic crust beneath the Lut Block, and the amalgamation of the northern and the southern subduction complexes (Fig. 11e). The North Makran can thus be considered as a true suture zone between two distinct accretionary complexes, which were associated with distinct subduction zones and recorded distinct accretionary histories (Fig. 12). Finally, the deposition of Eocene siliciclastic and carbonatic successions unconformably sealed the suture between the two distinct accretionary complexes (Fig. 11e, 12). Meanwhile, Eocene to Oligocene turbidites were deposited in an active trench basin located to the south of the North Makran domain. The history of the Makran continued with the progressive southward migration of both the trench-thrust top basins and the deformation front, leading to the imbrication of the Inner, Outer, and Coastal Makran from the Eocene to the present day (see Burg, 2018).

4.4. *Broad implication of the new model for the geodynamic reconstruction of the Alpine-Himalayan suture zones*

The new model for the North Makran suture zone significantly changes the Late Jurassic – Eocene geodynamic scenario for the Makran sector of the Neo-Tethys in two main aspects. The first concerns the physiography of the Neo-Tethys Ocean during the Late Jurassic – Cretaceous, which involved a unique oceanic basin that separated the Lut Block (i.e., the Eurasian margin) from the Arabian Plate. This ocean was characterized by the abundance of plume-related OIB-type magmatic rocks formed within seamounts. The second aspect involves the closure of the Neo-Tethys Ocean, which occurred through the generation of two coeval subduction zones. To critically evaluate our new model, we briefly compare it with the neighbouring sectors of the Alpine-Himalayan orogenic system, focusing the discussion on these two points.

The physiography of the Neo-Tethys ocean, as proposed in our model, is comparable to the geodynamic models suggested for the Neo-Tethys by several authors based on data from the neighbouring Zagros and Caucasus collisional belts (e.g., Ghasemi and Talboot, 2006; Saccani et al., 2013; Moghadam and Stern, 2015; Rolland et al., 2020). In these models, an oceanic lithosphere with MORB to OIB crustal rocks has been reconstructed based on to the features of ophiolites and *meta*-ophiolites. Similar to our model, the OIB-magmatic rocks have been genetically ascribed to Cretaceous mantle plume magmatism within the Neo-Tethys Ocean (e.g., Hässig et al., 2013; Rolland et al., 2020). In the Himalayan sector of the Alpine-Himalayan orogenic system, OIB-type basalts are associated with some Cretaceous ophiolites now scattered from the Pakistan-India border to Myanmar (e.g., Xia et al., 2008; Dai et al., 2012; Khogenkumar et al., 2016, 2021). These rocks have been interpreted as evidence of hot spot and plume-related magmatism that was responsible

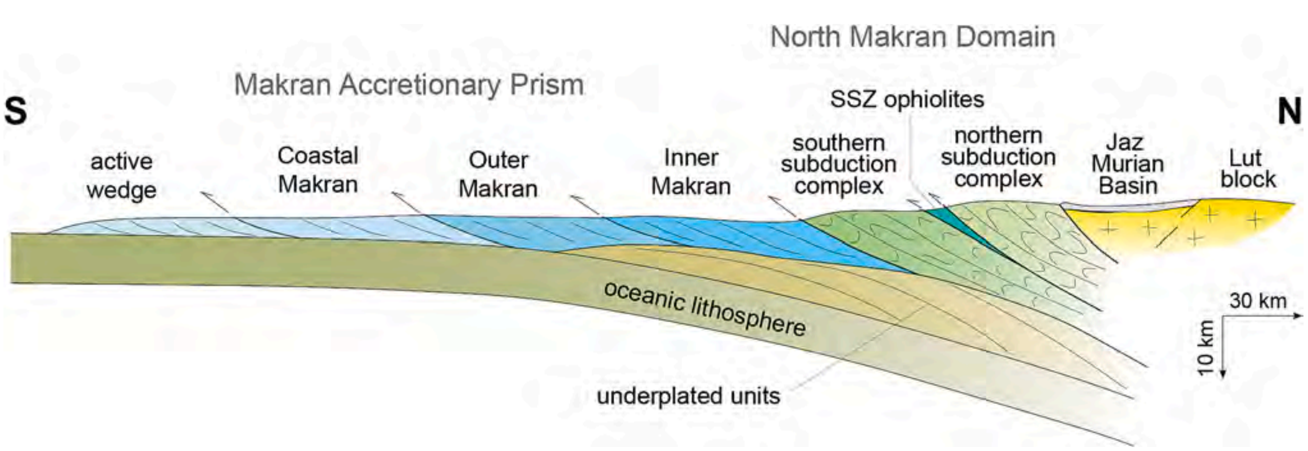

Fig. 12. Schematic present-day 2D schematic section of the Makran domain along a N-S transect showing the amalgamation of the Cretaceous – Paleocene southern and northern ophiolite-bearing subduction complexes with the post-Eocene – present-day Accretionary Prism (modified from Platt et al., 1985; Kopp et al., 2000; Burg, 2018). Abbreviation: SSZ: supra subduction zone.

for the formation of seamount and seamount chain within the Neo-Tethys Ocean during the Cretaceous (e.g., Khogenkumar et al., 2016). This comparison with the neighbouring segments of the Alpine-Himalayan suture zone validates our model, highlighting how the Neo-Tethys ocean was dominated by a Cretaceous mantle-plume activity, which produced a composite oceanic lithosphere characterized by MORB crustal rocks interspersed with patches of or isolated seamount of OIB-type basalts.

The Neo-Tethys ocean began its closure in the early Cretaceous in response to the general movement of the Africa-Arabia and India Plates toward the Eurasian Plate (e.g., Barrier et al., 2018; van Hinsbergen et al., 2019). In our new model, this convergence was accommodated by two subduction zones, associated with distinct subduction complexes and volcanic arcs. This conclusion fits well with the geodynamic models proposed for the neighbouring Zagros and Himalayan orogenic belts. In the Zagros belts, several authors proposed the existence of two coeval subduction zones within the Neo-Tethys during the Late Cretaceous (e.g., Ghasemi and Talbot, 2006; Agard et al., 2005; Saccani et al., 2013; Monsef et al., 2018; Bonnet et al., 2020b). Similar to our model, one subduction was intraoceanic and was associated with the formation of oceanic lithosphere in a supra-subduction zone setting. The remnants of this setting are now represented by the supra-subduction zone ophiolites that typically occur in the Zagros belt and in the Oman mountains, which can be correlated with the Sorkhband ophiolites in our model (e.g., Moghadam and Stern, 2015; Moghadam et al., 2021). A Late Cretaceous intraoceanic subduction is generally depicted in most geodynamic models for the Himalayan collisional belts from Pakistan to Myanmar (e.g., Malpas et al., 2003; Mahéo et al., 2004; Burg, 2011; Searle, 2019; Khogenkumar et al., 2021; Ullah et al., 2023; Salam et al., 2024), supporting the idea that the southern subduction zone proposed in our model was a regional-scale features that extended across the entire Neo-Tethys ocean during the Cretaceous. The second, northernmost subduction zone hypothesized in our model nucleated beneath the Eurasian margin and was responsible for the formation of a volcanic arc at the southern margin of the Lut Block (Fig. 11c, d). In the Zagros belt, some authors proposed a similar scenario with a subduction zone dipping beneath the continental crust of the Sanandaj-Sirjan block (e.g., Agard et al., 2005; Saccani et al., 2013; Monsef et al., 2018). However, other researchers proposed an alternative scenario implying a subduction associated with a forearc spreading centre close to the Eurasian margin (e.g., Moghadam and Stern, 2015; Bonnet et al., 2020b; Moghadam et al., 2023). In the Pakistani and Indian segments of the Alpine-Himalayan collisional systems, there is a general agreement on the nucleation of a subduction zone beneath the Eurasian margin resulting in the formation of a volcanic arc whose remnants are now found from Pakistan to the Himalayan belt (e.g., Malpas et al., 2003; Burg, 2011; Ullah et al., 2023). Some controversies among the various models concern the existence of a back-arc basin north of this arc, which closed with an additional subduction (e.g., Mahéo et al., 2004). Despite some differences that may be related to local complexities along the entire Alpine-Himalayan system, the comparison of our model with those proposed for neighbouring belts strongly validates our conclusions.

5. Conclusions

The North Makran domain, located in southeast Iran, is a large stack of tectonic units entirely exposed on land. It represents the backstop of the present-day Makran Accretionary Prism and preserves the pre-Eocene record of geodynamic events driven by the convergence between the Arabian and Eurasian Plates. Previous studies suggested that these tectonic units represent remnants of oceanic and continental domains (e.g., McCall, 2002; Hunziker et al., 2015; Burg, 2018; Saccani et al., 2018). Specifically, they originate from the North Makran Ocean, which was located south of the Lut Block, and the Bajgan-Durkan continental block. This continental block separated the North Makran Ocean from the main Neo-Tethys Ocean. This review, however, proposes a different scenario: the North Makran tectonic units derived from the North Makran Ocean and the Neo-Tethys, through two distinct north-dipping subductions, without any intervening microcontinent. The first, southernmost subduction initiated in the Early Cretaceous in an intra-oceanic setting within the Neo-Tethys Ocean, thus marking the separation of the North Makran Ocean (to the north) from the main Neo-Tethys Ocean (to the south). The northernmost subduction developed along the southern edge of the Lut Block during the Late Cretaceous, triggered by the increased convergence between Arabia and Eurasia (Agard et al., 2011). As result, two distinct subduction complexes – southern and northern – both bearing HP-LT metamorphic units, coexisted during the Late Cretaceous. The closure of the North Makran Ocean during the Paleocene was marked by basin-scale shortening, likely driven by the subduction of a seamount chain (the Durkan Complex) in the northern subduction zone (Fig. 11). Seamount subduction caused a decrease of the subduction rate, leading to abrupt shortening of the oceanic area between the two subduction zones to maintain ongoing plate convergence (Fig. 11e). This shortening propagated southward, affecting the southern intra-oceanic supra-subduction mantle (the Sorkhband ophiolites), which was compressed between the northern and the southern subduction complexes (Fig. 11e). This process resulted in the amalgamation of the two subduction complexes, incorporating slices of the Sorkhband ophiolites between them. (Fig. 12). Our model emphasizes the occurrence of dual subduction zones during the closure of the North Makran Ocean and underscore the critical role of seamount chain subduction. Similar processes have been documented in other convergent margins worldwide (e.g., Dominguez et al., 1998; Cloos, 1992; Kerr et al., 2002). The striking parallels between our model and those proposed for neighbouring Alpine-Himalayan suture zones strongly support our conclusions, offering valuable insights for future research on the Neo-Tethys realms at a regional-scale.

CRediT authorship contribution statement

Edoardo Barbero: Writing – review & editing, Writing – original draft, Visualization, Investigation, Conceptualization. **Luca Pandolfi:** Writing – review & editing, Project administration, Investigation, Conceptualization. **Morteza Delavari:** Writing – review & editing, Investigation, Conceptualization. **Asghar Dolati:** Writing – review & editing, Investigation, Conceptualization. **Emilio Saccani:** Writing – review & editing, Writing – original draft, Project administration, Investigation, Funding acquisition, Conceptualization. **Maria Di Rosa:** Writing – review & editing, Visualization, Investigation, Conceptualization. **Michele Marroni:** Writing – review & editing, Writing – original draft, Project administration, Investigation, Funding acquisition, Conceptualization.

Declaration of competing interest

The authors declare that they have no known competing financial interests or personal relationships that could have appeared to influence the work reported in this paper.

Acknowledgement

The research has been funded by the Darius Project (Head M. Marroni), PRA project of the Pisa University (Head S. Rocchi), and the IGG-CNR, FAR-2018 Project of the Ferrara University (Head E. Saccani). We sincerely thank Mr. Ahmad Behboodi for his fundamental assistance in organizing field work, and PhD student Ahmad Nateghpour from Kharazmi University for his help during field work. Rita Catanzariti, Marco Chiari, Federico Farina, Chiara Frassi, Antonio Langone, Valeria Luciani, Leila Vahedi, and Federica Zaccarini, are also thanked for the scientific contributions provided through the time. We would like to express our gratitude to an anonymous reviewer and to H.S. Moghadam and S. Ao for their thorough reviews from which we have greatly benefited in revising our paper. The Associate Editor J.M. Huizenga is warmly acknowledged for editorial handling and for his useful comments on the earlier version of this manuscript.

Data availability

Data will be made available on request.

References

Agard, P., Omrani, L., Jolivet, L., Mouthereau, F., 2005. Convergence history across Zagros (Iran): constraints from collisional and earlier deformation. Int. J. Earth Sci. (geol Rundsch) 94 (380–398), 401–419. https://doi.org/10.1007/s00531-005-0481-4.

Agard, P., Monié, P., Gerber, W., Omrani, J., Molinaro, M., Meyer, B., Labrousse, L., Vrielynck, B., Jolivet, L., Yamato, P., 2006. Transient, synobduction exhumation of Zagros blueschists inferred from P–T, deformation, time and kinematic constraints: Implications for Neotethyan wedge dynamics. J. Geophys. Res. 111 (B11).

Agard, P., Jolivet, L., Vrielynck, B., Burov, E., Monié, P., 2007. Plate acceleration: the obduction trigger? Earth Planet. Sci. Lett. 258 (3–4), 428–441.

Agard, P., Omarani, J., Jolivet, L., Whitechurch, H., Vrielynck, B., Spakman, W., Monié, P., Meyer, B., Wortel, R., 2011. Zagros orogeny: a subduction-dominated process. Geol. Mag. 148, 692–725. https://doi.org/10.1017/S001675681100046X.

Angiboust, S., Agard, P., Glodny, J., Omrani, J., Oncken, O., 2016. Zagros blueschists: Episodic underplating and long-lived cooling of a subduction zone. Earth Planet. Sci. Lett. 443, 48–58. https://doi.org/10.1016/j.epsl.2016.03.017.

Arvin, M., Babaei, A.A., Ghadami, Gh., Dargahi, S., Shakerardekani, A.R., 2005. The origin of the Kahnouj ophiolitic complex, SE of Iran: constraints from whole rock and mineral chemistry of the Bande-Zeyarat gabbroic complex. Ofioliti 30, 1–14.

Barbero, E., Delavari, M., Dolati, A., Saccani, E., Marroni, M., Catanzariti, R., Pandolfi, L., 2020a. The Ganj Complex reinterpreted as a Late Cretaceous volcanic arc: Implications for the geodynamic evolution of the North Makran domain (southeast Iran). J. Asian Earth Sci. 195. https://doi.org/10.1016/j.jseaes.2020.104306.

Barbero, E., Delavari, M., Dolati, A., Vahedi, L., Langone, A., Marroni, M., Pandolfi, L., Zaccarini, F., Saccani, E., 2020b. Early Cretaceous Plume–Ridge Interaction Recorded in the Band-e-Zeyarat Ophiolite (North Makran Iran): New Constraints from Petrological, Mineral Chemistry, and Geochronological Data. Minerals 10, 1100. https://doi.org/10.3390/min10121100.

Barbero, E., Pandolfi, L., Delavari, M., Dolati, A., Saccani, E., Catanzariti, R., Luciani, V., Chiari, M., Marroni, M., 2021a. The western Durkan Complex (Makran Accretionary Prism, SE Iran): A Late Cretaceous tectonically disrupted seamounts chain and its role in controlling deformation style. Geosci. Front. 12. https://doi.org/10.1016/j.gsf.2020.12.001.

Barbero, E., Zaccarini, F., Delavari, M., Dolati, A., Saccani, E., Marroni, M., Pandolfi, L., 2021b. New evidence for Late Cretaceous plume-related seamounts in the Middle East sector of the Neo-Tethys: Constraints from geochemistry, petrology, and mineral chemistry of the magmatic rocks from the western Durkan Complex (Makran Accretionary Prism, SE Iran). Lithos 396–397. https://doi.org/10.1016/j.lithos.2021.106228.

Barbero, E., Di Rosa, M., Pandolfi, L., Delavari, M., Dolati, A., Zaccarini, F., Saccani, E., Marroni, M., 2023a. Deformation history and processes during accretion of seamounts in subduction zones: The example of the Durkan Complex (Makran, SE Iran). Geosci. Front. 14 (2). https://doi.org/10.1016/j.gsf.2022.101522.

Barbero, E., Delavari, M., Dolati, A., Langone, A., Pandolfi, L., Marroni, M., and Saccani, E., 2023c. New geochemical and age data on the Bajgan Complex (Makran Accretionary Prism, SE Iran): Implications for the redefinition of its tectonic setting of Formation from Paleozoic continental basement to a Cretaceous Oceanic domain. In: International conference on Mediterranean Geoscience Union, MedGU 2021: Recent Research on Sedimentology, Stratigraphy, Paleontology, Tectonics, Geochemistry, Volcanology and Petroleum Geology 163-165.

Barbero, E., Pandolfi, L., Delavari, M., Dolati, A., Saccani, E., Catanzariti, R., Marroni, M., 2023b. The journey of the Band-e-Zeyarat ophiolite (Makran Accretionary Wedge, SE Iran) from the mid-ocean ridge to the accretionary complex: new insights from its sedimentary cover and associated basaltic dykes and sills. J. Geol. Soc. London 180 (6). https://doi.org/10.1144/jgs2023-043.

Barrier, E., Vrielynck, B., Brouillet, J.F., Brunet, M.F., 2018. Paleotectonic Reconstruction of the Central Tethyan Realm. Tectono-Sedimentary-Palinspastic maps from Late Permian to Pliocene. Atlas of 20 maps (scale: 1:15.000.000). CCGM/CGMW, Paris, http://www.ccgm.org.

Beccaluva, L., Di Girolamo, P., Macciotta, G., Morra, V., 1983. Magma affinities and fractionation trends in ophiolites. Ofioliti 8 (3), 307–324.

Behzadi, K.H., Shahabpour, J., 2011. An emplacement model for Esfandagheh and Faryab ultramafic-mafic complexes, Kerman province, south east Iran. Neues Jahrbuch Fur Geologie Und Paläontologie 262, 25–42.

Berberian, F., Muir, I.D., Pankhurst, R.J., Berberian, M., 1982. Late Cretaceous and early Miocene andean-type plutonic activity in northern Makran and Central Iran. J. Geol. Soc. London 139, 605–614.

Bonnet, G., Agard, P., Angiboust, S., Monié, P., Fournier, M., Caron, B., Omrani, J., 2020a. Structure and metamorphism of a subducted seamount (Zagros suture, Southern Iran). Geosphere 16, 62–81. https://doi.org/10.1130/GES02134.1.

Bonnet, G., Agard, P., Whitechurch, H., Fournier, M., Angiboust, S., Caron, B., Omrani, J., 2020b. Fossil seamount in southeast Zagros records intraoceanic arc to back-arc transition: New constraints for the evolution of the Neotethys. Gondwana Res. 81, 423–444. https://doi.org/10.1016/j.gr.2019.10.019.

Bortolotti, V., Chiari, M., Göncüoğlu, M.C., Principi, G., Saccani, E., Tekin, U.K., Tassinari, R., 2018. The Jurassic-Early Cretaceous basalt–chert association in the ophiolites of the Ankara Mélange, east of Ankara, Turkey: age and geochemistry. Geol. Mag. 155 (2), 451–478. https://doi.org/10.1017/S0016756817000401.

Bröcker, M., Omrani, H., Berndt, J., Moslempour, M.E., 2021. Unravelling metamorphic ages of suture zone rocks from the Sabzevar and Makran areas (Iran): Robust age constraints for the larger Arabia–Eurasian collision zone. J. Metam. Geol. 39, 1099–1129. https://doi.org/10.1111/jmg.12603.

Burg, J.-P., 2018. Geology of the onshore Makran accretionary wedge: Synthesis and tectonic interpretation. Earth Sci. Rev. 185, 1210–1231.

Burg, J.-P., Bernoulli, D., Smit, J., Dolati, A., Bahroudi, A., 2008. A giant catastrophic mud-and-debris flow in the Miocene Makran. Terra Nova 20, 188–193.

Burg, J.-P., Dolati, A., Bernoulli, D., Smit, J., 2013. Structural style of the Makran tertiary accretionary complex in SE Iran. In: Al Hosani, K., Roure, F., Ellison, R., Lokier, S. (Eds.), Lithosphere Dynamics and Sedimentary Basins: The Arabian Plate and Analogues. Frontiers in Earth Sciences, Springer, Heidelberg, pp. 239-259.

Burg, J.-P., 2011. The Asia–Kohistan–India collision: review and discussion. In: Brown, D., Ryan, P.D. (Eds.), Arc-Continent Collision. Frontiers in Earth Sciences. Springer-Verlag, Berlin, Heidelberg, pp. 279–309.

Chauvet, F., Lapierre, H., Maury, R.C., Bosch, D., Basile, C., Cotten, J., Brunet, P., Campillo, S., 2011. Triassic alkaline magmatism of the Hawasina Nappes: Post-breakup melting of the Oman lithospheric mantle modified by the Permian Neotethyan Plume. Lithos 122, 122–136.

Cloetingh, S., Koptev, A., Kovács, I., Gerya, T., Beniest, A., Willingshofer, E., Ehlers, T.A., Andrić-Tomašević, N., Botsyun, S., Eizenhöfer, P., François, T., Beekman, F., 2021. Plume-induced sinking of intra-continental lithospheric mantle: An overlooked mechanism of subduction initiation? Geochem. Geophys. Geosyst. 22, e2020GC009482. https://doi.org/10.1029/2020GC009482.

Cloos, M., 1992. Thrust-type subduction-zone earthquakes and seamount asperities: A physical model for seismic rupture. Geology 20 (7), 601–604. https://doi.org/10.1130/0091-7613(1992)020<0601:TTSZEA>2.3.CO;2.

Dai, J., Wang, C., Li, Y., 2012. Relicts of the Early Cretaceous seamounts in the central-western Yarlung Zangbo Suture Zone, southern Tibet. J. Asian Earth Sci. 53, 25–37. https://doi.org/10.1016/j.jseaes.2011.12.024.

Delaloye, M., Desmons, J., 1980. Ophiolites and mélange terranes in Iran: A geochronological study and its paleotectonic implications. Tectonophysics 68, 83–111.

Delavari, M., Dolati, A., Marroni, M., Pandolfi, L., Saccani, E., 2016. Association of MORB and SSZ ophiolites along the shear zone between Coloured Mélange and Bajgan Complexes (North Maran, Iran): Evidence from the Sorkhband area. Ofioliti 41, 21–34. https://doi.org/10.4454/ofioliti.v41i1.440.

Dercourt, J., Zonenshian, L.P., Ricou, L.-E., Kazmin, V.G., LePichon, X., Knipper, A.L., Grandjacquet, C., Sbortshikov, M., Geyssant, J., Lepvrier, C., Pechersky, D.H., Boulin, J., Sibuet, J.-C., Savostin, L.A., Sorokhtin, O., Westphal, M., Bazhenov, M.L., Lauer, J.P., Biju-Duval, B., 1986. Geological evolution of the Tethys Belt from the Atlantic to the Pamirs since the Lias. Tectonophysics 123, 241–315.

Desmons, J., Beccaluva, L., 1983. Mid-Ocean ridge and island-arc affinities in ophiolites from Iran: Palaeographic implications. Chem. Geol. 39, 39–63.

Dilek, Y., Furnes, H., 2009. Structure and geochemistry of Tethyan ophiolites and their petrogenesis in subduction rollback systems. Lithos 113, 1–20. https://doi.org/10.1016/j.lithos.2009.04.022.

Dilek, Y., Furnes, H., 2019. Tethyan ophiolites and Tethyan seaways. J. Geol. Soc. London 10. https://doi.org/10.1144/jgs2019-129.

Dolati, A., Burg, J.-P., 2013. Preliminary fault analysis and paleostress evolution in the Makran Fold-and-Thrust Belt in Iran. In: Al Hosani, K., Roure, F., Ellison, R., Lokier, S. (Eds.), Lithosphere Dynamics and Sedimentary Basins: The Arabian Plate and Analogues. Frontiers in Earth Sciences, Springer, Heidelberg, pp. 261–277.

Dolati, A., 2010. Stratigraphy, Structure Geology and Low-temperature Thermochronology Across the Makran Accretionary Wedge in Iran. PhD thesis, ETH Zurich, 165 pp.

Dominguez, S., Lallemand, S.E., Malavieille, J., von Huene, R., 1998. Upper plate deformation associated with seamount subduction. Tectonophysics 293, 207–224. https://doi.org/10.1016/S0040-1951(98)00086-9.

Dorani, M., Arvin, M., Oberhänsli, R., Dargahi, S., 2017. P-T evolution of metapelites from the Bajgan complex in the Makran accretionary prism, south eastern Iran. Geochemistry 77, 459–475. https://doi.org/10.1016/j.chemer.2017.07.004.

Engdahl, R.E., Jackson, J.A., Myers, S.C., Bergman, E.A., Priestley, K., 2006. Relocation and assessment of seismicity in the Iran region. Geophys. J. Int. 167, 761–778. https://doi.org/10.1111/j.1365-246X.2006.03127.x.

Esmaeili, R., Xiao, W., Ebrahimi, M., Zhang, J.E., Zhang, Z., El-Rahman, Y.A., Han, C., Wan, B., Ao, S., Song, D., Shahabi, S., Aouizerat, A., 2019. Makran ophiolitic basalts (SE Iran) record late Cretaceous Neotethys plume-ridge interaction. Int. Geol. Rev. https://doi.org/10.1080/00206814.2019.1658232.

Esmaeili, R., Xiao, W., Griffin, W.L., Moghadam, H.S., Zhang, Z., Ebrahimi, M., Zhang, J., Wan, B., Ao, S., Bhandari, S., 2020. Reconstructing the source and growth of the Makran Accretionary Complex: constraints from detrital zircon U-Pb geochronology. Tectonics 39 (2). https://doi.org/10.1029/2019TC005963.

Esmaeili, R., Ao, S., Shafaii Moghadam, H., Zhang, Z., Griffin, W.L., Ebrahimi, M., Xiao, W., Wan, B., Bhandari, S., 2021. Amphibolites from Makran accretionary complex record Permian-Triassic Neo-Tethyan evolution. Int. Geol. Rev. https://doi.org/10.1080/00206814.2021.1946663.

Farhoudi, G., Karig, D.E., 1977. Makran of Iran and Pakistan as an active arc system. Geology 5, 664. https://doi.org/10.1130/0091-7613(1977) 5<664:MOIAPA>2.0.CO;2.

Fergusson, C.L., Nutman, A.P., Mohajjel, M., Bennett, V.C., 2016. The Sanandaj–Sirjan Zone in the Neo-Tethyan suture, western Iran: Zircon U–Pb evidence of Late Palaeozoic rifting of northern Gondwana and mid-Jurassic orogenesis. Gondw. Res. 40, 43–57.
Festa, A., Barbero, E., Remitti, F., Ogata, K., Pini, G.A., 2022. Mélanges and chaotic rock units: Implications for exhumed subduction complexes and orogenic belts. Geosyst. Geoenvironm. 1 (2), 100030. https://doi.org/10.1016/j.geogeo.2022.100030.
Furnes, H., Dilek, Y., Zhao, G., Safonova, I., Santosh, M., 2020. Geochemical characterization of ophiolites in the Alpine-Himalayan Orogenic Belt: Magmatically and tectonically diverse evolution of the Mesozoic Neotethyan oceanic crust. Earth Sci. Rev. 208. https://doi.org/10.1016/j.earscirev.2020.103258.
Ghasemi, S.M., Mehrabi, B., Ganerod, M., Holwell, D.A., Yang, H.J., Karimi, S.B., 2022b. Origin of Fe-Ti mineralization in the Late Jurassic to Early Cretaceous Kahnouj ophiolitic complex, Makran accretionary prism. SE Iran. Lithos 426–427, 106784. https://doi.org/10.1016/j.lithos.2020.105832.
Ghasemi Siani, M., Mehrabi, M., Neubauer, F., Cao, S., Lentz, D.R., 2021. Geochronology, geochemistry, and origin of plagiogranitic rocks and related granitic dikes in the Dar Gaz district, Kahnouj ophiolite complex, SE Iran: analysis of their petrogenesis in a back-arc tectonic setting. Lithos 380–381. https://doi.org/10.1016/j.lithos.2020.105832.
Ghasemi Siani, M., Mehrabi, B., Neubauer, F., Cao, S., 2022a. Trace element geochemistry of zircons from the Kahnouj ophiolite complex: implications for petrogenesis and geodynamic setting Arabian. J. Geosci. 14, 1377. https://doi.org/10.1007/s12517-021-07575-5.
Ghasemi, A., Talbot, C.J., 2006. A new tectonic scenario for the Sanandaj–Sirjan Zone (Iran). J. Asian Earth Sci. 26 (6), 683–693. https://doi.org/10.1016/j.jseaes.2005.01.003.
Ghazi, A.M., Hassanipak, A.A., Mahoney, J.J., Duncon, R.A., 2004. Geochemical characteristics, 40Ar-39Ar ages and original tectonic setting of the Band-e-Zeyarat/Dar Anar ophiolite, Makran accretionary Prism, S.E. Iran. Tectonophysics 193, 175–196.
Glennie, K.W., Hughes Clarke, M.W., Boeuf, M.G.A., Pilaar, W.F.H., Reinhardt, B.M., 1990. Inter-relationship of Makran-Oman Mountains belts of convergence. In: Robertson, A.H.F., Searle, M.P., Ries, A.C. (Eds.), The Geology and Tectonics of the Oman Region. Geological Society, London Special Publications, pp. 773–786.
Grando, G., McClay, K., 2007. Morphotectonics domains and structural styles in the Makran accretionary prism, offshore Iran. Sed. Geol. 196, 157–179.
Haase, K.M., Devey, C.W., 1996. Geochemistry of lavas from the Ahu and Tupa volcanic fields, Easter Hotspot, Southeast Pacific: Implications for magma genesis near a spreading axis. Earth Planet. Sci. Lett. 137, 129–143.
Haghipour, N., Burg, J.-P., Kober, F., Zeilinger, G., Susan, I.-O., Kubik, P.W., Mohammad, F., 2012. Rate of crustal shortening and non-Coulomb behaviour of an active accretionary wedge: the folded fluvial terraces in Makran (SE, Iran). Earth Planet. Sci. Lett. 355–356, 187–198.
Hassanipak, A.A., Ghazi, A.M., Wampler, J.M., 1996. Rare earth element characteristics and K-Ar ages of the Bande-Zeyarat ophiolite complex, southeastern Iran. Canadian Journal of Earth Science 33, 1534–1542.
Hassanzadeh, J., Wernicke, B.P., 2016. The Neotethyan Sanandaj-Sirjan zone of Iran as an archetype for passive margin-arc transitions. Tectonics 35 (3), 586–621.
Hässig, M., Rolland, Y., Sosson, M., Galoyan, G., Müller, C., Avagyan, A., Sahakyan, L., 2013. New structural and petrological data on the Amasia ophiolites (NW Sevan–Akera suture zone, Lesser Caucasus): insights for a large-scale obduction in Armenia and NE Turkey. Tectonophysics 588, 135–153. https://doi.org/10.1016/j.tecto.2012.12.003.
Hunziker, D., 2014. Magmatic and metamorphic history of the North Makran ophiolites and blueschists (SE Iran): Influence of Fe3+/Fe2+ratios in blueschist facies minerals on geothermobarometric calculations. Doctoral Dissertation. Eidgenössische Technische Hochschule ETH Zurich no. 21778.
Hunziker, D., Burg, J.-P., Bouilhol, P., von Quadt, A., 2015. Jurassic rifting at the Eurasian Tethys margin: Geochemical and geochronological constraints from granitoids of North Makran, southeastern Iran. Tectonics 34, 571–593.
Hunziker, D., Burg, J.-P., Moulas, E., Reusser, E., Omrani, J., 2017. Formation and preservation of fresh lawsonite: geothermobarometry of the North Makran Blueschists, southeast Iran. J. Metam. Geol. 35 (8), 871–895. https://doi.org/10.1111/jmg.12259.
Jannessary, M.R., Melcher, F., Lodziak, J., Meisel, T.C., 2012. Review of platinum-group element distribution and mineralogy in chromitite ores from southern Iran. Ore Geology Review 48, 278–305.
Kananian, A., Juteau, T., Bellon, H., Darvishzadeh, A., Sabzehi, M., Whitechurch, H., Ricou, L.-E., 2001. The ophiolite massif of Kanuj (western Makran, southern Iran): new geological and geochronological data. Comptes Rendus De L'academie Des Science 332 (9), 543–552.
Kerr, A., Aspden, J., Tarney, J., Pilatasasig, L., 2002. The nature and provenance of accreted oceanic terranes in western Ecuador: geochemical and tectonic constraints. J. Geol. Soc. London 159, 577–594.
Khalatbari-Jafari, M., Babaie, H.A., Moslempour, M.E., Ghaderi, M., 2016. Mid-Ocean-ridge to suprasubduction geochemical transition in the hypabissal and extrusive sequences of major Upper Cretaceous ophiolites of Iran. Tectonic evolution, Collision and Seismicity of Southwest Asia. R. Sorkhabi. The Geological Society of America Special Paper 525, 229–289. https://doi.org/10.1130/2016.2525(07).
Khogenkumar, S., Krishnakanta Singh, A., Bikramaditya Singh, R.K., Khanna, P.P., Ibotombi Singh, N., Inaocha Singh, W., 2016. Coexistence of MORB and OIB-type mafic volcanics in the Manipur Ophiolite Complex, Indo-Myanmar Orogenic Belt, northeast India: Implication for heterogeneous mantle source at the spreading zone. J. Asian Earth Sci. 116, 42–58. https://doi.org/10.1016/j.jseaes.2015.11.007.
Khogenkumar, S., Krishnakanta Singh, A., Kumar, S., Lakhan, N., Chaubey, M., Imtisunep, S., Dutt, A., Oinam, G., 2021. Subduction versus non-subduction origin of the Nagaland-Manipur Ophiolites along the Indo-Myanmar Orogenic Belt, northeast India: Fact and fallacy. Geol. J. 56 (4), 1773–1794. https://doi.org/10.1002/gj.4030.
Kopp, C., Fruehn, J., Flueh, E.R., Reichert, C., Kukowski, N., Bialas, J., Klaeschen, D., 2000. Structure of the Makran subduction zone from wide-angle and reflection seismic data. Tectonophysics 329 (1–4), 171–191. https://doi.org/10.1016/S0040-1951(00)00195-5.
Le Roex, A.P., Dick, H.J.B., Erlank, A.J., Reid, A.M., Frey, F.A., Hart, S.R., 1983. Geochemistry, mineralogy and petrogenesis of lavas erupted along the Southwest Indian Ridge between the Bouvet triple junction and 11 degrees. East. Journal of Petrology 24 (3), 267–318.
Mahéo, G., Bertrand, H., Guillot, S., Villa, I.M., Keller, F., Capiez, P., 2004. The South Ladakh ophiolites (NW Himalaya, India): an intra-oceanic tholeiitic arc origin with implication for the closure of the Neo-Tethys. Chem. Geol. 203, 273–303. https://doi.org/10.1016/j.chemgeo.2003.10.007.
Malpas, J., Zhou, M.F., Robinson, P.T., Reynolds, P.H., 2003. Geochemical and geochronological constraints on the origin and emplacement of the Yarlung Zangbo ophiolites, Southern Tibet. Geol. Soc. Lond. Spec. Publ. 218, 191–206. https://doi.org/10.1144/GSL.SP.2003.218.01.11.
Marroni, M., Göncüoğlu, M.C., Frassi, C., Sayit, K., Pandolfi, L., Ellero, A., Ottria, G., 2020. The Intra-Pontide ophiolites in Northern Turkey revisited: From birth to death of a Neotethyan oceanic domain. Geosci. Front. 11, 129–149. https://doi.org/10.1016/j.gsf.2019.05.010.
McCall, G.J.H., 1997. The geotectonic history of the Makran and adjacent areas of southern Iran. J. Asian Earth Sci. 15, 517–531.
McCall, G.J.H., Kidd, R.G.W., 1982. The Makran southeastern Iran: the anatomy of a convergent margin active from Cretaceous to present. In: Leggett, J.K. (Eds.), Trench-forearc geology: sedimentation and tectonics of modern and ancient plate margins, Geological Society of London Special Publications vol. 10, pp. 387-397.
McCall, G.J.H., 1983. Mélanges of the Makran, southeastern Iran. In: In: McCall, G.J.H. (Eds.), Ophiolitic and related mélanges, Benchmark Papers in Geology 66. Hutchinson Ross Publishing Company, Stroudsburg, Pennsylvania, pp. 292–299.
McCall, G.J.H., 1985. Explanatory text of the Minab Quadrangle Map; 1:250,000; No. J13. Geological Survey of Iran, Tehran, pp. 530.
McCall, G.J.H., 2002. A summary of the geology of the Iranian Makran. In: Clift, P.D., Kroon, F.D., Gaedecke, C., Craig, J. (Eds.), The Tectonic and Climatic Evolution of the Arabian Sea Region, Geological Society of London Special Publications vol. 195, pp. 147-204.
Metcalfe, I., 2013. Gondwana dispersion and Asian accretion: Tectonic and palaeogeographic evolution of eastern Tethys. J. Asian Earth Sci. 66, 1–33. https://doi.org/10.1016/j.jseaes.2012.12.020.
Metcalfe, I., 2021. Multiple Tethyan ocean basins and orogenic belts in Asia. Gondw. Res. 100, 87–130. https://doi.org/10.1016/j.gr.2021.01.012.
Moghadam, H.S., Stern, R.J., 2015. Ophiolites of Iran: keys to understanding the tectonic evolution of SW Asia: (II) Mesozoic ophiolites. J. Asian Earth Sci. 100, 31–59.
Moghadam, H.S., Bröcker, M., Griffin, W.L., Li, X.-H., Chen, R.X., O'Reilly, S.Y., 2017. Subduction, high-P metamorphism, and collision fingerprints in South Iran: Constraints from zircon U-Pb and mica Rb-Sr geochronology. Geochem. Geophys. Geosyst. 18, 306–332. https://doi.org/10.1002/2016GC006585.
Moghadam, H.S., Li, Q.L., Griffin, W.L., Chiaradia, M., Hoernle, K., O'Reilly, S.Y., Esmaeili, R., 2021. The Middle-Late Cretaceous Zagros ophiolites, Iran: Linking of a 3000 km swath of subduction initiation fore-arc lithosphere from Troodos, Cyprus to Oman. Geol. Soc. Am. Bull. 134 (5–6), 1414–1442. https://doi.org/10.1130/B36041.1.
Moghadam, H.S., Arai, S., Griffin, W.L., Khedr, M., Saccani, E., Henry, H., O'Reilly, S.Y., Ghorbani, G., 2022. Geochemical variability among stratiform chromitites and ultramafic rocks from Western Makran. South Iran. Lithos 412–413, 106591. https://doi.org/10.1016/j.lithos.2021.106591.
Moghadam, H.S., Dilek, Y., Furnes, H., Ishizuka, O., Chiaradia, M., Li, Q., Karsli, O., Lucci, F., Asadi, A., 2023. Chemostratigraphy of the extrusive sequence of a Late Cretaceous Neotethyan ophiolite in southern Iran and its significance for the mode and tempo of subduction initiation magmatism and melt evolution in forearc tectonic settings. J. Geol. Soc. London 180. https://doi.org/10.1144/jgs2023-080.
Mohammadi, A., Burg, J.-P., Winkler, W., Ruh, J., von Quadt, A., 2016. Detrital zircon and provenance analysis of Late Cretaceous-Miocene onshore Iranian Makran strata: Implications for the tectonic setting. Geol. Soc. Am. Bull. 128 (9–10), 1481–1499, 10.1130/B31361.110.1130/2016113.
Mohammadi, A., Burg, J.-P., Guillong, M., Von Quadt, A., 2017. Arc magmatism witnessed by detrital zircon U-Pb geochronology, Hf isotopes and provenance analysis of Late Cretaceous-Miocene sandstones of onshore Western Makran. Am. J. Sci. 317 (8), 941–964.
Monsef, I., Monsef, R., Mata, J., Zhang, Z., Pirouz, M., Rezaeian, M., Esmaeili, R., Xiao, W., 2018. Evidence for an early-MORB to fore-arc evolution within the Zagros suture zone: Constraints from zircon U-Pb geochronology and geochemistry of the Neyriz ophiolite (South Iran). Gondw. Res. 62, 287–305. https://doi.org/10.1016/j.gr.2018.03.002.
Monsef, I., Rahgoshay, M., Pirouz, M., Chiaradia, M., Grégoire, M., Ceuleneer, G., 2019. The Eastern Makran Ophiolite (SE Iran): evidence for a Late Cretaceous fore-arc oceanic crust. Int. Geol. Rev. 1–27. https://doi.org/10.1080/00206814.2018.1507764.
Moslempour, M.E., Khalatbari-Jafari, M., Ghaderi, M., Yousefi, H., Shahdadi, S., 2015. Petrology, geochemistry and tectonics of the extrusive sequence of Fannuj-Maskutan Ophiolite, southeastern Iran. J. Geol. Soc. India 85, 604–618.

Motaghi, K., Shabanian, E., Nozad-Khalil, T., 2020. Deep structure of the western coast of the Makran subduction zone SE Iran. Tectonophysics 776. https://doi.org/10.1016/j.tecto.2019.228314.
Muñoz-Montecinos, J., Angiboust, S., Garcia-Casco, A., 2021. Blueschist-facies paleo-earthquakes in a serpentinite channel (Zagros suture, Iran) enlighten seismogenesis in Mariana-type subduction margins. Earth Planet. Sci. Lett. 573, 117135. https://doi.org/10.1016/j.epsl.2021.117135.
Najafzadeh, A.R., Arvin, M., Pan, Y., Ahmadipour, H., 2008. Podiform chromitites in the Sorkhband Ultramafic Complex, Southern Iran: Evidence for ophiolitic chromitite. J. Sci. Islamic Republic Iran 19, 49–65.
Niu, Y., 1997. Mantle melting and melt extraction processes beneath ocean ridges: evidence from abyssal peridotites. J. Petrol. 38, 1047–1074.
Omrani, H., Moazzen, M., Oberhänsli, R., Moslempour, M.E., 2017. Iranshahr blueschist: subduction of the inner Makran oceanic crust. J. Metam. Geol. 35, 373–392.
Pandey, D., Pandey, A., Whattam, S., 2019. Relict subduction initiation along a passive margin in the northwest Indian Ocean. Nat. Commun. https://doi.org/10.1038/s41467-019-10227-8.
Pandolfi, L., Barbero, E., Marroni, M., Delavari, M., Dolati, A., Di Rosa, M., Frassi, C., Langone, A., Farina, F., MacDonald, C.S., Saccani, E., 2021. The Bajgan Complex revealed as a Cretaceous ophiolite-bearing subduction complex: A key to unravel the geodynamics of Makran (southeast Iran). J. Asian Earth Sci. 222. https://doi.org/10.1016/j.jseaes.2021.104965.
Pearce, J.A., Norry, M.J., 1979. Petrogenetic implications of Ti, Zr, Y, and Nb variations in volcanic rocks. Contrib. Miner. Petrol. 69, 33–47.
Penney, C., Tavakoli, F., Saadat, A., Nankali, H.R., Sedighi, M., Khorrami, F., Sobouti, F., Rafi, Z., Copley, A., Jackson, J., Priestley, K., 2017. Megathrust and accretionary wedge properties and behaviour in the Makran subduction zone. Geophys. J. Int. 209, 1800–1830. https://doi.org/10.1093/gji/ggx126.
Platt, J.P., Leggett, J.K., Young, J., Raza, H., Alam, S., 1985. Large-scale sediment underplating in the Makran accretionary prism, southwest Pakistan. Geology 13 (7), 507–511.
Rajabzadeh, M.A., Moosavinasab, Z., 2013. Mineralogy and distribution of Platinum-Group Minerals (PGM) and other solid inclusions in the Faryab ophiolitic chromitites, Southern Iran. Mineral. Petrol. 107, 943–962.
Ramsay, J.G., 1967. Folding and Fracturing of Rocks. Mc Graw and Hill ed., 568 pp.
Rashidi, A., Kianimehr, H., Yamini-Fard, F., Tatar, M., Zafarani, H., 2022. Present Stress Map and Deformation Distribution in the NE Lut Block, Eastern Iran: Insights from Seismic and Geodetic Strain and Moment Rates. Pure Appl. Geophys. 179, 1887–1917. https://doi.org/10.1007/s00024-022-03015-x.
Regard, V., Hatzfeld, D., Molinaro, M., Aubourg, C., Bayer, R., Bellier, O., Yamini-Fard, F., Peyret, M., Abbassi, M., 2010. The transition between Makran subduction and the Zagros collision: recent advances in its structure and active deformation. Geol. Soc. Lond. Spec. Publ. 330 (1), 43–64.
Ricou, L.E., 1994. Tethys reconstructed: plates continental fragments and their boundaries since 260 Ma from Central America to South-eastern Asia. Geodin. Acta 7, 169–218.
Robertson, A. H. F., Searle, M. P., 1990. The northern Oman Tethyan continental margin: Stratigraphy, structure, concepts, and controversies. In: Robertson, A.H.F., Searle, M. P., and Ries, A.C., eds., The Geology and Tectonics of the Oman Region: Geological Society, London, Special Publication 49, p. 3–25, Doi: 10.1144/GSL.SP.1992.049.01.02.
Rodriguez, M., Arnould, M., Coltice, N., Soret, M., 2021. Long-term evolution of a plume-induced subduction in the Neotethys realm. Earth Planet. Sci. Lett. 561, 116798. https://doi.org/10.1016/j.epsl.2021.116798.
Rolland, Y., Hässig, M., Bosch, D., Bruguier, O., Melis, R., Galoyan, G., Topuz, G., Sahakyan, L., Avagyan, A., Sosson, M., 2020. The East Anatolia–Lesser Caucasus ophiolite: an exceptional case of large-scale obduction, synthesis of data and numerical modelling. Geosci. Front. 11 (1), 83–108. https://doi.org/10.1016/j.gsf.2018.12.009.
Saccani, E., 2015. A new method of discriminating different types of post-Archean ophiolitic basalts and their tectonic significance using Th-Nb and Ce-Dy-Yb systematics. Geosci. Front. 6, 481–501.
Saccani, E., Photiades, A., Padoa, E., 2003. Geochemistry, petrogenesis and tectono-magmatic significance of volcanic and subvolcanic rocks from the Koziakas Mélange (Western Thessaly, Greece). Ofioliti 28, 43–57.
Saccani, E., Allahyari, K., Beccaluva, L., Bianchini, G., 2013. Geochemistry and petrology of the Kermanshah ophiolites (Iran): Implication for the interaction between passive rifting, oceanic accretion, and plume-components in the Southern Neo-Tethys Ocean. Gondw. Res. 24, 392–411. https://doi.org/10.1016/j.gr.2012.1010.1009.
Saccani, E., Delavari, M., Dolati, A., Marroni, M., Pandolfi, L., Chiari, M., Barbero, E., 2018. New insights into the geodynamics of Neo-Tethys in the Makran area: Evidence from age and petrology of ophiolites from the Coloured Mélange Complex (SE Iran). Gondw. Res. 62, 306–327. https://doi.org/10.1016/j.gr.2017.07.013.
Saccani, E., Delavari, M., Dolati, A., Pandolfi, L., Barbero, E., Brombin, V., Marroni, M., 2022a. Geochemistry of volcanic rocks and dykes from the Remeshk-Mokhtarabad and Fannuj-Maskutan Ophiolites (Makran Accretionary Prism, SE Iran): New constraints for magma generation in the Middle East Neo-Tethys. Geosyst. Geoenvironm. https://doi.org/10.1016/j.geogeo.2022.100140.
Saccani, E., Delavari, M., Dolati, A., Pandolfi, L., Barbero, E., Tassinari, R., Marroni, M., 2022b. Geochemistry of basaltic blueschists from the Deyader Metamorphic Complex (Makran Accretionary Prism, SE Iran): New constraints for magma generation in the Makran sector of the Neo-Tethys. J. Asian Earth Sci. https://doi.org/10.1016/j.jseaes.2022.105141.
Saccani, E., Barbero, E., Delavari, M., Dolati, A., Brombin, V., Marroni, M., Pandolfi, L., 2024. Geochemistry and magmatic petrology of metaophiolites from the Bajgan Complex (Makran Accretionary Prism, SE Iran): New insights on the nature of the Early Cretaceous Middle East Neo-Tethys. J. Geol. Soc. 181. https://doi.org/10.1144/jgs2024-043.
Safonova, I., Maruyama, S., Kojima, S., Komiya, T., Krivonogov, S., Koshida, K., 2016. Recognizing OIB and MORB in accretionary complexes: a new approach based on ocean plate stratigraphy, petrology, and geochemistry. Gondw. Res. 33, 92–114. https://doi.org/10.1016/j.gr.2015.06.013.
Salam, H., Turab, S.A., Ali, A., Jan, M.Q., Sulaiman, N., Basori, M.B.I., 2024. Kahi mélange complex in Kurram and Waziristan, NW Pakistan: An integrated approach for tectonic implications to India–Afghan suturing. Gondw. Res. 126, 79–95. https://doi.org/10.1016/j.gr.2023.10.001.
Searle, M.P., 2019. Timing of subduction initiation, arc formation, ophiolite obduction and India–Asia collision in the Himalaya. In: Treloar, P.J. & Searle, M.P. (Eds), Himalayan Tectonics: A Modern Synthesis: Geological Society London, Special Publications, 483, 19-37, Doi: 10.1144/SP483.8.
Sengör, A.M.C., 1984. The Cimmeride orogenic system and the tectonics of Eurasia. Geological Society of America Special. Publication 195, 82 p.
Şengör, A.M.C., Altiner, D., Cin, A., Ustaömer, T., Hsü, K.J., 1988. Origin and assembly of the Tethyside orogenic collage at the expense of Gondwana Land. Geochem. Soc. Spec. Publ. https://doi.org/10.1144/GSL.SP.1988.037.01.09.
Şengör, A.M.C., Yilmaz, 1981. Y. Tethyan evolution of Turkey; a plate tectonic approach. Tectonophysics 75, 181–241.
Sepidbar, F., Lucci, F., Biabangard, H., Zaki Khedr, M., Jiantang, P., 2020. Geochemistry and tectonic significance of the Fannuj-Maskutan SSZ-type ophiolite (Inner Makran, SE Iran). International Geology Review. Doi: 10.1080/00206814.2020.1753118.
Serri, G., 1981. The petrochemistry of ophiolite gabbroic complexes: a key for the classification of ophiolites into low-Ti and high-Ti types. Earth Planet. Sci. Lett. 52, 203–212.
Shaker Ardakani, A.R., Arvin, M., Oberhänsli, R., Mocek, B., Moeinzadeh, S.H., 2009. Morphology and petrogenesis of pillow lavas from the Ganj Ophiolitic Complex, Southeastern Kerman Iran. J. Sci. Islamic Republic of Iran 20, 139–151.
Stampfli, G.M., Hochard, C., 2009. Plate tectonics of the Alpine realm. In: Murphy, J.B., Hynes, A.J., Keppie, J.D. (Eds.), Ancient orogens and modern analogues: Geological Society, London, Special Publications, 327, pp. 89–111.
Stampfli, G.M., Borel, G.D., 2002. A plate tectonic model for the Palaeozoic and Mesozoic constrained by dynamic plate boundaries and restored synthetic oceanic isochrones. Earth Planet. Sci. Lett. 169, 17–33.
Stampfli, G.M., 2000. Tethyan oceans. In: Bozkurt, E., Winchester, J., Piper, J.A. (Eds.), Tectonics and Magmatism in Turkey and the Surrounding Area, vol. 173. Geological Society of London, Special Publications, pp. 1–23.
Stern, R.J., Moghadam, H.S., Pirouz, M., Mooney, W., 2021. The Geodynamic Evolution of Iran. Annu. Rev. Earth Planet. Sci. 49, 9–36. https://doi.org/10.1146/annurev-earth-071620-052109.
Stöcklin, J., 1968. Structural history and tectonics of Iran: A review. American Association of Petroleum Geology 52, 1229–1258.
Stoneley, R., 2005. The Zendan Fault of southern Iran. Proc. Geol. Assoc. 116, 311–313. https://doi.org/10.1016/S0016-7878(05)80049-5.
Sun, S.-S., McDonough, W.F., 1989. Chemical and isotopic systematics of oceanic basalts: implications for mantle composition and processes. Geol. Soc. Lond. Spec. Publ. 42 (1), 313–345. https://doi.org/10.1144/GSL.SP.1989.042.
Takin, M., 1972. Iranian geology and continental drift in the Middle East. Nature 235, 147–150.
Taylor, S.R., McLennan, S.M., 1985. The Continental Crust: its composition and evolution: an examination of the geochemical record preserved in sedimentary rocks. Blackwell Scientific Publication, Oxford, p. 312.
Ullah, I., Xue, C., Yang, T., Furnes, H., Dilek, Y., Wand, W., Ghaffar, A., 2023. Double arc–continent collision record in the latest Mesozoic–Cenozoic tectonic history of the Himalayan–Tibetan orogenic belt in western Pakistan. J. Geol. Soc. London 180. https://doi.org/10.1144/jgs2023-07.
van Hinsbergen, D.J.J., Lippert, P.C., Li, S., Huang, W., Advokaat, E.L., Spakman, W., 2019. Reconstructing Greater India: Paleogeographic, kinematic, and geodynamic perspectives. Tectonophysics 760, 69–94. https://doi.org/10.1016/j.tecto.2018.04.006.
Wan, B., Chu, Y., Chen, L., Liang, X., Zhang, Z., Ao, S., Talebian, M., 2021. Paleo-Tethys subduction induced slab-drag opening the Neo-Tethys: Evidence from an Iranian segment of Gondwana. Earth Sci. Rev. 221, 103788. https://doi.org/10.1016/j.earscirev.2021.103788.
Whattam, S.A., Stern, R.J., 2015. Late Cretaceous plume-induced subduction initiation along the southern margin of the Caribbean and NW South America: The first documented example with implications for the onset of plate tectonics. Gondw. Res. 27, 38–63. https://doi.org/10.1016/j.gr.2014.07.011.
White, R.S., Klitgord, K., 1976. Sediment deformation and plate tectonics in the Gulf of Oman. Earth Planet. Sci. Lett. 32, 199–209. https://doi.org/10.1016/0012-821X(76)90059-5.
Workman, R.K., Hart, S.R., 2005. Major and trace element composition of the depleted MORB mantle (DMM). Earth Planet. Sci. Lett. 321, 53–72.
Xia, B., Chen, G.-W., Wang, R., Wang, Q., 2008. Seamount volcanism associated with the Xigaze ophiolite, Southern Tibet. J. Asian Earth Sci. 32, 396–405. https://doi.org/10.1016/j.jseaes.2007.11.008.
Zhang, Z., Xiao, W., Ji, W., Majidifard, M.R., Rezaeian, M., Talebian, M., Xiang, D., Chen, L., Wan, B., Ao, S., Esmaeili, R., 2018. Geochemistry, zircon U-Pb and Hf isotope for granitoids, NW Sanandaj-Sirjan zone, Iran: Implications for Mesozoic-Cenozoic episodic magmatism during Neo-Tethyan lithospheric subduction. Gondw. Res. 62, 227–245.
Zhou, X., Li, Z.H., Gerya, T., Stern, R.J., 2020. Lateral propagation–induced subduction initiation at passive continental margins controlled by preexisting lithospheric weakness. Sci. Adv. 6 (10). https://doi.org/10.1126/sciadv.aaz1048.